Optimal Error Estimates of Ultra-weak Discontinuous Galerkin Methods with Generalized Numerical Fluxes for Multi-dimensional Convection-Diffusion and Biharmonic Equations

Yuan Chen, Yulong Xing[1]

Abstract

In this paper, we study ultra-weak discontinuous Galerkin methods with generalized numerical fluxes for multi-dimensional high order partial differential equations on both unstructured simplex and Cartesian meshes. The equations we consider as examples are the non-linear convection-diffusion equation and the biharmonic equation. Optimal error estimates are obtained for both equations under certain conditions, and the key step is to carefully design global projections to eliminate numerical errors on the cell interface terms of ultra-weak schemes on general dimensions. The well-posedness and approximation capability of these global projections are obtained for arbitrary order polynomial space based on a wide class of generalized numerical fluxes on regular meshes. These projections can serve as general analytical tools to be naturally applied to a wide class of high order equations. Numerical experiments are conducted to demonstrate these theoretical results.

MSC (2020): Primary 65M12, 65M15, 65M60; Secondary 35G25
Keywords: Ultra-weak Discontinuous Galerkin Method, Optimal Error Estimate, High order PDEs, Generalized numerical Fluxes, Unstructured meshes

1   Introduction

In this paper, we consider ultra-weak discontinuous Galerkin (DG) methods with generalized numerical fluxes for high order partial differential equations (PDEs) in multi-dimensional spaces. Let $\Omega \subset \mathbb{R}^d$, $d \geq 1$, the two examples considered in this paper are:

- the nonlinear convection-diffusion equation

$$u_t + \nabla \cdot \mathbf{f}(u) - \varepsilon \Delta u \; = \; 0, \tag{1.1}$$

   where $\mathbf{f}$ is the general nonlinear convection term, and $\varepsilon > 0$ is the diffusion coefficient.

- the biharmonic equation

$$u_t + \Delta^2 u \; = \; 0. \tag{1.2}$$

For simplicity of analysis and computation, we only consider periodic boundary conditions on the rectangular domain Ω. The results can be extended to other boundary conditions and shapes of domains with suitable conditions.

The DG method is a class of Finite Element Methods (FEM) that employ discontinuous piecewise polynomials as trial and test spaces. It was first introduced in [42] for solving a steady state linear hyperbolic equation in the framework of neutron transport problems. Simultaneously in the 1970s, a class of Interior Penalty Discontinuous Galerkin (IPDG) was studied for elliptic and parabolic problems [1, 5, 27]. In the late 1990s, Local Discontinuous Galerkin (LDG) was developed by Cockburn and Shu [24] for nonlinear convection-diffusion equations. The idea of LDG is to introduce auxiliary variables and rewrite the equation into an equivalent system of first order equations. It is well-known that numerical flux is an important ingredient in the design and analysis of the DG method, due to the fact that discontinuous polynomial spaces do not require continuity on the boundaries of elements for flexibility of applications. The role of numerical fluxes is to control the behavior of numerical solutions on element boundaries, which directly affect, and even determine the accuracy and stability behavior of DG schemes. In [2], the authors summarized the aforementioned DG methods into a unified framework with only differences in the choice numerical fluxes. In the last decade, there are some new DG methods proposed for high order PDEs, here we only name a few. Direct Discontinuous Galerkin (DDG) method was introduced in [35] to solve diffusion problems. The idea of DDG methods is to directly derive the weak formulation of numerical solutions without introducing auxiliary variables, which is closely related to the classical IPDG. For DDG methods, high order spatial derivatives may be included in the schemes to enrich the stability. Ultra-weak DG method which will be studied in this paper was proposed in [18] for solving time-dependent PDEs with higher order spatial derivatives. The spirit of this method is to successively apply integration by parts on the weak formulation of PDEs and move all high order spatial derivatives to the test functions. The numerical fluxes are carefully chosen to guarantee numerical stability. Ultra-weak DG method was developed and extended to solve the one-dimensional Schrödinger equation [15], dispersive wave equations [31], etc. Recently, an ultra-weak local DG method was introduced in [49], which combines features of LDG and ultra-weak DG methods.

The a priori error estimates of DG methods have been studied for a long period. In [2], the early work of DG methods for diffusion problems is summarized and analyzed using one unified framework with different numerical fluxes. IPDG and LDG are both included in this framework and proved to have optimal convergence under certain assumptions. A wide range of other classical DG methods such as [6, 7, 11, 43] are included in this class. For convection-diffusion equations, [25, 26] obtained $\mathcal{O}(h^k)$ suboptimal estimate for the modified [7] and vanilla IPDG [27] methods. Here and in what follows, k denotes the degree of piecewise polynomials in the discontinuous polynomial spaces. Within the LDG framework, the first $\mathcal{O}(h^k)$ suboptimal L^2 error estimate for one-dimensional linear convection-diffusion equations with generalized numerical fluxes was obtained in [24]. Only sub-optimal results hold since L^2 projection could not treat the numerical errors on element boundaries optimally. In [12, 13], a special case of numerical fluxes, alternating numerical fluxes, are chosen to obtain optimal $\mathcal{O}(h^{k+1})$ convergence rate using Gauss-Radau projections. This projection could eliminate error terms on element boundaries since it interpolates functions on boundaries. The authors then extended this result into multi-dimensional Cartesian meshes by discovering the local superconvergence phenomenon [23]. In [37], an optimal error estimate of DG methods with upwind-biased flux was obtained for the linear hyperbolic conservation law on one- and two-dimensional Cartesian meshes. The difficulty of this work focuses on the design and analysis of a global type projection. This work was then extended to convection-diffusion equations with generalized alternating fluxes using the technique of generalized Gauss-Radau projections [16]. For the DDG method, Liu et al. [33, 34, 35] derived optimal error estimates for

one- and multi-dimensional convection-diffusion problems. For the ultra-weak DG method, Cheng and Shu considered the alternating fluxes combined with a $\mathcal{O}(h^{-1})$ penalty term and proved the sub-optimal $\mathcal{O}(h^k)$ convergence for one-dimensional convection-diffusion equations in [18]. Only sub-optimality is obtained because the chosen Gauss-Radau projections may not be compatible with the convection terms on the boundaries of elements. In [8], a global projection was introduced to provide the error estimate of an ultra-weak energy-conserving DG method for the generalized Korteweg-de Vries (gKdV) equation. Recently, in [49, 50], the authors studied the ultra-weak local DG scheme for the time-dependent biharmonic equation and nonlinear fourth-order wave equations on one- and two-dimensional Cartesian meshes. Optimal error analysis is obtained through the use of Gauss-Radau projections.

In recent years, there is a growing trend in investigating the theoretical behavior of generalized numerical fluxes. For convection-diffusion equations, we have mentioned [37] with upwind-biased flux and [16] with generalized alternating fluxes. For two-way wave equations, [17] proposed and studied a class of numerical fluxes, named $\alpha\beta$ fluxes, which yield optimal error estimate. Recently [47] extended the range of parameters in the numerical fluxes and, by using the novel energy argument, derived optimal error estimates of DG methods with generalized numerical fluxes for wave equations on unstructured simplex meshes. In [48], similar energy argument was carried out to construct a global projection on special simplex meshes in multi dimensions satisfying the so-called flow condition, and optimal error estimates are proved for upwind-biased DG methods for multi-dimensional linear advection equations on such meshes. DG methods with generalized numerical fluxes were recently studied for stochastic Maxwell equations with additive or multiplicative noises in [45, 46]. For one-dimensional models containing high order derivatives, LDG methods with $\alpha\beta$ fluxes were studied in [30]. In [15], an optimal error estimate for one-dimensional Schrödinger equation is achieved for ultra-weak schemes with generalized numerical fluxes. The error analysis is rather cumbersome due to the construction of global projections, which is aggravated in the cases of ultra-weak schemes since the projections for this type of scheme require coupling of functions and their derivatives (as compared with LDG-type schemes). This feature could also explain the lack of such results in the ultra-weak DG method for multi-dimensional problems. It is therefore interesting and necessary to develop analysis tools suitable for ultra-weak DG methods in general cases with multi-dimensional settings and generalized numerical fluxes.

In this paper, we focus on the generalization and development of analysis tools for the optimal error estimate of ultra-weak DG methods with generalized numerical fluxes. The main objective of this paper is threefold. First, we design novel global projections suitable for the analysis of ultra-weak type methods on multi-dimensional settings with unstructured meshes. In addition, properties of such projections including the well-posedness and optimal approximation capability will be studied. Second, we apply these tools to study ultra-weak DG methods for general dimensional nonlinear convection-diffusion equations and biharmonic equations. The optimal convergence is obtained by taking advantage of the carefully designed projections. Third, we also consider generalized numerical fluxes in a general formulation with various parameters, and study the general behavior of ultra-weak schemes under this setting. The tools we build in the present work can be applied not only to convection-diffusion and biharmonic equations, but to other high-dimensional problems such as Schrödinger [15] and wave [50] equations, etc. Furthermore, we believe the spirit of current work could also be extended to other high order problems such as the gKdV equation [8, 18, 29] and problems with higher order spatial derivatives [49].

In the analysis of projection error, different from the approaches in [22, 47], we do not consider Gauss-Radau type projections on unstructured simplex meshes in this paper. This follows the nature of our problem: instead of coupling auxiliary variables, Gauss-Radau type projections for ultra-weak type schemes have to deal with the aforementioned coupling of function and its

derivatives. If we adopt a similar definition as LDG type projections [22, 47], it may even produce an overdetermined global linear system. Moreover, the decoupling work of functions with their derivatives is rather harder than that of auxiliary variables, even in one dimension. Therefore, we consider generating projections directly from the ultra-weak schemes on simplex meshes and survey the range of parameters that could guarantee good properties. This setting is flexible and could be extended to other meshes and discontinuous spaces easily. A similar technique has been applied to analyze multi-dimensional DDG methods in [34]. We emphasize that compared with [34], the compatible parameter set of our method can be explicitly written out and computed, which could be useful in the computation of an application problem. Moreover, if Cartesian meshes are used, we could still take advantage of the tensor structure and design tensor product projections from the one-dimensional projections studied in [15]. Thanks to the structure of the Cartesian mesh, we could extend the range of parameters with optimal error. Superconvergence properties corresponding to results of [23] are studied for these tensor projections to overcome the lack of orthogonality. With these carefully designed projections, we can improve and extend error estimates for convection-diffusion and biharmonic equations in the literature [18, 49] under multi-dimensional and generalized numerical fluxes settings. At the end of this paper, some numerical examples are provided to further investigate the general behavior of different numerical fluxes.

As a DG method, the ultra-weak DG method automatically enjoys the common advantages of DG methods, such as easiness to accommodate arbitrary h-p adaptivity, high parallel efficiency, flexibility in handling geometry and meshes, etc. When applied to convection-diffusion equation, the ultra-weak DG method avoids using auxiliary variables or rewriting the original equation into a larger system. As a result, the stencil is more compact than methods such as LDG, which leads to more efficient computation. Compared with earlier classical DG methods [7, 41], the provable stability and optimal convergence which will be shown in the present paper also provides stronger theoretical guarantee. For time-dependent biharmonic equations, the standard discontinuous polynomial spaces are used, instead of C^1 conforming element or mixed elements [4, 20] used in FEM. This reduces the difficulty brought by approximated spaces such as tedious coding and Ladyzhenskaya-Babuska-Brezzi (LBB) conditions. The theoretical analysis in this paper could provide provable stability and convergence, especially for polynomial order $k = 1, 2$, which usually bring difficulties for methods of fourth order problems, see [10, 28, 38, 39]. Moreover, designed to solve high spatial order PDEs, the ultra-weak DG method is easy to be generalized to other high order equations, such as gKdV equation, fifth, sixth, seventh and even general nth order PDEs.

The rest of the paper is organized as follows: In Section 2, we introduce notations, assumptions, ultra-weak DG scheme, and some preliminary analysis results. In Section 3, we develop a couple of projections designed for ultra-weak schemes which are critical tools for optimal error estimates. In Sections 4 and 5, we derive optimal error estimates for the multi-dimensional nonlinear convection-diffusion equation and biharmonic equation, respectively. Numerical experiments are provided in Section 6 to validate and explore theoretical results. Finally, a brief conclusion will be given in Section 7.

2 Ultra-weak Scheme

2.1 Notations and Assumptions

In this section, we introduce the notations and assumptions that will be used in this paper. In the one-dimensional case, we consider Ω as an interval $[a, b]$, where $a, b \in \mathbb{R}$. Let $\mathcal{T}_h = \{I_i\}_{i=1}^N$ to be a partition of Ω, where $I_i = (x_{i-1/2}, x_{i+1/2})$ has the length $h_i = x_{i+1/2} - x_{i-1/2}$. The global mesh size is set as $h \equiv \max_{1 \le i \le N} h_i$. We assume the partition $\mathcal{T}_h$ is quasi-uniform [9], i.e., there exists a

constant C independent of h, such that $Ch \leq h_i \leq h$, for $i = 1, 2, ..., N$ as h goes to 0. We also use $\mathcal{E}_h$ to represent the set of boundary points of partition $\mathcal{T}_h$, i.e., $\mathcal{E}_h = \{x_{i+1/2}\}$, $i = 0, 1, ..., N$.

In higher dimensional spaces with $d \geq 2$, two classes of meshes will be considered in this paper: simplex mesh and Cartesian mesh. We introduce the setting of these two classes of meshes respectively. Let $\mathcal{T}_h$ be a simplex mesh of Ω and $\mathcal{E}_h$ be the set of faces of $\mathcal{T}_h$. For $T \in \mathcal{T}_h$, we denote the local mesh size to be $h_T = \text{diam}(T)$ and global mesh size $h = \max_{T \in \mathcal{T}_h} h_T$, where diam means diameter of a given geometric object. For any face $e \in \mathcal{E}_h$, we define its size to be $h_e = \text{diam}(e)$.

On the other hand, we use $\mathcal{K}_h$ to denote a Cartesian mesh on Ω. With spatial variables $X = (x^1, x^2, ..., x^d)$, the rectangular domain Ω can be represented in the form of $\Omega = \prod_{j=1}^{d} [a_j, b_j]$. Then we can write Ω as:

$$\Omega = \bigcup_{T \in \mathcal{K}_h} T, \tag{2.1}$$

where each $T \in \mathcal{K}_h$ can be written as $T = I_{\alpha_1}^1 \times I_{\alpha_2}^2 \times ... \times I_{\alpha_d}^d$, for some indexes $(\alpha_1, \alpha_2, ..., \alpha_d)$. For each dimension $j = 1, 2, ..., d$, $[a_j, b_j]$ is partitioned to N_j subintervals, i.e., $[a_j, b_j] = \bigcup_{\alpha_j=1}^{N_j} I_{\alpha_j}^j = \bigcup_{\alpha_j=1}^{N_j} [x_{\alpha_j - 1/2}^j, x_{\alpha_j + 1/2}^j]$ and the index α_j satisfies $1 \leq \alpha_j \leq N_j$. In this case, the definition of $\mathcal{E}_h$, mesh sizes h_e, and h directly follows the definition of the corresponding terminologies in the last paragraph.

Similar to the one-dimensional case, we also assume high dimensional meshes to be quasi-uniform. It is well-known that quasi-uniform meshes are non-degenerate [9]. In this paper, we will frequently use the following corollary: $\exists \, \sigma$ independent of h, such that

$$\frac{|e|}{|T|} \leq \frac{\sigma}{h_e}, \text{ for } \forall e \in \mathcal{E}_h(T), \ \forall T \in \mathcal{T}_h \text{ or } \mathcal{K}_h, \tag{2.2}$$

here $|\cdot|$ denotes the Lebesgue measure of each geometric object.

For simplicity of notations, we denote the standard L^2 norms of any function on a domain $\widetilde{\Omega}$ by $\|\cdot\|_{\widetilde{\Omega}}$. For example, for function v defined on Ω, $\|v\|_\Omega$ and $\|v\|_e$ represents the L^2 norm of v on the domain Ω and trace of v on a face e (if well-defined) respectively. Moreover, with these meshes on Ω defined as above, we are able to construct mesh-dependent norms. Here we take the simplex mesh $\mathcal{T}_h$ as an example. We use $W^{k,p}(\mathcal{T}_h)$, $k \geq 0$, $1 \leq p \leq \infty$ to denote the broken Sobolev space on $\mathcal{T}_h$, which can be defined as:

$$W^{k,p}(\mathcal{T}_h) = \{v \in L^2(\Omega) : \ v|_T \in W^{k,p}(T), \forall T \in \mathcal{T}_h\}. \tag{2.3}$$

This space is equipped with the following norm for $1 \leq p \leq \infty$:

$$\|v\|_{W^{k,p}(\mathcal{T}_h)} = \sum_{T \in \mathcal{T}_h} \|v\|_{W^{k,p}(T)}, \ 1 \leq p < \infty; \qquad \|v\|_{W^{k,\infty}(\mathcal{T}_h)} = \max_{T \in \mathcal{T}_h} \|v\|_{W^{k,\infty}(T)}. \tag{2.4}$$

By convention, when $p = 2$, we denote $W^{k,2}(\mathcal{T}_h)$ by $H^s(\mathcal{T}_h)$. For semi-norms, similar definitions could apply and we just denote the corresponding Sobolev semi-norm by $|v|_{W^{k,p}(\mathcal{T}_h)}$ for $1 \leq p \leq \infty$. For functions on norm vector spaces V with additional time variable within $t \in [0, L]$, here L represents a positive termination time, we use $L^p(0, L; V)$, $W^{k,p}(0, L; V)$ to denote the corresponding spaces.

To properly handle boundaries of elements and define the DG method. We have to deal with computations on traces of elements. Here we mention the related concepts and operators. We first note that the face set $\mathcal{E}_h$ can be split into $\mathcal{E}_h^b$, the boundary face set which contains faces located at the boundary of Ω, and the interior face set $\mathcal{E}_h^i = \mathcal{E}_h \backslash \mathcal{E}_h^b$. Then we associate one normal vector $\mathbf{n}$ to each $e \in \mathcal{E}_h$. For $e \in \mathcal{E}_h^b$, this vector points from the interior of the domain Ω to the exterior

side. For $e \in \mathcal{E}_h^i$, the direction of this vector only needs to be fixed with respect to e. In our work, we do not assign this direction. Without loss of generality, for each $e \in \mathcal{E}_h^i$, we denote the vector $\mathbf{n}$ pointing from T_e^1 to T_e^2, which are two neighbor elements of e. Note that functions in the broken Sobolev spaces on $\mathcal{T}_h$ may be double-valued on traces $e \in \mathcal{E}_h^i = \mathcal{E}_h \backslash \mathcal{E}_h^b$. For these functions, we define the operators $[\![\cdot]\!]$ and $\{\!\{\cdot\}\!\}$ on e to be:

$$[\![v]\!]_e = v|_{T_e^1} - v|_{T_e^2}, \qquad \{\!\{v\}\!\}_e = \frac{1}{2}(v|_{T_e^1} + v|_{T_e^2}), \qquad \text{on } e \in \mathcal{E}_h^i. \tag{2.5}$$

To adapt the above trace operators with the periodic boundary condition, we pair the faces on opposite boundaries. Each $e \in \mathcal{E}_h^b$ forms a boundary face pair $(e, \hat{e})$ with the corresponding symmetrical face $\hat{e}$ on the opposite boundary. For simplex meshes, we assume our triangulation makes this possible. Then we denote T_e^1 and $T_{\hat{e}}^2$ as the elements associated to e and $\hat{e}$, with which the operators $[\![\cdot]\!]$ and $\{\!\{\cdot\}\!\}$ on boundary face pair $(e, \hat{e})$ can be defined similarly:

$$[\![v]\!]_{(e,\hat{e})} = v|_{T_e^1} - v|_{T_{\hat{e}}^2}, \qquad \{\!\{v\}\!\}_{(e,\hat{e})} = \frac{1}{2}(v|_{T_e^1} + v|_{T_{\hat{e}}^2}), \qquad \text{for each boundary pair}(e, \hat{e}). \tag{2.6}$$

For the normal vector, we assign $\mathbf{n}_{(e,\hat{e})}$ pointing out from T_e^1 to the exterior of the domain, and is naturally identical to the normal vector pointing from exterior to $T_{\hat{e}}^2$. We may omit these subscripts if it does not cause any confusion. Note that in the following context, when we sum with respect to $\mathcal{E}_h$, it means sum with respect to all the faces in $\mathcal{E}_h^i$ and all face pairs $(e, \hat{e})$ on the boundary.

Remark 2.1. *In one dimension, we set $\sigma = 1$ in (2.2) for any partition $\mathcal{T}_h$, for the convenience of providing a unified trace inequality. Moreover, the concept of normal vectors can be adapted in one dimension without special treatment by defining the outer normal vector of each interval I to be $\mathbf{n} = -1$ on the left node, and $\mathbf{n} = 1$ on the right node. With this setting, it's possible that our definition of $[\![\cdot]\!]_e$ is slightly different from that in the literature.*

2.2 Preliminary Analysis

In this subsection, we list some important results that are commonly used in the analysis of finite element type methods. The following inequality reads the trace inequality for $H^1(T)$ element [9]: for any $T \in \mathcal{T}_h$ or $\mathcal{K}_h$,

$$\text{(Trace inequality)}. \quad \|v\|_{L^2(e)} \leq C \left(h_e^{-1/2} \|v\|_{L^2(T)} + h_e^{1/2} |v|_{H^1(T)} \right), \quad \forall v \in H^1(T), \tag{2.7}$$

where e is a face of T.

We define the mesh-dependent discontinuous piecewise polynomial space on $\mathcal{T}_h$:

$$V_h^k = \{v \in L^2(\mathcal{T}_h) : v|_T \in \mathcal{P}^k(T), \quad \forall T \in \mathcal{T}_h\}, \tag{2.8}$$

where $\mathcal{P}^k$ is the polynomial space of degree at most k. To enforce periodic boundary conditions, the following subspaces of V_h^k will be used in the following sections:

$$
\begin{aligned}
V_h^{k,0} &= \{v \in L^2(\mathcal{T}_h) : \int_\Omega v \, dX = 0, \ v|_T \in \mathcal{P}^k(T), \ \forall T \in \mathcal{T}_h\}, \\
V_h^{k,u} &= \{v + \frac{1}{|\Omega|} \int_\Omega u \, dX : v \in V_h^{k,0}\}.
\end{aligned}
\tag{2.9}
$$

Refined inequalities on polynomial space include trace inequality [51, 52] and inverse inequality (for example, see Theorem 3.2.6 of [21]):

(Trace inequality).	$\|v\|_{L^2(e)} \leq \sqrt{\dfrac{\sigma(k+1)(k+d)}{d}} h_e^{-1/2}\|v\|_{L^2(T)},$	$\forall v \in \mathcal{P}^k(T),$
(Inverse inequality).	$|v|_{H^1(T)} \leq Ch^{-1}\|v\|_{L^2(T)},$	$\forall v \in \mathcal{P}^k(T),$
(L_∞ Inverse inequality).	$\|v\|_{L^\infty(T)} \leq Ch^{-d/2}\|v\|_{L^2(T)},$	$\forall v \in \mathcal{P}^k(T).$

$$(2.10)$$

Similar to the polynomial spaces defined above, we introduce the discontinuous tensor product polynomial space S_h^k:

$$S_h^k = \{v \in L^2(\Omega) : \ v|_T \in \mathcal{Q}^k(T), \ \ \forall T \in \mathcal{K}_h\}, \tag{2.11}$$

where $\mathcal{Q}_k$ is the polynomial space of degree at most k for every spatial variable. Similar subspace $S_h^{k,0}$, $S_h^{k,u}$ and inverse inequalities can be established for this space as well. Here we only rewrite and derive the coefficients of the trace inequality.

Lemma 2.1. *Let K be a rectangular element, say $K = I_{\alpha_1}^1 \times I_{\alpha_2}^2 \times ... \times I_{\alpha_d}^d$, e be one of its faces with $h_e = diam(e)$. For a function $v \in \mathcal{Q}_k(T)$, the following trace inequality holds:*

$$\|v\|_{L^2(e)} \leq \sqrt{\sigma}(k+1)h_e^{-1/2}\|v\|_{L^2(T)}. \tag{2.12}$$

The proof of the above lemma is given in Appendix A.1. It can be seen that the constant of trace inequality in high-dimensional Cartesian meshes inherits that of the one-dimensional case.

2.3 Ultra-weak Discretization

The idea of ultra-weak DG methods [18] is to apply integration by parts repeatedly on the weak formulation of equations so that high order spatial derivatives can be moved to test functions. Then the numerical fluxes are carefully chosen to ensure stability and convergence.

For the negative Laplacian operator $-\Delta u$ which is common to many PDEs, we can derive its ultra-weak discretization as follows. Assume $u, v \in H^s(\Omega)$, $s \geq 2$, let us start with performing integration by parts twice to the bilinear form $(-\Delta u, v)_T$:

$$(-\Delta u, v)_T = (\nabla u, \nabla v)_T - \langle \partial_{\mathbf{n}} u, v \rangle_{\partial T} = -(u, \Delta v)_T + \langle u, \partial_{\mathbf{n}} v \rangle_{\partial T} - \langle \partial_{\mathbf{n}} u, v \rangle_{\partial T}, \tag{2.13}$$

where the test function v is taken from the piecewise polynomial space V_h^k or S_h^k. The notation $(\cdot, \cdot)_T$ denotes the standard inner product of L^2 space on element T, while the inner product on face e is denoted by $\langle \cdot, \cdot \rangle_e$. Note that in one dimension, $\langle \cdot, \cdot \rangle$ will degenerate to multiplication at point e. The functions u and $\partial_{\mathbf{n}} u$ defined on trace space are called physical fluxes. We sum the above equality for all elements T and substitute u and $\partial_{\mathbf{n}} u$ by single value functions $\widehat{u}$ and $\widetilde{\partial_{\mathbf{n}} u}$ on face e, which leads to

$$-\sum_T (u, \Delta v)_T + \sum_e \left[\langle \widehat{u}, [\![\partial_{\mathbf{n}} v]\!] \rangle_e - \langle \widetilde{\partial_{\mathbf{n}} u}, [\![v]\!] \rangle_e \right], \tag{2.14}$$

Using integration by parts on the first term of (2.14), we could define the bilinear form $a_h(\cdot, \cdot) : H^s(\Omega) \times H^s(\Omega) \mapsto \mathbb{R}$, $s > 3/2$ in the following form:

$$a_h(u, v) := \sum_T (\nabla u, \nabla v)_T - \sum_e \langle [\![u\partial_{\mathbf{n}} v]\!], 1 \rangle_e + \sum_e \left[\langle \widehat{u}, [\![\partial_{\mathbf{n}} v]\!] \rangle_e - \langle \widetilde{\partial_{\mathbf{n}} u}, [\![v]\!] \rangle_e \right]. \tag{2.15}$$

7

Here, the $\widehat{u}$ and $\widetilde{\partial_{\mathbf{n}} u}$ are the so-called numerical fluxes. In this paper, we consider generalized numerical fluxes with parameters $\alpha_1, \alpha_2, \beta_1, \beta_2 \in \mathbb{R}$:

$$\widetilde{\partial_{\mathbf{n}} u} = \{\!\{\partial_{\mathbf{n}} u\}\!\} + \alpha_1 [\![\partial_{\mathbf{n}} u]\!] + \beta_1 [\![u]\!], \quad \widehat{u} = \{\!\{u\}\!\} + \alpha_2 [\![u]\!] + \beta_2 [\![\partial_{\mathbf{n}} u]\!]. \tag{2.16}$$

This general form of the numerical flux was studied for the one-dimensional linear Schrödinger equation in [14]. Note that our definitions naturally guarantee that these numerical fluxes are consistent and conservative (as known as adjoint consistent [2]).

In our present work, we only consider the scaling invariant form, that is $\alpha_1 = -\alpha_2 = \alpha$, $\beta_1 = c_1/h_e$, $\beta_2 = c_2 h_e$, which leads to

$$\widetilde{\partial_{\mathbf{n}} u} = \{\!\{\partial_{\mathbf{n}} u\}\!\} + \alpha [\![\partial_{\mathbf{n}} u]\!] + \frac{c_1}{h_e} [\![u]\!], \quad \widehat{u} = \{\!\{u\}\!\} - \alpha [\![u]\!] + c_2 h_e [\![\partial_{\mathbf{n}} u]\!]. \tag{2.17}$$

The generalized numerical fluxes defined above include a large class of well-known numerical fluxes, such as central flux ($\alpha = c_1 = c_2 = 0$), alternating flux ($\alpha = 1/2$, $c_1 = c_2 = 0$), $\alpha\beta$ fluxes [17] ($\alpha^2 + c_1 c_2 = 1/4$), etc. In addition, the flux considered for the one-dimensional convection-diffusion equation in the original ultra-weak DG work by Cheng and Shu [18] is a particular case of the generalized fluxes, where $\alpha = 1/2$, c_1 is negative with sufficient large absolute value and $c_2 = 0$. Moreover, the bilinear form of the IPDG method [27] can also be rewritten in form (2.15) and included in this flux family by letting $\alpha = 0$, $c_1 \leq 0$ and $c_2 = 0$. For the convenience of notations, we denote Θ to be a universal set of the parameter triple (α, c_1, c_2). The suitable parameter set Θ will be discussed in the following sections, for the purpose to provide sufficient stability and/or accuracy of the approximation.

3 Projections

One critical tool in the analysis of DG methods is the projection which is carefully chosen for the purpose of providing optimal a priori error estimate. In this section, we design a couple of projections for the ultra-weak scheme with generalized numerical fluxes. The well-posedness and optimal approximation capability of these projections will also be studied.

3.1 Ultra-Weak Projection

We first introduce a projection rising directly from the formulation of the ultra-weak scheme. In this section, we take polynomial spaces V_h^k on $\mathcal{T}_h$ as a representative example to illustrate the idea. See Remark 3.5 for the extension to S_h^k on $\mathcal{K}_h$, and a similar strategy can be applied for other meshes and spaces.

We consider the following projection $\Pi_h^{\mathtt{UW}} : H^s(\Omega) \mapsto V_h^{k,u}$, $s > 3/2$, induced by $a_h(\cdot, \cdot)$:

$$a_h(\Pi_h^{\mathtt{UW}} u - u, v_h) = 0, \text{ for any } v_h \in V_h^{k,0}. \tag{3.1}$$

As we could see later, this projection is designed to eliminate the errors of numerical solutions on the faces. The parameters α, c_1, c_2 could be chosen to ensure suitable approximation capability, and we restrict the parameter set Θ to the sub-class $\Theta_{UW} = \Theta_1^{UW} \cup \Theta_2^{UW}$:

$$\Theta_1^{UW} = \{(\alpha, c_1, c_2) : c_1 < 0, c_2 > 0, c_1 < -\frac{\alpha^2}{c_2} - \frac{\sigma(k+1)(k+d)}{d}\},$$

$$\Theta_2^{UW} = \cup_{\epsilon > 0, \gamma \in (0,1)} \Theta_{\epsilon, \gamma}^{UW}, \tag{3.2}$$

$$\Theta_{\epsilon, \gamma}^{UW} = \{(\alpha, c_1, c_2) : c_1 < 0, c_2 \leq 0, \epsilon|\alpha| - c_2 < \frac{\gamma d}{2\sigma(k+1)(k+d)}, -c_1 - \frac{|\alpha|}{\epsilon} > \frac{\sigma(k+1)(k+d)}{d(1-\gamma)}\},$$

which will be explained in the following analysis.

Remark 3.1. *We restrict the test functions to $V_h^{k,0}$ in the definition* (3.1). *Indeed, for any projection $\Pi_h^{\mathtt{UW}} u$ satisfying the definition, the orthogonality holds for a wider class of test functions v_h:*

$$a_h(\Pi_h^{\mathtt{UW}} u - u, v_h) = 0, \ for \ any \ v_h \in V_h^k. \tag{3.3}$$

This is easy to see with, for example, (3.6), *since $a_h(w, v)$ only involves jumps and derivatives of v, which is invariant with respect to constant-shifts.*

Remark 3.2. *The admissible parameter set Θ_{UW} looks complicated. However, the set is computable for any dimension d and polynomial k. The only quantity relatively difficult to be computed is σ, defined in* (2.2). *For some typical structured meshes, we could compute σ easily. For example, in two dimensions, $\sigma = 4$ for structured mesh consisted of isosceles right triangles, and $\sigma = 1$ for Cartesian mesh consisted of squares. For unstructured triangular mesh, σ can also be computed numerically. Actually, this constant is bounded by the reciprocal of $\sin^2\theta$, where θ is the smallest angle of triangular elements. Therefore, this condition also suggests using meshes that are not too 'bad'* [44].

Remark 3.3. *We remark that the range of parameters Θ_{UW} is a generalization of such range of IPDG methods. As we can see in the following Lemmas and numerical experiments, the involvement of the extra penalization term $\langle [\![\partial_{\mathbf{n}} u]\!], [\![\partial_{\mathbf{n}} v]\!]\rangle_e$ enlarges and generalizes the admissible parameters range of IPDG methods.*

Remark 3.4. *To illustrate the range of Θ_{UW}, we draw graphs of cross sections of the set $\mathbb{R}^3$ and compare with the classical numerical fluxes when $k = d = \sigma = 1$ (see Figure 3.1). In the left one of Figure 3.1, we plot the Θ_1^{UW} when $\alpha = 1/2$ with blue and the area will extend to the left-upper corner of the c_1-c_2 plane. Within our knowledge, there are no other existing numerical fluxes belonging to this area. In the middle one, we plot the Θ_2^{UW} at $\alpha = 1/2$ and use a red dot line to represent the parameters of the original ultra-weak DG method* [18]. *In the right sub-figure, we plot Θ_2^{UW} at $\alpha = 0$ and mark the (Symmetric) IPDG flux with a red dot line.*
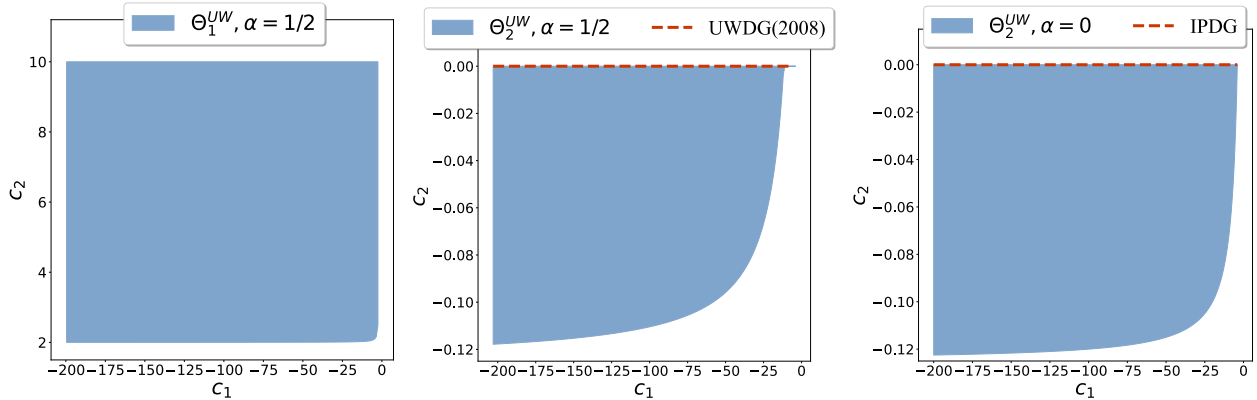
Figure 3.1: Illustrations of Θ_1^{UW} on c_1-c_2 plane with $\alpha = 1/2$ (Left), Θ_2^{UW} on c_1-c_2 plane with $\alpha = 1/2$ (Middle) and Θ_2^{UW} on c_1-c_2 plane with $\alpha = 0$ (Right) as $k = d = \sigma = 1$.

In addition, we introduce the mesh dependent energy norm $\|\cdot\|_E$ and the augmented norm $\|\!|\cdot|\!\|$

on $V_h^{k,0}$:

$$\|v\|_E^2 = \sum_{T \in \mathcal{T}_h} \|\nabla v\|_T^2 + \sum_{e \in \mathcal{E}_h} \frac{1}{h_e} \|[\![v]\!]\|_e^2,$$

$$\||v|\|^2 = \|v\|_E^2 + \sum_{e \in \mathcal{E}_h} \left[h_e \|\{\!\{\partial_\mathbf{n} v\}\!\}\|_e^2 + h_e \|[\![\partial_\mathbf{n} v]\!]\|_e^2 \right]. \tag{3.4}$$

It can be seen these two norms are equivalent on $V_h^{k,0}$. Next, we present some properties of $a_h(\cdot, \cdot)$ in order to study the projection $\Pi_h^{\mathtt{UW}}$.

Lemma 3.1 (Continuity). *For $w, v \in H^s(\mathcal{T}_h)$, $s > 3/2$, $a(\cdot, \cdot)$ is continuous, i.e., there exists a constant $C^\star$ independent of h, such that:*

$$|a_h(w, v)| \leq C^\star \||w|\| \||v|\|. \tag{3.5}$$

Proof. Using integration by parts and the identity $[\![fg]\!] = [\![f]\!] \{\!\{g\}\!\} + [\![g]\!] \{\!\{f\}\!\}$, we can write $a_h(w, v)$ as:

$$a_h(w, v) = \sum_{T \in \mathcal{T}_h} (\nabla w, \nabla v)_T - \sum_{e \in \mathcal{E}_h} \left[\langle [\![w]\!], \{\!\{\partial_\mathbf{n} v\}\!\} \rangle_e + \langle \{\!\{\partial_\mathbf{n} w\}\!\}, [\![v]\!] \rangle_e \right] \tag{3.6}$$
$$- \sum_{e \in \mathcal{E}_h} \left[\alpha \langle [\![w]\!], [\![\partial_\mathbf{n} v]\!] \rangle_e + \alpha \langle [\![\partial_\mathbf{n} w]\!], [\![v]\!] \rangle_e - c_2 h_e \langle [\![\partial_\mathbf{n} w]\!], [\![\partial_\mathbf{n} v]\!] \rangle_e + \frac{c_1}{h_e} \langle [\![w]\!], [\![v]\!] \rangle_e \right].$$

Applying Cauchy-Schwarz inequality yields

$$\sum_{T \in \mathcal{T}_h} |(\nabla w, \nabla v)_T| \leq \sum_{T \in \mathcal{T}_h} \|\nabla w\|_T \|\nabla v\|_T \leq C \||w|\| \||v|\|. \tag{3.7}$$

The second term can be bounded as:

$$\sum_{e \in \mathcal{E}_h} |\langle [\![w]\!], \{\!\{\partial_\mathbf{n} v\}\!\} \rangle_e| \leq \sum_{e \in \mathcal{E}_h} \frac{1}{\sqrt{h_e}} \|[\![w]\!]\|_e \sqrt{h_e} \|\{\!\{\partial_\mathbf{n} v\}\!\}\|_e \leq C \||w|\| \||v|\|, \tag{3.8}$$

and all the other terms can be bounded similarly. $\qquad \square$

Lemma 3.2 (Coercivity). *Let $w \in V_h^k$, and assume $(\alpha, c_1, c_2) \in \Theta_{UW}$, then $a(\cdot, \cdot)$ is strongly coercive, i.e., there exists a constant $C_\star$ independent of h, such that:*

$$a_h(w, w) \geq C_\star \||w|\|^2. \tag{3.9}$$

Proof. As a result of the norm equivalence of $\|\cdot\|_E$ and $\||\cdot|\|$, we need only to prove the coercivity result for $\|\cdot\|_E$. Also by the structure of a_h and $\||\cdot|\|$, we only need to prove for $w \in V_h^{k,0}$. Assume $\|v\|_E \geq \underline{C} \||v|\|$ on $v \in V_h^{k,0}$. From (3.6), we have

$$a_h(w, w) = \sum_{T \in \mathcal{T}_h} (\nabla w, \nabla w)_T - \sum_{e \in \mathcal{E}_h} \left[2\langle [\![w]\!], \{\!\{\partial_\mathbf{n} w\}\!\} \rangle_e + 2\alpha \langle [\![w]\!], [\![\partial_\mathbf{n} w]\!] \rangle_e \right. \tag{3.10}$$
$$\left. + \frac{c_1}{h_e} \|[\![w]\!]\|_e^2 - c_2 h_e \|[\![\partial_\mathbf{n} w]\!]\|_e^2 \right].$$

Next we consider two different cases, each corresponding to the set Θ_1^{UW} or Θ_2^{UW}, respectively.

Case 1. $c_1 < 0$, $c_2 > 0$, *provided* $c_1 < -\alpha^2/c_2 - \sigma(k+1)(k+d)/d$.

For any $e \in \mathcal{E}_h$, we have

$$|2\langle \llbracket w \rrbracket, \{\!\!\{\partial_{\mathbf{n}} w\}\!\!\}\rangle_e| \leq \frac{\sigma(k+1)(k+d)}{dh_e(1-\gamma)} \|\llbracket w \rrbracket\|_e^2 + \frac{(1-\gamma)dh_e}{\sigma(k+1)(k+d)} \|\{\!\!\{\partial_{\mathbf{n}} w\}\!\!\}\|_e^2,$$

where $\gamma \in (0,1)$ is a constant to be chosen. Applying the trace inequality (2.10) yields

$$\frac{(1-\gamma)dh_e}{\sigma(k+1)(k+d)} \|\{\!\!\{\partial_{\mathbf{n}} w\}\!\!\}\|_e^2 \leq \frac{1-\gamma}{2} \left(\|\partial_{\mathbf{n}} w\|_{T_e^1}^2 + \|\partial_{\mathbf{n}} w\|_{T_e^2}^2 \right) \leq \frac{1-\gamma}{2} \left(\|\nabla w\|_{T_e^1}^2 + \|\nabla w\|_{T_e^2}^2 \right),$$

where T_e^1 and T_e^2 are the two elements adjacent to the face e. Then we combine the above two inequalities and sum them w.r.t. $e \in \mathcal{E}_h$ to obtain the estimate

$$-\sum_{e \in \mathcal{E}_h} 2\langle \llbracket w \rrbracket, \{\!\!\{\partial_{\mathbf{n}} w\}\!\!\}\rangle_e \geq -\sum_{T \in \mathcal{T}_h} (1-\gamma) \|\nabla w\|_T^2 - \sum_{e \in \mathcal{E}_h} \frac{\sigma(k+1)(k+d)}{dh_e(1-\gamma)} \|\llbracket w \rrbracket\|_e^2. \tag{3.11}$$

We can follow similar lines and have the following estimate:

$$-2\alpha\langle \llbracket \partial_{\mathbf{n}} w \rrbracket, \llbracket w \rrbracket\rangle_e \geq -\left(c_2 h_e \|\llbracket \partial_{\mathbf{n}} w \rrbracket\|_e^2 + \frac{\alpha^2 \|\llbracket w \rrbracket\|_e^2}{c_2 h_e} \right). \tag{3.12}$$

Combining the inequalities (3.11)-(3.12) with (3.10) yields

$$a_h(w,w) \geq \gamma \sum_{T \in \mathcal{T}_h} \|\nabla w\|_T^2 + \left(-c_1 - \frac{\alpha^2}{c_2} - \frac{\sigma(k+1)(k+d)}{d(1-\gamma)} \right) \sum_{e \in \mathcal{E}_h} \frac{\|\llbracket w \rrbracket\|_e^2}{h_e}. \tag{3.13}$$

Taking $C_\gamma = \min\{\gamma, -c_1 - \frac{\alpha^2}{c_2} - \frac{\sigma(k+1)(k+d)}{d(1-\gamma)}\}$ and $C_\star = \underline{C}^2 \max_{\gamma \in (0,1)} C_\gamma$. We have $C_\star > 0$ provided the assumption $c_1 < -\alpha^2/c_2 - \sigma(k+1)(k+d)/d$, and this leads to the coercivity (3.9).

Case 2. $c_1 < 0$, $c_2 \leq 0$, provided $\epsilon|\alpha| - c_2 < \gamma d/2\sigma(k+1)(k+d)$ and $-c_1 - |\alpha|/\epsilon > \sigma(k+1)(k+d)/d(1-\gamma)$, for some $\epsilon > 0$ and $\gamma \in (0,1)$.

For any fixed $\epsilon > 0$, we have the following estimate

$$-2\alpha\langle \llbracket \partial_{\mathbf{n}} w \rrbracket, \llbracket w \rrbracket\rangle_e \geq -|\alpha| \left(\epsilon h_e \|\llbracket \partial_{\mathbf{n}} w \rrbracket\|_e^2 + \frac{\|\llbracket w \rrbracket\|_e^2}{\epsilon h_e} \right), \tag{3.14}$$

and apply the trace inequality to obtain

$$-(\epsilon|\alpha| - c_2)h_e \|\llbracket \partial_{\mathbf{n}} w \rrbracket\|_e^2 \geq -2(\epsilon|\alpha| - c_2)\frac{\sigma(k+1)(k+d)}{d} \cdot \frac{1}{2} \left(\|\partial_{\mathbf{n}} w\|_{T_e^1}^2 + \|\partial_{\mathbf{n}} w\|_{T_e^2}^2 \right). \tag{3.15}$$

Combining the inequalities (3.11), (3.14), (3.15) with (3.10) leads to

$$\begin{aligned} a_h(w,w) \geq & \left(\gamma - 2(\epsilon|\alpha| - c_2)\frac{\sigma(k+1)(k+d)}{d} \right) \sum_{T \in \mathcal{T}_h} \|\nabla w\|_T^2 \\ & + \left(-c_1 - \frac{|\alpha|}{\epsilon} - \frac{\sigma(k+1)(k+d)}{d(1-\gamma)} \right) \sum_{e \in \mathcal{E}_h} \frac{\|\llbracket w \rrbracket\|_e^2}{h_e}. \end{aligned} \tag{3.16}$$

Provided $\epsilon|\alpha| - c_2 < \gamma d/2\sigma(k+1)(k+d)$ and $-c_1 - |\alpha|/\epsilon > \sigma(k+1)(k+d)/d(1-\gamma)$, we can take $C_\star$ to be minimum of two coefficients in (3.16) multiplied by $\underline{C}^2$ to derive the coercivity (3.9). $\qquad \square$

Now we are ready to analyze the approximation capability of the projection Π_h^{UW} in (3.1).

Theorem 3.1. *Let $(\alpha, c_1, c_2) \in \Theta_{UW}$ and $u \in H^s(\mathcal{T}_h)$, $s > 3/2$, then the projection* 3.3 *is well-defined. Moreover, if $u \in H^{k+1}(\mathcal{T}_h)$, then the following approximation results hold:*

$$
\begin{aligned}
\left\| \left\| u - \Pi_h^{\text{UW}} u \right\| \right\| &\leq Ch^k |u|_{H^{k+1}(\Omega)}, \\
|u - \Pi_h^{\text{UW}} u|_{H^1(\mathcal{T}_h)} &\leq Ch^k |u|_{H^{k+1}(\Omega)}, \\
\left\| u - \Pi_h^{\text{UW}} u \right\|_{L^2(\mathcal{T}_h)} &\leq Ch^{k+1} |u|_{H^{k+1}(\Omega)}, \\
\left\| u - \Pi_h^{\text{UW}} u \right\|_{L^2(\mathcal{E}_h)} &\leq Ch^{k+1/2} |u|_{H^{k+1}(\Omega)}.
\end{aligned}
\tag{3.17}
$$

Proof. The existence and uniqueness both follow from the Lax-Milgram Theorem. We start with proving the approximation capability for the augmented norm $\|\|\cdot\|\|$. We have the following approximation results from Bramble-Hilbert Lemma and the standard scaling argument:

$$
|u - P_h^k u|_{H^s(\mathcal{T}_h)} \leq Ch^{k+1-s} |u|_{H^{k+1}(\mathcal{T}_h)},
\tag{3.18}
$$

where P_h^k is the L^2 projection defined as $P_h^k : L^2(\Omega) \mapsto V_h^k$, such that for $\forall T \in \mathcal{T}_h$, it holds that

$$
(P_h^k u, v)_T = (u, v)_T, \qquad \forall v \in \mathcal{P}^k(T).
\tag{3.19}
$$

Note that $\Pi_h^{\text{UW}} u - P_h^k u \in V_h^{k,0}$, we use the continuity and coercivity properties of a_h to have:

$$
\begin{aligned}
C_\star \left\| \left\| \Pi_h^{\text{UW}} u - P_h^k u \right\| \right\|^2 &\leq a_h(\Pi_h^{\text{UW}} u - P_h^k u, \Pi_h^{\text{UW}} u - P_h^k u) = a_h(\Pi_h^{\text{UW}} u - P_h^k u, u - P_h^k u) \\
&\leq C^\star \left\| \left\| \Pi_h^{\text{UW}} u - P_h^k u \right\| \right\| \left\| \left\| u - P_h^k u \right\| \right\|,
\end{aligned}
\tag{3.20}
$$

where the first inequality arises from Lemma 3.2, and the equality follows from the orthogonality property of the projection (3.3). This produces the following property:

$$
\left\| \left\| \Pi_h^{\text{UW}} u - P_h^k u \right\| \right\| \leq \frac{C^\star}{C_\star} \left\| \left\| u - P_h^k u \right\| \right\|.
\tag{3.21}
$$

We can estimate $\left\| \left\| u - P_h^k u \right\| \right\|$ by using the trace inequality (2.7) and the approximation (3.18):

$$
\begin{aligned}
\left\| \left\| u - P_h^k u \right\| \right\|^2 &\leq C \left(h^{-2} \left\| u - P_h^k u \right\|_{L^2(\mathcal{T}_h)}^2 + \left| u - P_h^k u \right|_{H^1(\mathcal{T}_h)}^2 + h^2 \left| u - P_h^k u \right|_{H^2(\mathcal{T}_h)}^2 \right) \\
&\leq Ch^{2k} |u|_{H^{k+1}(\mathcal{T}_h)}^2.
\end{aligned}
\tag{3.22}
$$

Applying triangular inequality and combining (3.21)-(3.22) yield

$$
\left\| \left\| u - \Pi_h^{\text{UW}} u \right\| \right\| \leq \left\| \left\| \Pi_h^{\text{UW}} u - P_h^k u \right\| \right\| + \left\| \left\| u - P_h^k u \right\| \right\| \leq Ch^k |u|_{H^{k+1}(\mathcal{T}_h)}.
\tag{3.23}
$$

Next, we estimate the L^2 norm by a traditional duality argument. Denote the projection error by $\eta_h^\star = \Pi_h^{\text{UW}} u - u \in L^2(\Omega)$. Let $\omega \in H^2(\Omega)$ be the solution of the following auxiliary problem:

$$
\begin{aligned}
-\Delta \omega &= \eta_h^\star, & \text{on } \Omega, & \tag{3.24a} \\
\omega &= 0, & \text{on } \partial\Omega. & \tag{3.24b}
\end{aligned}
$$

The elliptic regularity ensures that there exists C only depending on Ω, such that:

$$
|\omega|_{H^2(\Omega)} \leq C \left\| \eta_h^\star \right\|_{L^2(\Omega)}.
\tag{3.25}
$$

Since $\omega \in H^2(\Omega)$, we have the following relation:

$$\|\eta_h^\star\|_\Omega^2 = (\eta_h^\star, \eta_h^\star)_\Omega = (-\Delta\omega, \eta_h^\star)_\Omega = a_h(\omega, \eta_h^\star), \qquad (3.26)$$

where the last equality could be seen by repeating the steps to derive ultra-weak schemes

$$
\begin{aligned}
(-\Delta\omega, \eta_h^\star)_\Omega &= \sum_{T \in \mathcal{T}_h} -(\omega, \Delta\eta_h^\star)_T + \langle\omega, \partial_{\mathbf{n}}\eta_h^\star\rangle_{\partial T} - \langle\partial_{\mathbf{n}}\omega, \eta_h^\star\rangle_{\partial T} \\
&= -\sum_{T \in \mathcal{T}_h} (\omega, \Delta\eta_h^\star)_T + \sum_{e \in \mathcal{E}_h} \langle\omega, [\![\partial_{\mathbf{n}}\eta_h^\star]\!]\rangle_e - \langle\partial_{\mathbf{n}}\omega, [\![\eta_h^\star]\!]\rangle_e \\
&= -\sum_{T \in \mathcal{T}_h} (\omega, \Delta\eta_h^\star)_T + \sum_{e \in \mathcal{E}_h} \langle\widehat{\omega}, [\![\partial_{\mathbf{n}}\eta_h^\star]\!]\rangle_e - \langle\widetilde{\partial_{\mathbf{n}}\omega}, [\![\eta_h^\star]\!]\rangle_e,
\end{aligned}
\qquad (3.27)
$$

and the consistency of numerical fluxes as mentioned in Section 2 was used in the last step. The orthogonality condition (3.3) and symmetric property of $a_h(\cdot, \cdot)$ lead to $a_h(P_h^1\omega, \eta_h^\star) = 0$, where $P_h^1\omega$, the piecewise L^2 projection of ω, belongs to V_h^1. Combining (3.26), (3.22), and the approximation capability of P_h^1 under $\|\!|\cdot|\!\|$ yields

$$\|\eta_h^\star\|_\Omega^2 = a_h(\omega - P_h^1\omega, \eta_h^\star) \le C^*\|\!|\omega - P_h^1\omega|\!\| \, \|\!|\eta_h^\star|\!\| \le Ch|\omega|_{H^2(\Omega)}\|\!|\eta_h^\star|\!\| \le Ch \, \|\eta_h^\star\|_\Omega \, \|\!|\eta_h^\star|\!\|, \quad (3.28)$$

which, combined with (3.23), leads to the estimate in the L^2 norm

$$\|\eta_h^\star\|_\Omega \le Ch\|\!|\eta_h^\star|\!\| \le Ch^{k+1}|u|_{H^{k+1}(\Omega)}. \qquad (3.29)$$

Then, we use inverse inequality to get:

$$|P_h^k u - \Pi_h^{\mathtt{UW}} u|_{H^1(\mathcal{T}_h)} \le Ch^{-1}\left\|P_h^k u - \Pi_h^{\mathtt{UW}} u\right\|_{L^2(\mathcal{T}_h)} \le Ch^{-1}\left(\left\|u - \Pi_h^{\mathtt{UW}} u\right\|_{L^2(\mathcal{T}_h)} + \left\|u - P_h^k u\right\|_{L^2(\mathcal{T}_h)}\right),$$

and the estimate for the H^1 norm can be easily obtained by applying triangular inequality:

$$|u - \Pi_h^{\mathtt{UW}} u|_{H^1(\mathcal{T}_h)} \le |u - P_h^k u|_{H^1(\mathcal{T}_h)} + |P_h^k u - \Pi_h^{\mathtt{UW}} u|_{H^1(\mathcal{T}_h)} \le Ch^k|u|_{H^{k+1}(\Omega)}. \qquad (3.30)$$

The estimate for error on faces can be obtained in a similar way by using trace inequality. This completes the proof. $\qquad\square$

Remark 3.5. *It can be seen that a similar projection can be established for S_h^k on a Cartesian mesh $\mathcal{K}_h$. The set Θ_{UW} can be obtained through a simple modification of that of simplex mesh cases. Recall the trace inequalities established in Lemma 2.1, and it's easy to see for the Cartesian mesh case, the only modification in the definition of Θ_{UW} is to take $d = 1$ in (3.2). We note that the σ value is also the same as the one-dimensional case. This also shows that this set Θ_{UW} is independent of dimension d on Cartesian meshes if tensor product spaces are used. In [34], a similar conclusion holds for parameters of DDG method on Cartesian meshes.*

3.2 Gauss-Radau Type Projection

In the previous section, we demonstrate that the ultra-weak projection enjoys nice properties on arbitrary meshes when the parameters belong to the set Θ_{UW}. On Cartesian meshes, we could extend and improve the range of parameters by taking advantage of the structure of tensor polynomial spaces.

We first recall the one-dimensional Gauss-Radau type projection $\Pi_h^{\mathrm{GR}} : H^s(\Omega) \mapsto V_h^{k,u}$, $s > 3/2$ for ultra-weak schemes studied in [15]:

$$\left(\Pi_h^{\mathrm{GR}}u, v\right)_{I_j} = (u, v)_{I_j}, \qquad \forall v \in \mathcal{P}^{k-2}(I_j), \ \forall j = 1, 2, ..., N, \tag{3.31a}$$

$$\mathcal{F}_1(\Pi_h^{\mathrm{GR}}u) = \mathcal{F}_1(u), \qquad \text{at } x_{j+\frac{1}{2}}, \ \forall j = 1, 2, ..., N, \tag{3.31b}$$

$$\mathcal{F}_2(\Pi_h^{\mathrm{GR}}u) = \mathcal{F}_2(u), \qquad \text{at } x_{j+\frac{1}{2}}, \ \forall j = 1, 2, ..., N. \tag{3.31c}$$

with $\mathcal{F}_1$ and $\mathcal{F}_2$ given by

$$\mathcal{F}_1(u_h) = \{\!\{(u_h)_x\}\!\} + \alpha \,[\![(u_h)_x]\!] + \frac{c_1}{h_j}\,[\![u_h]\!], \tag{3.32a}$$

$$\mathcal{F}_2(u_h) = \{\!\{u_h\}\!\} - \alpha\,[\![u_h]\!] + c_2 h_j\,[\![(u_h)_x]\!]. \tag{3.32b}$$

In [15], two important quantities were introduced and used in the analysis

$$\Gamma_j = \frac{\widetilde{\Gamma}}{h_j}, \quad \Lambda_j = \frac{\widetilde{\Lambda}}{h_j}, \quad j = 1, 2, ..., N, \tag{3.33}$$

where the constants $\widetilde{\Gamma}$ and $\widetilde{\Lambda}$ are defined by

$$\begin{aligned}
\widetilde{\Gamma} &:= -c_1 - k^2\left(k^2 - 1\right)c_2 - 2k^2\left(\alpha^2 + c_1 c_2 + \frac{1}{4}\right), \\
\widetilde{\Lambda} &:= -2k\left(\alpha^2 + c_1 c_2 - \frac{1}{4}\right).
\end{aligned} \tag{3.34}$$

Note that these quantities are slightly different from those in [15], due to the fact that our definition of $[\![\cdot]\!]$ is opposite. For this case, we could define the parameter set Θ_{GR}

$$\Theta_{GR} = \left\{\alpha^2 + c_1 c_2 = \frac{1}{4}, \widetilde{\Gamma} \neq 0\right\} \cup \left\{\alpha^2 + c_1 c_2 \neq \frac{1}{4}, \left|\widetilde{\Gamma}\right| > \left|\widetilde{\Lambda}\right|\right\}. \tag{3.35}$$

Many well-known numerical fluxes belong to this set. Examples include the aforementioned upwind flux, alternating flux, $\alpha\beta$ flux, central flux (when $k \geq 2$), and the generalized alternating flux (see [16]) etc.

Remark 3.6. *We illustrate the range of Θ_{GR} using graphs of cross sections of the set within $\mathbb{R}^3$ as well. In the first plot of Figure 3.2, we plot the set Θ^{GR} when $\alpha = 1/2$ and $d = 1$ with the color blue. In this case, we mark the $\alpha\beta$ flux [17] using the red dot line and the alternating flux at the origin as a particular case. In the middle figure, we change the polynomial order to $k = 2$ in which a significant difference is observed and most of the lower half domain with $c_2 < 0$ is now included. This is due to the effect of the term $k^2(k^2 - 1)c_2$ in Γ_j which was zero when $k = 1$. In the right figure, we plot the α-c_1 plane cross section when $c_2 = 0$, $k = 2$. The central flux, generalized alternating flux [16], $\alpha\beta$ flux, and alternating flux are marked on the graph.*

For this parameter set, the approximation capability of the one-dimensional Gauss-Radau type projection (3.31) has been studied in [15]. Below, we recall the following projection error and provide a slightly modified proof in Appendix A.2. For simplicity, we assume Ω is uniformly partitioned, i.e. $h_j = h$ in the following analysis.

Lemma 3.3. *For $(\alpha, c_1, c_2) \in \Theta_{GR}$, $u \in H^s(\Omega)$, $s > 3/2$, the one-dimensional projection (3.31) is well-defined. Moreover, the following estimate holds for $u \in H^{s+1}(\Omega)$, $s \geq 0$,*

$$\left\|u - \Pi_h^{\mathrm{GR}}u\right\|_{L^2(\mathcal{T}_h)} + h^{1/2}\left\|u - \Pi_h^{\mathrm{GR}}u\right\|_{L^2(\mathcal{E}_h)} \leq Ch^{\min\{k+1, s+1\}}|u|_{H^{s+1}(\mathcal{T}_h)}. \tag{3.36}$$
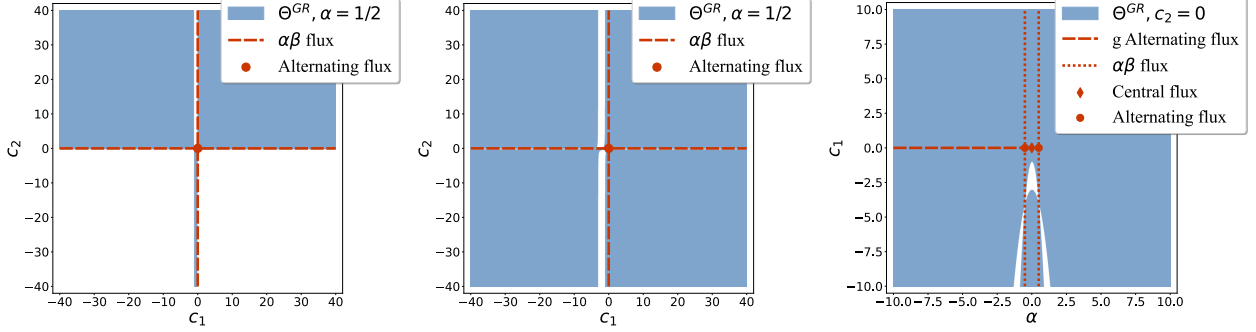
Figure 3.2: An illustration of Θ^{GR} on c_1-c_2 plane with $\alpha = 1/2$ and $k = 1$ (Left), Θ^{GR} on c_1-c_2 plane with $\alpha = 1/2$ and $k = 2$ (Middle) and Θ^{GR} on α-c_2 plane with $\alpha = 0$ and $k = 2$ (Right). In all three plots, some typical numerical fluxes are marked in red.

Next, we explore the multi-dimensional extension of the Gauss-Radau type projection (3.31) on Cartesian meshes, and could take advantage of the tensor product polynomial space S_h^k to define tensor product projections. On the d dimensional rectangular domain ($d \geq 2$), we define

$$\Pi_h^{\mathsf{GR}} u = \left(\Pi_h^1 \otimes ... \otimes \Pi_h^d \right) u, \tag{3.37}$$

where $\otimes$ denotes the tensor product and Π_h^j is the one-dimensional Gauss-Radau type projection (3.31) on the spatial variable x^j, $1 \leq j \leq d$. To study the approximation property of this projection, we restrict ourselves to two-dimensional cases to illustrate the idea, although the same analysis can be extended to higher dimension ($d \geq 3$) through induction.

For the convenience of displaying our idea, we denote $\Pi_h^{\mathsf{GR}} = \Pi_h^x \otimes \Pi_h^y$, and the domain as $\Omega = I \times J$. I (in x-direction) is split into intervals $I_i = [x_{i-1/2}, x_{i+1/2}]$, $i = 1, 2, ..., N_x$ and J (in y-direction) is split into intervals $J_j = [y_{j-1/2}, y_{j+1/2}]$, $i = 1, 2, ..., N_y$. We can observe that the projection Π_h^{GR} satisfies the following conditions

$$\left(\Pi_h^{\mathsf{GR}} u, v \right)_T = (u, v)_T, \qquad \forall v \in \mathcal{Q}^{k-2}(T), \ \forall T \in \mathcal{K}_h, \tag{3.38a}$$

$$\langle \mathcal{F}_1(\Pi_h^{\mathsf{GR}} u), w \rangle_e = \langle \mathcal{F}_1(u), w \rangle_e, \qquad \forall w \in \mathcal{P}^{k-2}(e), \ \forall e \in \mathcal{E}_h, \tag{3.38b}$$

$$\langle \mathcal{F}_2(\Pi_h^{\mathsf{GR}} u), \mu \rangle_e = \langle \mathcal{F}_2(u), \mu \rangle_e, \qquad \forall \mu \in \mathcal{P}^{k-2}(e), \ \forall e \in \mathcal{E}_h. \tag{3.38c}$$

We then prove the following approximation capability for this projection.

Theorem 3.2. *Let $d = 2$ and $u \in H^s(\mathcal{K}_h)$, $s > 3/2$, $(\alpha, c_1, c_2) \in \Theta_{GR}$, then the projection (3.37) is well-defined. Moreover, if $u \in H^{k+1}(\mathcal{K}_h)$, the following estimate holds*

$$\left\| u - \Pi_h^{\mathsf{GR}} u \right\|_{L^2(\mathcal{K}_h)} + h^{1/2} \left\| u - \Pi_h^{\mathsf{GR}} u \right\|_{L^2(\mathcal{E}_h)} \leq Ch^{k+1} |u|_{H^{k+1}(\mathcal{K}_h)}. \tag{3.39}$$

Proof. We can write $\Pi_h^x \otimes \Pi_h^y$ as $\Pi_h^x \circ \Pi_h^y$. Note that $\Pi_h^y u$ is a piecewise polynomial function in y direction, and a H^{k+1} smooth function in x direction. As a result, $\Pi_h^x \circ \Pi_h^y u$ can be uniquely defined. Then we have

$$\left\| u - \Pi_h^{\mathsf{GR}} u \right\|_{L^2(\mathcal{K}_h)} = \left\| u - \Pi_h^x u + \Pi_h^x (u - \Pi_h^y u) \right\|_{L^2(\mathcal{K}_h)} \tag{3.40}$$

$$= \left\| u - \Pi_h^x u + u - \Pi_h^y u + \Pi_h^x (u - \Pi_h^y u) - (u - \Pi_h^y u) \right\|_{L^2(\mathcal{K}_h)}$$

$$\leq \left\| u - \Pi_h^x u \right\|_{L^2(\mathcal{K}_h)} + \left\| u - \Pi_h^y u \right\|_{L^2(\mathcal{K}_h)} + \left\| \Pi_h^x (u - \Pi_h^y u) - (u - \Pi_h^y u) \right\|_{L^2(\mathcal{K}_h)}.$$

15

The first term on the right-hand side can be estimated by utilizing the one-dimensional projection error in Lemma 3.3

$$
\begin{aligned}
\|u - \Pi_h^x u\|_{L^2(\mathcal{K}_h)}^2 &= \sum_{j=1}^{N_y} \sum_{i=1}^{N_x} \int_{y_{j-\frac{1}{2}}}^{y_{j+\frac{1}{2}}} \int_{x_{i-\frac{1}{2}}}^{x_{i+\frac{1}{2}}} (u - \Pi_h^x u)^2 \; dxdy \\
&\leq Ch^{2(k+1)} \sum_{j=1}^{N_y} \int_{y_{j-\frac{1}{2}}}^{y_{j+\frac{1}{2}}} \left(\sum_{i=1}^{N_x} \int_{x_{i-\frac{1}{2}}}^{x_{i+\frac{1}{2}}} (\partial_x^{k+1} u)^2 \; dx \right) dy \\
&\leq Ch^{2(k+1)} |u|_{H^{k+1}(\mathcal{K}_h)}^2.
\end{aligned}
\tag{3.41}
$$

Similarly, we have

$$
\left\| u - \Pi_h^y u \right\|_{L^2(\mathcal{K}_h)}^2 \leq Ch^{2(k+1)} |u|_{H^{k+1}(\mathcal{K}_h)}^2.
\tag{3.42}
$$

To bound the last term, we first consider the following estimate for a function $w(x) \in H^1(I)$:

$$
\|w - \Pi_h^x w\|_{L^2(\mathcal{I}_h)} \leq Ch|w|_{H^1(\mathcal{I}_h)}.
\tag{3.43}
$$

with $\mathcal{I}_h$ being the partition of interval I. For any fixed $y \in J$, choosing $w = u - \Pi_h^y u \in H^1(I)$ yields

$$
\begin{aligned}
\left\| \Pi_h^x(u - \Pi_h^y u) - (u - \Pi_h^y u) \right\|_{L^2(\mathcal{K}_h)}^2 &= \sum_{j=1}^{N_y} \int_{y_{j-\frac{1}{2}}}^{y_{j+\frac{1}{2}}} \left\| \Pi_h^x(u - \Pi_h^y u) - (u - \Pi_h^y u) \right\|_{L^2(\mathcal{I}_h)}^2 \; dy \\
&\leq \sum_{j=1}^{N_y} \sum_{i=1}^{N_x} \int_{y_{j-\frac{1}{2}}}^{y_{j+\frac{1}{2}}} \int_{x_{i-\frac{1}{2}}}^{x_{i+\frac{1}{2}}} Ch^2 \left(\partial_x(u - \Pi_h^y u) \right)^2 \; dxdy \\
&= \sum_{j=1}^{N_y} \sum_{i=1}^{N_x} \int_{x_{i-\frac{1}{2}}}^{x_{i+\frac{1}{2}}} \int_{y_{j-\frac{1}{2}}}^{y_{j+\frac{1}{2}}} Ch^2 \left(\partial_x u - \Pi_h^y \partial_x u \right)^2 \; dydx \\
&\leq Ch^{2(k+1)} \sum_{j=1}^{N_y} \sum_{i=1}^{N_x} \int_{x_{i-\frac{1}{2}}}^{x_{i+\frac{1}{2}}} \int_{y_{j-\frac{1}{2}}}^{y_{j+\frac{1}{2}}} \left(\partial_y^k \partial_x u \right)^2 \; dydx \leq Ch^{2(k+1)} |u|_{H^{k+1}(\mathcal{K}_h)}^2,
\end{aligned}
\tag{3.44}
$$

where the one-dimensional projection error in Lemma 3.3 is again used. The error estimate in the L^2 norm follows by plugging (3.41) and (3.44) into (3.40). We can also derive the semi-H^1 norm estimate with the assistance of L^2 projection P_h^k and inverse inequality (2.10)

$$
|u - \Pi_h^{\mathrm{GR}} u|_{H^1(\mathcal{K}_h)} \leq |u - P_h^k u|_{H^1(\mathcal{K}_h)} + |P_h^k u - \Pi_h^{\mathrm{GR}} u|_{H^1(\mathcal{K}_h)} \leq Ch^k |u|_{H^{k+1}(\mathcal{K}_h)}.
\tag{3.45}
$$

Then the error estimate in the trace norms can be derived by applying trace inequality (2.7)

$$
\left\| u - \Pi_h^{\mathrm{GR}} u \right\|_{L^2(\mathcal{E}_h)} \leq h^{-1/2} \left\| u - \Pi_h^{\mathrm{GR}} u \right\|_{L^2(\mathcal{K}_h)} + h^{1/2} |u - \Pi_h^{\mathrm{GR}} u|_{H^1(\mathcal{K}_h)} \leq Ch^{k+1/2} |u|_{H^{k+1}(\mathcal{K}_h)}.
\tag{3.46}
$$

This completes the proof. $\qquad\square$

In the rest of this section, we discuss some properties of the Gauss-Radau type projection. It is well known that in the higher dimension, the tensor product of Gauss-Radau type projections may fail to satisfy the orthogonality condition. Fortunately, motivated by [16, 23], we can uncover the superconvergent properties of the projection (3.37), which compensate the orthogonality and will be proved to be sufficient for optimal error bounds. The following lemma shows the approximation capability on higher order polynomial spaces.

Lemma 3.4. *Let $(\alpha, c_1, c_2) \in \Theta_{GR}$, $k \geq 1$, $d \geq 2$, $d < 2(k+1)$. The following result*

$$a_h(u - \Pi_h^{\mathrm{GR}} u, v) = 0 \tag{3.47}$$

holds for any $u \in V_h^{k+2}$ and $v \in S_h^k$.

Proof. Let $\eta_h^\star = u - \Pi_h^{\mathrm{GR}} u$. On Cartesian meshes we can decompose $a_h(u - \Pi_h^{\mathrm{GR}} u, v)$ as

$$a_h(u - \Pi_h^{\mathrm{GR}} u, v) = \sum_{i=1}^{d} a_h^i(\eta_h^\star, v), \tag{3.48}$$

where, for each coordinate, a_h^i is defined by

$$a_h^i(\eta_h^\star, v) = -\sum_{K \in \mathcal{K}_h} \left(\eta_h^\star, \partial_{x^i}^2 v\right)_K + \sum_{e \in \mathcal{E}_{h,i}} \left[\langle \widehat{\eta_h^\star}^i, [\![\partial_{x^i} v]\!]\rangle_e - \langle \widetilde{\partial_\mathbf{n} \eta_h^\star}^i, [\![v]\!]\rangle_e\right]. \tag{3.49}$$

Here, we write $\mathcal{E}_h$ into $\mathcal{E}_h = \cup_{i=1}^{d} \mathcal{E}_{h,i}$, where $\mathcal{E}_{h,i}$ contains faces of $K \in \mathcal{K}_h$ which have fixed value on the x^i dimension. It is clear that operators $[\![\cdot]\!]$ and $\{\!\!\{\cdot\}\!\!\}$ are well-defined on each $\mathcal{E}_h^i$. The $\widehat{u}^i$ and $\widetilde{\partial_\mathbf{n} u}^i$ in the above definition are $\widehat{u}$ and $\widetilde{\partial_\mathbf{n} u}$ restricted on $\mathcal{E}_{h,i}$ which can be defined as:

$$\widetilde{\partial_\mathbf{n} u}^i = \{\!\!\{\partial_{x^i} u\}\!\!\} + \alpha_1 [\![\partial_{x^i} u]\!] + \frac{c_1}{h} [\![u]\!], \quad \widehat{u}^i = \{\!\!\{u\}\!\!\} + \alpha_2 [\![u]\!] + c_2 h [\![\partial_{x^i} u]\!]. \tag{3.50}$$

For ease of presentation, we consider the two-dimensional case and denote x^1, x^2 by x, y, respectively. The result (3.47) automatically holds for $u \in S_h^k$, since the projection Π_h^{GR} preserves k-th order tensor product polynomials. To prove the result for any $u \in V_h^{k+2}$, it is sufficient to show it for the extra terms x^{k+1}, y^{k+1}, xy^{k+1}, $x^{k+1}y$, x^{k+2} and y^{k+2} with the bilinear form a_h^1 only. We start by validating the case $u = x^{k+1}$, which leads to $\eta_h^\star = x^{k+1} - \Pi_h^{\mathrm{GR}} x^{k+1} = x^{k+1} - \Pi_h^x x^{k+1}$. Since $\partial_x^2 v$ is a polynomial in x with order up to $k-2$, applying the definition of the projection Π_h^x leads to

$$\sum_{K \in \mathcal{K}_h} \left(\eta_h^\star, \partial_x^2 v\right)_K = \sum_{K \in \mathcal{K}_h} \left(x^{k+1} - \Pi_h^x x^{k+1}, \partial_x^2 v\right)_K = 0. \tag{3.51}$$

We also have $\widehat{\eta_h^\star}^1 = 0$ and $\widetilde{\partial_\mathbf{n} \eta_h^\star}^1 = 0$ which again follows from the definition of Π_h^x in (3.31). This leads to the conclusion that $a_h^1(\eta_h^\star, v) = 0$ for any $v \in S_h^k$, and the same proof also applies to x^{k+2} and yx^{k+1}. For $u = y^{k+1}$ and y^{k+2}, we use integration by parts to rewrite (3.49) as:

$$a_h^1(\eta_h^\star, v) = \sum_{k \in \mathcal{K}_h} (\partial_x \eta_h^\star, \partial_x v)_K - \sum_{e \in \mathcal{E}_{h,1}} \left[\langle [\![\eta_h^\star \partial_x v]\!], 1\rangle_e - \langle \widehat{\eta_h^\star}^1, [\![\partial_x v]\!]\rangle_e + \langle \widetilde{\partial_\mathbf{n} \eta_h^\star}^1, [\![v]\!]\rangle_e\right]. \tag{3.52}$$

Since $u = y^{k+1}$ or $u = y^{k+2}$ are independent of x, so $\partial_x \eta_h^\star = 0$ thus the first term of (3.52) is 0. In addition, on each $e \in \mathcal{E}_{h,1}$, we can deduce $\eta_h^\star$ is continuous with respect to x, because u is independent of x. By the definition of $[\![\cdot]\!]$ and consistency of numerical fluxes, we have:

$$\langle [\![\eta_h^\star \partial_x v]\!], 1\rangle_e - \langle \widehat{\eta_h^\star}^1, [\![\partial_x v]\!]\rangle_e + \langle \widetilde{\partial_\mathbf{n} \eta_h^\star}^1, [\![v]\!]\rangle_e = \langle \eta_h^\star [\![\partial_x v]\!], 1\rangle_e - \langle \eta_h^\star, [\![\partial_x v]\!]\rangle_e + \langle \partial_x \eta_h^\star, [\![v]\!]\rangle_e, \tag{3.53}$$

which reduces to 0 since the first two terms cancel and $\partial_x \eta_h^\star = 0$ in the last term. Lastly, for $u = xy^{k+1}$, we apply integration by parts again to have:

$$a_h^1(\eta_h^\star, v) = -\sum_{k \in \mathcal{K}_h} (\partial_x^2 \eta_h^\star, v)_K + \sum_{e \in \mathcal{E}_{h,1}} \left[\langle [\![\partial_x \eta_h^\star v]\!], 1\rangle_e - \langle [\![\eta_h^\star \partial_x v]\!], 1\rangle_e + \langle \widehat{\eta_h^\star}^1, [\![\partial_x v]\!]\rangle_e - \langle \widetilde{\partial_\mathbf{n} \eta_h^\star}^1, [\![v]\!]\rangle_e\right]. \tag{3.54}$$

Then since $k \geq 1$, we have $u - \Pi_h^{\mathrm{GR}}u = x(y^{k+1} - \Pi_h^y y^{k+1}) := x\eta_{h,y}^\star$, and $\partial_x^2 \eta_h^\star = 0$. For the rest of terms, we have for each $e \in \mathcal{E}_{h,1}$:

$$
\begin{aligned}
&\langle [\![\partial_x \eta_h^\star v]\!], 1 \rangle_e - \langle [\![\eta_h^\star \partial_x v]\!], 1 \rangle_e + \langle \widehat{\eta_h^\star}^1, [\![\partial_x v]\!] \rangle_e - \langle \widetilde{\partial_{\mathbf{n}} \eta_h^\star}^1, [\![v]\!] \rangle_e \\
&= \langle \eta_{h,y}^\star [\![v]\!], 1 \rangle_e - \langle x\eta_{h,y}^\star [\![\partial_x v]\!], 1 \rangle_e + \langle x\eta_{h,y}^\star, [\![\partial_x v]\!] \rangle_e - \langle \eta_{h,y}^\star, [\![v]\!] \rangle_e = 0.
\end{aligned}
\tag{3.55}
$$

This finishes the proof of this Lemma. $\qquad\square$

With the above results, we could obtain the following superconvergent result for a_h.

Lemma 3.5. *Let* $(\alpha, c_1, c_2) \in \Theta_{GR}$, $k \geq 1$, $d \geq 2$, $d < 2(k+1)$ *and assume* $u \in H^{k+3}(\mathcal{K}_h)$, *then the linear functional* $u \mapsto a_h(u - \Pi_h^{\mathrm{GR}}u, v)$ *with* $v \in S_h^k$ *is bounded on the domain of* u. *Additionally, the following estimate holds:*

$$
\left| a_h(u - \Pi_h^{\mathrm{GR}}u, v) \right| \leq Ch^{k+1} |u|_{H^{k+3}(\mathcal{K}_h)} \|v\|_{L^2(\Omega)}.
\tag{3.56}
$$

Proof. We will prove the result for each $a_h^i(\eta_h^\star, v)$ defined in (3.49), with $\eta_h^\star = u - \Pi_h^{\mathrm{GR}}u$. Each of the three right-hand terms of $a_h^i(\eta_h^\star, v)$ will be bounded respectively. Applying Cauchy-Schwarz inequality yields

$$
\left| \sum_{K \in \mathcal{K}_h} (\eta_h^\star, \partial_{x^i}^2 v)_K \right| \leq \|\eta_h^\star\|_{\mathcal{K}_h} \|\partial_{x^i}^2 v\|_{\mathcal{K}_h}.
\tag{3.57}
$$

The second term can be bounded as follows

$$
\begin{aligned}
\left| \sum_{e \in \mathcal{E}_{h,i}} \langle \widehat{\eta_h^\star}^i, [\![\partial_{x^i} v]\!] \rangle_e \right| &= \left| \sum_{e \in \mathcal{E}_{h,i}} \langle \{\!\!\{\eta_h^\star\}\!\!\} - \alpha [\![\eta_h^\star]\!] + c_2 h_e [\![\partial_{x^i} \eta_h^\star]\!], [\![\partial_{x^i} v]\!] \rangle_e \right| \\
&\leq C \sum_{e \in \mathcal{E}_{h,i}} (\|\{\!\!\{\eta_h^\star\}\!\!\}\|_e + \|[\![\eta_h^\star]\!]\|_e + h\|[\![\partial_{x^i} \eta_h^\star]\!]\|_e) \|[\![\partial_{x^i} v]\!]\|_e \\
&\leq C \sum_{e \in \mathcal{E}_{h,i}} \sum_{j=1,2} \left(h^{-1/2} \|\eta_h^\star\|_{L^2(K_e^j)} + h^{1/2} |\eta_h^\star|_{H^1(K_e^j)} \right) h^{-1/2} \|\partial_{x^i} v\|_{L^2(K_e^j)} \\
&\quad + C \sum_{e \in \mathcal{E}_{h,i}} \sum_{j=1,2} \left(h^{1/2} \|\partial_{x^i} \eta_h^\star\|_{L^2(K_e^j)} + h^{3/2} |\partial_{x^i} \eta_h^\star|_{H^1(K_e^j)} \right) h^{-1/2} \|\partial_{x^i} v\|_{L^2(K_e^j)} \\
&\leq C \left(h^{-1} \|\eta_h^\star\|_{\mathcal{K}_h} + |\eta_h^\star|_{H^1(\mathcal{K}_h)} + h|\eta_h^\star|_{H^2(\mathcal{K}_h)} \right) |v|_{H^1(\mathcal{K}_h)},
\end{aligned}
\tag{3.58}
$$

where the trace inequality (2.10) for v and (2.7) for $\eta_h^\star$ on the x^i dimension was used, and K_e^j, $j = 1, 2$ are two neighbor elements sharing the face e. Similarly, we have the estimate of the last term

$$
\begin{aligned}
\left| \sum_{e \in \mathcal{E}_{h,i}} \langle \widetilde{\partial_{\mathbf{n}} \eta^\star}^i, [\![v]\!] \rangle_e \right| &= \left| \sum_{e \in \mathcal{E}_{h,i}} \langle \{\!\!\{\partial_{x^i} \eta^\star\}\!\!\} + \alpha [\![\partial_{x^i} \eta^\star]\!] + \frac{c_1}{h_e} [\![\eta^\star]\!], [\![v]\!] \rangle_e \right| \\
&\leq C \left(h^{-2} \|\eta_h^\star\|_{\mathcal{K}_h} + h^{-1} |\eta_h^\star|_{H^1(\mathcal{K}_h)} + |\eta_h^\star|_{H^2(\mathcal{K}_h)} \right) \|v\|_{\mathcal{K}_h}.
\end{aligned}
\tag{3.59}
$$

Combining three estimates above with inverse inequality (2.10) and approximation capability of Π_h^{GR}, we have

$$
\left| a_h^i(\eta_h^\star, v) \right| \leq C \left(h^{-2} \|\eta_h^\star\|_{\mathcal{K}_h} + h^{-1} |\eta_h^\star|_{H^1(\mathcal{K}_h)} + |\eta_h^\star|_{H^2(\mathcal{K}_h)} \right) \|v\|_{\mathcal{K}_h} \leq Ch^{k-1} |u|_{H^{k+1}(\mathcal{K}_h)} \|v\|_{\mathcal{K}_h}.
\tag{3.60}
$$

18

Since this holds for all $i = 1, 2, ..., d$, we have the following estimates

$$\left| a_h(u - \Pi_h^{\text{GR}} u, v) \right| \le Ch^{k-1} |u|_{H^{k+1}(\mathcal{K}_h)} \|v\|. \tag{3.61}$$

Inspired by [16], we use Lemma 3.4 to deduce that for any $\chi \in V_h^{k+2}$:

$$\left| a_h(u - \Pi_h^{\text{GR}} u, v) \right| = \left| a_h(u - \chi - \Pi_h^{\text{GR}}(u - \chi), v) \right| \le Ch^{k-1} |u - \chi|_{H^{k+1}(\mathcal{K}_h)} \|v\|. \tag{3.62}$$

Then we have the following estimate using the standard estimation [19]:

$$\left| a_h(u - \Pi_h^{\text{GR}} u, v) \right| \le Ch^{k-1} \inf_{\chi \in V_h^{k+2}} |u - \chi|_{H^{k+1}(\mathcal{K}_h)} \|v\| \le Ch^{k+1} |u|_{H^{k+3}(\mathcal{K}_h)} \|v\|, \tag{3.63}$$

which proves our superconvergent result. $\qquad\qquad\qquad\qquad\qquad\qquad\qquad\qquad\qquad\qquad\qquad\square$

Remark 3.7. *When $d = 1$, the Cartesian mesh and simplex mesh both degenerate into interval partitions. Therefore, the orthogonality condition also holds for Θ_{GR}, and the optimal error estimate holds on both Θ_{GR} and Θ_{UW}.*

Remark 3.8. *The above two Lemmas are a generalization of [49, Lemmas 6.2, 6.3] with slight differences in regularity requirements. We remark that we could also obtain results similar to [49, Lemma 6.3] with a Taylor expansion argument.*

Remark 3.9. *The regularity condition H^{k+3} here is analogous to the superconvergence result in [16, 23], in which the authors obtained H^{k+2}. The reason is that the Laplacian operator is written into a first order system in [23] with an LDG scheme, while the second order is retained in the ultra-weak scheme.*

4   Convection-Diffusion Equation

In this section, we study the ultra-weak DG method for nonlinear convection-diffusion equations on $\Omega \in \mathbb{R}^d$:

$$u_t + \nabla \cdot \mathbf{f}(u) - \varepsilon \Delta u = 0, \qquad\qquad \text{on } \Omega \times [0, L], \tag{4.1a}$$
$$u(X, 0) = g(X), \qquad\qquad \text{on } \Omega, \tag{4.1b}$$

with periodic boundary conditions and the diffusion coefficient $\varepsilon > 0$. The stability analysis and optimal error estimates are derived for the semi-discrete method with the special projections designed above. For convenience, in the following analysis, we take $\mathcal{T}_h$ and V_h^k as an example to illustrate the idea.

4.1   Ultra-weak DG scheme

We multiply (4.1a) with a test function $v \in V_h^k$ to obtain

$$(u_t, v)_T + (\nabla \cdot \mathbf{f}, v)_T + \varepsilon(-\Delta u, v)_T = 0, \tag{4.2}$$

on each element T. The diffusion term $(-\Delta u, v)_T$ can be discretized by the ultra-weak discretization $a_h(u, v)$. The convection component of (4.2) can be approximated by $F_h(u, v)$ in the form

$$F_h(u, v) = - \sum_{T \in \mathcal{T}_h} (\mathbf{f}(u), \nabla v)_T + \sum_{e \in \mathcal{E}_h} \langle \widehat{\mathbf{f}} \cdot \mathbf{n}, [\![v]\!] \rangle_e. \tag{4.3}$$

Here $\widehat{\mathbf{f}} \cdot \mathbf{n} := \widehat{\mathbf{f}}(u^-, u^+)$ is a monotone numerical flux of the nonlinear term $\mathbf{f}$ which admits the following restrictions:

- $\widehat{\mathbf{f}}(u^-, u^+)$ is locally Lipschitz continuous;

- $\widehat{\mathbf{f}}(u^-, u^+) \cdot \mathbf{n}$ is consistent with the normal physical flux, namely $\widehat{\mathbf{f}}_{\mathbf{n}}(w, w) \cdot \mathbf{n} = \mathbf{f}(w) \cdot \mathbf{n}$;

- $\widehat{\mathbf{f}}(u^-, u^+)$ is a nondecreasing function of u^-, and a nonincreasing function of u^+.

Combining these together, we now have the ultra-weak DG semi-discrete scheme for problem (4.1): find $u_h(t) : [0, T] \mapsto V_h^k$, such that:

$$((u_h)_t, v_h)_\Omega + F_h(u_h, v_h) + \varepsilon a_h(u_h, v_h) = 0, \quad \forall v_h \in V_h^k, \tag{4.4}$$

subjected to the initial conditions:

$$u_h(0) = \mathcal{P}_h g. \tag{4.5}$$

Here $\mathcal{P}_h$ stands for an approximation operator of the initial value g in the space V_h^k, such as the nodal interpolation or L^2 projection. In this paper, we take $\mathcal{P}_h$ to be the L^2 projection P_h^k.

Remark 4.1. *It is remarked in [15] that the specific DDG scheme for the Schrödinger equation [36] could be reformulated as a particular case of the ultra-weak DG scheme with generalized numerical fluxes. Motivated by that, we comment that the proposed ultra-weak scheme and DDG scheme [34] for the convection-diffusion equation share some similarities. To see this, we can take $\alpha = 0$ in the numerical fluxes (2.17) and it can be observed that the only difference between these two methods is the treatment of numerical fluxes of normal derivatives. To be precise, the term $\langle [\![\partial_{\mathbf{n}} u]\!], [\![\partial_{\mathbf{n}} v]\!] \rangle_e$ in the ultra-weak scheme is substituted by $\langle [\![\partial_{\mathbf{n}}^2 u]\!], [\![v]\!] \rangle_e$ in the DDG scheme. It is well-known that the DDG scheme focuses on the behavior of high order derivatives across element faces, while the ultra-weak scheme preserves the symmetric structure and has a relatively low requirement of regularity on element faces.*

4.2 Stability and Error Analysis

We provide the stability analysis of the scheme (4.4) in the following theorem.

Theorem 4.1 (Stability)**.** *Given $a_h(\cdot, \cdot)$ which satisfies semi-positivity, the scheme (4.4) is L^2 stable, i.e.*

$$\frac{d}{dt} \|u_h\|_\Omega^2 \leq 0. \tag{4.6}$$

Proof. Let $v_h = u_h$ in the scheme (4.4), we get the following energy equation

$$\frac{d}{dt} \|u_h\|_\Omega^2 + F_h(u_h, u_h) + \varepsilon a_h(u_h, u_h) = 0. \tag{4.7}$$

Due to the semi-positivity of $a_h(\cdot, \cdot)$, we have $a(u_h, u_h) \geq 0$. Next, we claim that $F_h(u_h, u_h) \geq 0$, which follows from a multi-dimensional extension of the cell entropy inequality [32]. We write $\mathbf{f} = (f_i)_{i=1}^d$, and introduce the notations $F_i(u) = \int_0^u f_i(s) ds$, $\mathbf{F} = (F_i)_{i=1}^d$. By Divergence Theorem, on any element T, we have

$$(\mathbf{f}(u_h), \nabla u_h)_T = (\nabla \cdot \mathbf{F}(u_h), 1)_T = \langle \mathbf{F}(u_h) \cdot \mathbf{n}, 1 \rangle_{\partial T}. \tag{4.8}$$

Taking sum over $T \in \mathcal{T}_h$ and combining with the definition (4.3) yield

$$F_h(u_h, u_h) = -\sum_{e \in \mathcal{E}_h} \langle [\![\mathbf{F}(u_h) \cdot \mathbf{n}]\!], 1 \rangle_e + \sum_{e \in \mathcal{E}_h} \langle \widehat{\mathbf{f}}(u_h^-, u_h^+) \cdot \mathbf{n}, [\![u_h]\!] \rangle_e. \tag{4.9}$$

Following the same technique as in [32] by using mean value theorem and consistency of $\widehat{\mathbf{f}} \cdot \mathbf{n}$ leads to

$$
\begin{aligned}
F_h(u_h, u_h) &= -\sum_{e \in \mathcal{E}_h} \langle \mathbf{f}(\xi) \cdot \mathbf{n}, [\![u_h]\!] \rangle_e + \sum_{e \in \mathcal{E}_h} \langle \widehat{\mathbf{f}}(u_h^-, u_h^+) \cdot \mathbf{n}, [\![u_h]\!] \rangle_e \\
&= \sum_{e \in \mathcal{E}_h} \langle (\widehat{\mathbf{f}}(u_h^-, u_h^+) \cdot \mathbf{n} - \widehat{\mathbf{f}}(\xi, \xi) \cdot \mathbf{n}), [\![u_h]\!] \rangle_e \geq 0,
\end{aligned}
\tag{4.10}
$$

where $\xi(X)$ locates between $u_h^-(X)$ and $u_h^+(X)$ for every X on each e. The last inequality follows from the monotonicity of the numerical flux $\widehat{\mathbf{f}}$. Combining the semi-positivity of $a_h(\cdot, \cdot)$ and $F_h(\cdot, \cdot)$ with (4.7), we obtain the L^2 stability (4.6) of our scheme. $\qquad \square$

Remark 4.2. *We remark that a_h is positive when $(\alpha, c_1, c_2) \in \Theta_{UW}$, although here we do not require this stronger condition for stability analysis.*

Next, we present the optimal error estimate of the ultra-weak DG method (4.4). Let us start by introducing some ancillary quantities concerning the monotone flux $\widehat{\mathbf{f}} \cdot \mathbf{n}$, which are commonly used in the literature. The following operator α was proposed in [54], and was later applied to analyze the LDG method for the KdV equation in [53], the ultra-weak DG method [18] and the DDG method [33, 34]. For any piecewise smooth function $p \in L^2(\Omega)$, on the set $\mathcal{E}_h$, we define

$$
\alpha(\widehat{\mathbf{f}} \cdot \mathbf{n}; p) \equiv \alpha \left(\widehat{\mathbf{f}} \cdot \mathbf{n}; p^-, p^+ \right) := \begin{cases} [\![p]\!]^{-1} \left[\widehat{\mathbf{f}}(p^-, p^+) \cdot \mathbf{n} - \mathbf{f}(\{\!\{p\}\!\}) \cdot \mathbf{n} \right], & \text{if } [\![p]\!] \neq 0, \\ \frac{1}{2} |\mathbf{f}'(\{\!\{p\}\!\}) \cdot \mathbf{n}|, & \text{if } [\![p]\!] = 0. \end{cases}
\tag{4.11}
$$

From the monotonicity of the monotone flux $\widehat{\mathbf{f}}$, we know that $\alpha(\widehat{\mathbf{f}} \cdot \mathbf{n}; p) \geq 0$ on $\mathcal{E}_h$, and, in addition, $\alpha(\widehat{\mathbf{f}} \cdot \mathbf{n}; p) \leq C_{\mathbf{f}, \widehat{\mathbf{f}}}$, in which the constant $C_{\mathbf{f}, \widehat{\mathbf{f}}}$ depends on the Lipschitz continuity constant of $\widehat{\mathbf{f}}$ and $|\mathbf{f}'|$. Therefore, suitable regularity assumption of $\mathbf{f}$ can ensure $\alpha(\widehat{\mathbf{f}} \cdot \mathbf{n}; p)$ is bounded from above.

Theorem 4.2 (Error Estimate). *Let $(\alpha, c_1, c_2) \in \Theta_{UW}$, $k \geq (d-1)/2$, assume $u \in W^{1,\infty}(0, L; W^{k+1,\infty})$ and the non-linear function $\mathbf{f} \in C^3$, we have the following error estimates for the scheme (4.4): for every fixed $t \in [0, L]$,*

$$
\|u - u_h\|_\Omega + h|u - u_h|_{H^1(\mathcal{T}_h)} \leq \widehat{C} e^{\varepsilon^{-1} C t} h^{k+1},
\tag{4.12}
$$

where the constant C, $\widehat{C}$ is independent of h and ε, but depends on $\|\mathbf{f}''(u)\|_{L^\infty}$, $C_{\mathbf{f}, \widehat{\mathbf{f}}}$, $|g|_{H^{k+1}}$ $\|u\|_{L^\infty(0, L; W^{1,\infty})}$ and $\|u\|_{W^{1,\infty}(0, L; H^{k+1})}$.

Proof. Utilizing the ultra-weak projection Π_h^{UW} specified in (3.3), we decompose the numerical error $e_h = u - u_h$ into $e_h = \xi_h^\star - \eta_h^\star$, where $\eta_h^\star = \Pi_h^{\mathsf{UW}} u - u$ and $\xi_h^\star = \Pi_h^{\mathsf{UW}} u - u_h$. By consistency of the scheme and weak formulation of the convection-diffusion equation, we have the error equation

$$
((e_h)_t, v_h)_\Omega + \varepsilon a_h(e_h, v_h) + F_h(u, v_h) - F_h(u_h, v_h) = 0.
\tag{4.13}
$$

By taking $v_h = \xi_h^\star$ and using $e_h = \xi_h^\star - \eta_h^\star$, we have

$$
((\xi_h^\star)_t, \xi_h^\star)_\Omega + \varepsilon a_h(\xi_h^\star, \xi_h^\star) = ((\eta_h^\star)_t, \xi_h^\star)_\Omega + \varepsilon a_h(\eta_h^\star, \xi_h^\star) + \mathcal{H},
\tag{4.14}
$$

where $\mathcal{H} := -F_h(u, \xi_h^\star) + F_h(u_h, \xi_h^\star)$ takes the form

$$
\mathcal{H} = \sum_{T \in \mathcal{T}_h} (\mathbf{f}(u) - \mathbf{f}(u_h), \nabla \xi_h^\star)_T + \sum_{e \in \mathcal{E}_h} \langle \mathbf{f}(u) \cdot \mathbf{n} - \widehat{\mathbf{f}}(u_h^-, u_h^+) \cdot \mathbf{n}, [\![\xi_h^\star]\!] \rangle_e.
\tag{4.15}
$$

Following the orthogonality (3.3) of the projection, the coercivity of $a_h(\cdot, \cdot)$ in Lemma 3.2, we have

$$((\xi_h^\star)_t, \xi_h^\star)_\Omega + \varepsilon C_\star \|\xi_h^\star\|_E^2 \leq ((\eta_h^\star)_t, \xi_h^\star)_\Omega + \mathcal{H}. \tag{4.16}$$

Next, we estimate the term $\mathcal{H}$. Following the approaches in [33, 34, 53], we take $\mathbf{f}(\{\!\{u_h\}\!\}) \cdot \mathbf{n}$ as an intermediate value and obtain

$$\mathcal{H} = \sum_{T \in \mathcal{T}_h} (\mathbf{f}(u) - \mathbf{f}(u_h), \nabla \xi_h^\star)_T + \sum_{e \in \mathcal{E}_h} \langle \mathbf{f}(u) \cdot \mathbf{n} - \mathbf{f}(\{\!\{u_h\}\!\}) \cdot \mathbf{n}, [\![\xi_h^\star]\!] \rangle_e$$
$$+ \sum_{e \in \mathcal{E}_h} \left\langle \widehat{\mathbf{f}}(\{\!\{u_h\}\!\}, \{\!\{u_h\}\!\}) \cdot \mathbf{n} - \widehat{\mathbf{f}}(u_h^-, u_h^+) \cdot \mathbf{n}, [\![\xi_h^\star]\!] \right\rangle_e. \tag{4.17}$$

Using the definition (4.11) of $\alpha(\widehat{\mathbf{f}} \cdot \mathbf{n}; u_h)$, we obtain

$$\mathcal{H} = \sum_{T \in \mathcal{T}_h} (\mathbf{f}(u) - \mathbf{f}(u_h), \nabla \xi_h^\star)_T + \sum_{e \in \mathcal{E}_h} \langle \mathbf{f}(u) \cdot \mathbf{n} - \mathbf{f}(\{\!\{u_h\}\!\}) \cdot \mathbf{n}, [\![\xi_h^\star]\!] \rangle_e - \sum_{e \in \mathcal{E}_h} \langle \alpha(\widehat{\mathbf{f}} \cdot \mathbf{n}; u_h), [\![u_h]\!] [\![\xi_h^\star]\!] \rangle_e. \tag{4.18}$$

Applying the second order Taylor expansion (4.19) for each component $f_i, i = 1, ..., d$ of the nonlinear term $\mathbf{f}$ leads to

$$f_i(u) - f_i(u_h) = f_i'(u)e_h - \frac{f_i''(\kappa_i)}{2}e_h^2 = f_i'(u)(\xi_h^\star - \eta_h^\star) - \frac{f_i''(\kappa_i)}{2}(\xi_h^\star - \eta_h^\star)^2,$$
$$f_i(u) - f_i(\{\!\{u_h\}\!\}) = f_i'(u)\{\!\{e_h\}\!\} - \frac{f_i''(\varepsilon_i)}{2}\{\!\{e_h\}\!\}^2 = f_i'(u)(\{\!\{\xi_h^\star\}\!\} - \{\!\{\eta_h^\star\}\!\}) - \frac{f_i''(\varepsilon_i)}{2}(\{\!\{\xi_h^\star\}\!\} - \{\!\{\eta_h^\star\}\!\})^2, \tag{4.19}$$

where κ_i and ε_i are the points of Lagrange form remainder. Then we can decompose $\mathcal{H}$ into $\mathcal{H} = \mathcal{H}_1 + \mathcal{H}_2 + \mathcal{H}_3 + \mathcal{H}_4$ with each term taking the form

$$\mathcal{H}_1 = \sum_{T \in \mathcal{T}_h} (\mathbf{f}'(u), \xi_h^\star \nabla \xi_h^\star)_T + \sum_{e \in \mathcal{E}_h} \langle \mathbf{f}'(u) \cdot \mathbf{n}, \{\!\{\xi_h^\star\}\!\} [\![\xi_h^\star]\!] \rangle_e,$$
$$\mathcal{H}_2 = -\sum_{T \in \mathcal{T}_h} (\mathbf{f}'(u)\eta_h^\star, \nabla \xi_h^\star)_T - \sum_{e \in \mathcal{E}_h} \langle \mathbf{f}'(u) \cdot \mathbf{n} \{\!\{\eta_h^\star\}\!\}, [\![\xi_h^\star]\!] \rangle_e,$$
$$\mathcal{H}_3 = -\frac{1}{2} \sum_{T \in \mathcal{T}_h} (\mathbf{f}_\kappa'', (\xi_h^\star - \eta_h^\star)^2 \nabla \xi_h^\star)_T - \frac{1}{2} \sum_{e \in \mathcal{E}_h} \langle \mathbf{f}_\varepsilon'' \cdot \mathbf{n}, (\{\!\{\xi_h^\star\}\!\} - \{\!\{\eta_h^\star\}\!\})^2 [\![\xi_h^\star]\!] \rangle_e, \tag{4.20}$$
$$\mathcal{H}_4 = -\sum_{e \in \mathcal{E}_h} \langle \alpha(\widehat{\mathbf{f}} \cdot \mathbf{n}; u_h), [\![\xi_h^\star]\!]^2 \rangle_e + \sum_{e \in \mathcal{E}_h} \langle \alpha(\widehat{\mathbf{f}} \cdot \mathbf{n}; u_h), [\![\eta_h^\star]\!] [\![\xi_h^\star]\!] \rangle_e,$$

where $\mathbf{f}_\kappa'' := (f_i''(\kappa_i))_{i=1}^d$ and $\mathbf{f}_\varepsilon'' := (f_i''(\varepsilon_i))_{i=1}^d$. The fact $[\![u_h]\!] = [\![u_h - u]\!]$ was used to drive $\mathcal{H}_4$, since $u \in C^0(\Omega)$ by Sobolev embedding.

Each of these terms can be bounded as follows. $\mathcal{H}_1$ can be treated by using integration by parts

$$\mathcal{H}_1 = -\frac{1}{2} \sum_{T \in \mathcal{T}_h} (\mathbf{f}''(u) \cdot \nabla u, (\xi_h^\star)^2)_T \leq \|\mathbf{f}''(u)\|_{L^\infty(\Omega)} \|\nabla u\|_{L^\infty(\Omega)} \|\xi_h^\star\|_\Omega^2 \leq C \|\xi_h^\star\|_\Omega^2. \tag{4.21}$$

$\mathcal{H}_2$ is bounded by applying Young's inequality, trace inequality (2.7) and the approximation error

of the projection $\Pi_h^{\mathtt{UW}}$

$$\mathcal{H}_2 \leq \frac{1}{3}\varepsilon C_\star \left(\sum_{T\in\mathcal{T}_h} \|\nabla\xi_h^\star\|_T^2 + \sum_{e\in\mathcal{E}_h} \frac{\|[\![\xi_h^\star]\!]\|_e^2}{h_e} \right) + \frac{3}{4\varepsilon C_\star} \left(\sum_{T\in\mathcal{T}_h} \|\mathbf{f}'(u)\eta_h^\star\|_T^2 + \sum_{e\in\mathcal{E}_h} h_e \left\|\langle \mathbf{f}'(u)\cdot\mathbf{n}\,\{\!\{\eta_h^\star\}\!\}\rangle\right\|_e^2 \right)$$

$$\leq \frac{1}{3}\varepsilon C_\star \|\xi_h^\star\|_E^2 + \frac{3\|\mathbf{f}'(u)\|_{L^\infty(\Omega)}^2}{4\varepsilon C_\star} \left(\sum_{T\in\mathcal{T}_h} \|\eta_h^\star\|_T^2 + \sum_{e\in\mathcal{E}_h} h_e \|\{\!\{\eta_h^\star\}\!\}\|_e^2 \right) \tag{4.22}$$

$$\leq \frac{1}{3}\varepsilon C_\star \|\xi_h^\star\|_E^2 + \varepsilon^{-1} C \left(\|\eta_h^\star\|_\Omega^2 + h^2 |\eta_h^\star|_{H^1(\mathcal{T}_h)}^2 \right) \leq \frac{1}{3}\varepsilon C_\star \|\xi_h^\star\|_E^2 + \varepsilon^{-1} C h^{2k+2}.$$

Similarly, we can bound $\mathcal{H}_3$ by utilizing Young's inequality, trace inequality (2.7), inverse inequality (2.10), and the approximation error of the projection $\Pi_h^{\mathtt{UW}}$

$$\mathcal{H}_3 \leq \frac{1}{3}\varepsilon C_\star \left(\sum_{T\in\mathcal{T}_h} \|\nabla\xi_h^\star\|_T^2 + \sum_{e\in\mathcal{E}_h} \frac{\|[\![\xi_h^\star]\!]\|_e^2}{h_e} \right)$$

$$+ \frac{3\|\mathbf{f}''(u)\|_{L^\infty(\Omega)}\|\xi_h^\star - \eta_h^\star\|_{L^\infty(\mathcal{T}_h)}^2}{16\varepsilon C_\star} \left(\|\xi_h^\star - \eta_h^\star\|_\Omega^2 + h^2 |\xi_h^\star - \eta_h^\star|_{H^1(\mathcal{T}_h)}^2 \right) \tag{4.23}$$

$$\leq \frac{1}{3}\varepsilon C_\star \|\xi_h^\star\|_E^2 + \varepsilon^{-1} C \|\xi_h^\star - \eta_h^\star\|_{L^\infty(\mathcal{T}_h)}^2 \left(\|\xi_h^\star\|_\Omega^2 + h^{2k+2} \right).$$

By applying inverse inequality (2.10) to $\xi_h^\star$, we obtain following estimate for the L^∞ norm

$$\|\xi_h^\star - \eta_h^\star\|_{L^\infty(\mathcal{T}_h)} \leq \|\xi_h^\star\|_{L^\infty(\mathcal{T}_h)} + \|\eta_h^\star\|_{L^\infty(\mathcal{T}_h)} \leq C h^{-d/2} \|\xi_h^\star\|_\Omega + \|\eta_h^\star\|_{L^\infty(\mathcal{T}_h)}. \tag{4.24}$$

The infinity norm error estimate of the projection error $\eta_h^\star$ can be written as

$$\|\eta_h^\star\|_{L^\infty(\mathcal{T}_h)} = \max_{T\in\mathcal{T}_h} \|\eta_h^\star\|_{L^\infty(T)} \leq \left\|u - P_h^k u\right\|_{L^\infty(\widetilde{T})} + \left\|P_h^k u - \Pi_h^\star u\right\|_{L^\infty(\widetilde{T})}. \tag{4.25}$$

Here $\widetilde{T}$ represents the element in $\mathcal{T}_h$ where the maximum is achieved. Then we use L^∞, L^2 approximation capability of L^2 projection operator [19, 21], L^∞ inverse inequality (2.10), triangular inequality and the approximation error of the projection $\Pi_h^\star$ to obtain

$$\|\eta_h^\star\|_{L^\infty(\mathcal{T}_h)} \leq C h^{k+1-d/2} + C h^{-d/2} \left(\left\|P_h^k u - u\right\|_{\widetilde{T}} + \|u - \Pi_h^\star u\|_{\widetilde{T}} \right) \leq C h^{k+1-d/2}. \tag{4.26}$$

Combining (4.23), (4.24) and (4.26) yields

$$\mathcal{H}_3 \leq \frac{1}{3}\varepsilon C_\star \|\xi_h^\star\|_E^2 + \varepsilon^{-1} C \left(h^{-d} \|\xi_h^\star\|_\Omega^2 + h^{2k+2-d} \right) \left(\|\xi_h^\star\|_\Omega^2 + h^{2k+2} \right). \tag{4.27}$$

Finally, we have the following bound for $\mathcal{H}_4$:

$$\mathcal{H}_4 \leq \sum_{e\in\mathcal{E}_h} \langle \alpha(\widehat{\mathbf{f}}\cdot\mathbf{n}; u_h), [\![\eta_h^\star]\!]\,[\![\xi_h^\star]\!]\rangle_e \leq C_{\mathbf{f},\widehat{\mathbf{f}}} \left(\sum_{e\in\mathcal{E}_h} \frac{\varepsilon C_\star \|[\![\xi_h^\star]\!]\|_e^2}{3 h_e C_{\mathbf{f},\widehat{\mathbf{f}}}} + \sum_{e\in\mathcal{E}_h} \frac{3 C_{\mathbf{f},\widehat{\mathbf{f}}} h_e}{4\varepsilon C_\star} \|[\![\eta_h^\star]\!]\|_e^2 \right)$$

$$\leq \frac{1}{3}\varepsilon C_\star \|\xi_h^\star\|_E^2 + \varepsilon^{-1} C \left(\|\eta_h^\star\|_\Omega^2 + h^2 |\eta_h^\star|_{H^1}^2 \right) \leq \frac{1}{3}\varepsilon C_\star \|\xi_h^\star\|_E^2 + \varepsilon^{-1} C h^{2k+2}. \tag{4.28}$$

Combining the above estimates for each term leads to

$$\mathcal{H} \leq \varepsilon C_\star \|\xi_h^\star\|_E^2 + C \|\xi_h^\star\|_\Omega^2 + \varepsilon^{-1} C \left(h^{-d} \|\xi_h^\star\|_\Omega^2 + h^{2+2k-d} \right) \left(\|\xi_h^\star\|_\Omega^2 + h^{2k+2} \right) + \varepsilon^{-1} C h^{2k+2}. \tag{4.29}$$

Then we plug (4.29) into (4.16) to obtain

$$
\begin{aligned}
\frac{d}{dt}\|\xi_h^\star\|_\Omega^2 + \varepsilon C_\star \|\xi_h^\star\|_E^2 \leq{}& \varepsilon C_\star \|\xi_h^\star\|_E^2 + \frac{1}{2}\|(\eta_h^\star)_t\|_\Omega^2 + C\|\xi_h^\star\|_\Omega^2 \\
& + \varepsilon^{-1}C\left(h^{-d}\|\xi_h^\star\|_\Omega^2 + h^{2+2k-d}\right)\left(\|\xi_h^\star\|_\Omega^2 + h^{2k+2}\right) + \varepsilon^{-1}Ch^{2k+2}.
\end{aligned}
\tag{4.30}
$$

Since $(\eta_h^\star)_t = (\Pi_h^\star u - u)_t = \Pi_h^\star u_t - u_t$, its projection error also satisfies Theorem 3.1, therefore, without loss of generality, we assume $\varepsilon \leq 1$ and have

$$
\frac{d}{dt}\|\xi_h^\star\|_\Omega^2 \leq \varepsilon^{-1}C\left(1 + h^{-d}\|\xi_h^\star\|_\Omega^2 + h^{2+2k-d}\right)\left(\|\xi_h^\star\|_\Omega^2 + h^{2k+2}\right).
\tag{4.31}
$$

The assumption $k \geq (d-1)/2$ leads to $2k+2-d \geq 1$, hence $h^{2k+2-d} \leq h$ under the condition $h < 1$, therefore, the above equation becomes

$$
\frac{d}{dt}\|\xi_h^\star\|_\Omega^2 \leq \varepsilon^{-1}C\left(1 + h^{-d}\|\xi_h^\star\|_\Omega^2\right)\left(\|\xi_h^\star\|_\Omega^2 + h^{2k+2}\right).
\tag{4.32}
$$

Let us introduce the notation $W(t) = \|\xi_h^\star\|_\Omega^2 / h^{2k+2}$. We have

$$
\frac{dW}{dt} \leq \varepsilon^{-1}C(1 + h^{2k+2-d}W)(1 + W) \leq \varepsilon^{-1}C(1 + hW)(1 + W),
\tag{4.33}
$$

which is equivalent to

$$
\frac{d}{dt}\left(\frac{W(t)+1}{hW(t)+1}\right) \leq \varepsilon^{-1}C(1-h)\frac{W(t)+1}{hW(t)+1}.
\tag{4.34}
$$

Since the approximation of the initial condition, we have the initial error $\xi_h^\star(0) = \Pi_h^{\mathtt{UW}}u(0) - u_h(0)$, which leads to $W(0) \leq C'$ where C' is independent of h and ε. Applying Grönwall's inequality to obtain

$$
\frac{W(t)+1}{hW(t)+1} \leq \frac{W(0)+1}{hW(0)+1}e^{\varepsilon^{-1}C(1-h)t} \leq (C'+1)e^{\varepsilon^{-1}C(1-h)t},
\tag{4.35}
$$

which leads to

$$
W(t) \leq \frac{(C'+1)e^{\varepsilon^{-1}C(1-h)t} - 1}{1 - (C'+1)e^{\varepsilon^{-1}C(1-h)t}h}.
\tag{4.36}
$$

If we take h (depending on ε) to be small enough so that $1 - (C'+1)e^{\varepsilon^{-1}C(1-h)t}h > 1/2$, we have $W(t) \leq 2((C'+1)e^{\varepsilon^{-1}C(1-h)t} - 1) \leq 2(C'+1)e^{\varepsilon^{-1}Ct}$. With $\widehat{C} := 2(C'+1)$, we then have $\|\xi_h^\star(t)\|_\Omega^2 \leq \widehat{C}e^{\varepsilon^{-1}Ct}h^{2k+2}$. Combining this with the projection error of $\eta_h^\star$ leads to the optimal error estimate

$$
\|u - u_h\|_\Omega \leq \widehat{C}e^{\varepsilon^{-1}Ct}h^{k+1}.
\tag{4.37}
$$

The error estimate in the semi-H^1 norm

$$
|u - u_h|_{H^1(\mathcal{T}_h)} \leq \widehat{C}e^{\varepsilon^{-1}Ct}h^k
\tag{4.38}
$$

can be derived following the same technique in (3.30). The combination of these leads to (4.12), and this completes the proof. $\square$

Remark 4.3. *Though this proof holds for any fixed diffusion constant $\varepsilon > 0$, it is not uniform with respect to ε. In Section 6, we numerically test the convergence behavior for the case of vanishing ε, for which an optimal result is shown, see Example 6.5. In fact, for convection dominated case ($\varepsilon = 0$), only suboptimal $\mathcal{O}(h^k)$ result can be obtained, see [53] via the study of LDG methods. It could be improved in some special cases, for example, $k + 1/2$ order in 1D case [53] or $k + 1$ order with upwind flux in 1D case [55].*

Remark 4.4. *If we relax the requirement on coercivity of a_h, this optimal error estimate may not be obtained, since the $\|\xi_h^\star\|_E$ term in the estimation of $\mathcal{H}$ would dominate $\mathcal{O}(h^k)$ order of convergence as studied in [18]. From this perspective, the coercivity condition has enhanced our estimation, although it limits the set of parameters (α, c_1, c_2). Note that for the case of $\mathbf{f} = 0$, i.e., the model (4.1) reduces to heat equation, in this case coercivity is not necessary. Once the stability condition is satisfied, i.e., a_h is semi-positive, the optimal error estimate could be obtained with the same technique as the above theorem.*

Remark 4.5. *For $d = 1, 2, 3$, the condition $k \geq (d-1)/2$ is equivalent to $k \geq 1$. So polynomials with positive order can be used without concerns.*

5   Biharmonic Equation

In this section, we employ the time-dependent fourth order biharmonic equation to demonstrate the application of the ultra-weak discretization to equations with high order spatial derivatives. We consider the following time-dependent biharmonic equation on $\Omega \subset \mathbb{R}^d$, $d \geq 1$ with periodic boundary condition:

$$
\begin{aligned}
u_t + \Delta^2 u &= 0, & \text{on } \Omega \times [0, L], & \qquad (5.1\text{a}) \\
u(X, 0) &= g(X), & \text{on } \Omega. & \qquad (5.1\text{b})
\end{aligned}
$$

5.1   A Local Ultra-Weak DG Scheme

The biharmonic equation (5.1a) can be written into the following system by introducing an auxiliary variable q:

$$
\begin{aligned}
u_t + \Delta q &= 0, \\
q - \Delta u &= 0.
\end{aligned} \qquad (5.2)
$$

To enhance the stability of the ultra-weak DG method, we consider the local ultra-weak DG scheme recently developed in [49], which can be written as: find $u_h, q_h \in V_h^k$, for $\forall v_h, w_h \in V_h^k$:

$$
\begin{aligned}
((u_h)_t, v_h)_\Omega - a_h(q_h, v_h) &= 0, \\
(q_h, w_h)_\Omega + a_h(u_h, w_h) &= 0,
\end{aligned} \qquad (5.3)
$$

where $a_h(\cdot, \cdot)$ is the ultra-weak discretization defined in (2.15) with generalized numerical fluxes (2.17), subjected to the initial conditions

$$
u_h(0) = \mathcal{P}_h g. \qquad (5.4)
$$

Remark 5.1. *Here we use the same spatial discretization for the two Laplacian operators, i.e., with the same parameters (α, c_1, c_2). We remark here it is possible to choose different parameter sets as long as the stability condition is guaranteed. In [49], the authors studied four alternating fluxes, two of which are special cases of our setting above. The other two fluxes belong to the class of generalized numerical fluxes with $\alpha_1 = \alpha_2$.*

5.2   Stability and Error Analysis

We can immediately derive the following stability result of this scheme (5.3).

Theorem 5.1 (Stability)**.** *Let* $(\alpha, c_1, c_2) \in \mathbb{R}^3$, *the local ultra-weak scheme* (5.3) *is* L^2 *stable, i.e.*

$$\frac{d}{dt} \|u_h\|_\Omega^2 \le 0. \tag{5.5}$$

Proof. Let $v_h = u_h$, $w_h = q_h$ in scheme (5.3), we get the following energy equation by symmetric property:

$$\frac{d}{dt} \|u_h\|_\Omega^2 + \|q_h\|_\Omega^2 = 0. \tag{5.6}$$

This proves the L^2 stability. □

For the parameter $(\alpha, c_1, c_2) \in \Theta_{UW}$, we could take advantage of the properties of ultra-weak projection to have the following error estimates on both unstructured simplex and Cartesian meshes. Similar to the convection-diffusion equation, we take V_h^k on the mesh $\mathcal{T}_h$ as an example to illustrate this, and it is easy to show it for the other cases.

Theorem 5.2 (Error Estimate on Triangular Mesh or Cartesian Mesh)**.** *Let* $(\alpha, c_1, c_2) \in \Theta_{UW} \cup \Theta_{GR}$ *when* $d = 1$, *or* $(\alpha, c_1, c_2) \in \Theta_{UW}$ *for* $d \ge 2$. *Assume the exact solution* $u \in H^1(0, L; H^{k+1}) \cap L^2(0, L; H^{k+3})$ *and initial condition* $g \in H^{k+1}(\mathcal{T}_h)$, *then we have the following error estimate for scheme* (5.3)*: for every fixed* $t \in [0, L]$,

$$\|u - u_h\|_\Omega + \|q - q_h\|_{L^2(0,t;L^2)} \le Ch^{k+1}, \tag{5.7}$$

where C is independent with h and may depend on $|u|_{H^1(0,L;H^{k+1})}$, $\|q\|_{L^2(0,L;H^{k+1})}$, $|u|_{H^{k+1}(\Omega)}$ *and* $|g|_{H^{k+1}(\Omega)}$.

Proof. Let $\Pi_h^\star$ be the ultra-weak or Gauss-Raudu type projection. We denote $\eta_{u,h}^\star = \Pi_h^\star u - u$, $\xi_{u,h}^\star = \Pi_h^\star u - u_h$, $\eta_{q,h}^\star = \Pi_h^\star q - q$ and $\xi_{q,h}^\star = \Pi_h^\star q - q_h$, where all the projections satisfies the orthogonality condition. We could take either ultra weak projection (3.1) or Gauss-Raudu projection (3.31) under our assumption of parameters. The error terms can be decomposed into $e_u = \xi_{u,h}^\star - \eta_{u,h}^\star$ and $e_q = \xi_{q,h}^\star - \eta_{q,h}^\star$. We take $v_h = \xi_{u,h}^\star$, $w_h = \xi_{q,h}^\star$ in error equations associated with scheme (5.3) to get:

$$\begin{aligned}
((\xi_{u,h}^\star)_t, \xi_{u,h}^\star)_\Omega - a_h(\xi_{q,h}^\star, \xi_{u,h}^\star) + a_h(\eta_{q,h}^\star, \xi_{u,h}^\star) &= ((\eta_{u,h}^\star)_t, \xi_{u,h}^\star)_\Omega, \\
(\xi_{q,h}^\star, \xi_{q,h}^\star)_\Omega + a_h(\xi_{u,h}^\star, \xi_{q,h}^\star) - a_h(\eta_{u,h}^\star, \xi_{q,h}^\star) &= (\eta_{q,h}^\star, \xi_{q,h}^\star)_\Omega.
\end{aligned} \tag{5.8}$$

We add these two equations and use symmetricity of $a_h(\cdot, \cdot)$ and orthognality property of ultra-weak projections $\Pi_h^\star$ to have:

$$\frac{d}{dt} \|\xi_{u,h}^\star\|_\Omega^2 + \|\xi_{q,h}^\star\|_\Omega^2 = ((\eta_{u,h}^\star)_t, \xi_{u,h}^\star)_\Omega + (\eta_{q,h}^\star, \xi_{q,h}^\star)_\Omega. \tag{5.9}$$

By Cauchy-Schwarz inequality and Young's inequality:

$$\frac{d}{dt} \|\xi_{u,h}^\star\|_\Omega^2 + \|\xi_{q,h}^\star\|_\Omega^2 \le \frac{1}{2} \left(\|(\eta_{u,h}^\star)_t\|_\Omega^2 + \|\xi_{u,h}^\star\|_\Omega^2 + \|\eta_{q,h}^\star\|_\Omega^2 + \|\xi_{q,h}^\star\|_\Omega^2 \right), \tag{5.10}$$

which leads to

$$\frac{d}{dt} \|\xi_{u,h}^\star\|_\Omega^2 + \|\xi_{q,h}^\star\|_\Omega^2 \le C \left(\|(\eta_{u,h}^\star)_t\|_\Omega^2 + \|\xi_{u,h}^\star\|_\Omega^2 + \|\eta_{q,h}^\star\|_\Omega^2 \right). \tag{5.11}$$

We then take integration over $[0, t]$ to obtain:

$$\|\xi_{u,h}^\star(t)\|_\Omega^2 + \int_0^t \|\xi_{q,h}^\star(s)\|_\Omega^2 \, ds \le C \left(\int_0^t \|(\eta_{u,h}^\star)_t\|_\Omega^2 \, ds + \int_0^t \|\xi_{u,h}^\star\|_\Omega^2 \, ds + \int_0^t \|\eta_{q,h}^\star\|_\Omega^2 \, ds + \|\xi_{u,h}^\star(0)\|_\Omega^2 \right). \tag{5.12}$$

Applying Gronwall inequality yields

$$\left\|\xi_{u,h}^{\star}(t)\right\|_{\Omega}^{2} + \int_{0}^{t} \left\|\xi_{q,h}^{\star}(s)\right\|_{\Omega}^{2} ds \leq C \left(\int_{0}^{t} \left\|(\eta_{u,h}^{\star})_{t}\right\|_{\Omega}^{2} ds + \int_{0}^{t} \left\|\eta_{q,h}^{\star}\right\|_{\Omega}^{2} ds + \left\|\xi_{u,h}^{\star}(0)\right\|_{\Omega}^{2} \right). \tag{5.13}$$

By the approximation capability, we have:

$$\left\|\xi_{u,h}^{\star}(t)\right\|_{\Omega}^{2} + \left\|\xi_{q,h}^{\star}\right\|_{L^{2}(0,t;L^{2})}^{2} \leq Ch^{2k+2} \left(|u|_{H^{1}(0,T;H^{k+1})}^{2} + \|q\|_{L^{2}(0,T;H^{k+1})}^{2} + |g|_{H^{k+1}(\mathcal{T}_{h})}^{2} \right). \tag{5.14}$$

Then by triangular inequality and approximation capability of the ultra-weak projection, we have the following estimate

$$\|u - u_{h}\|_{\Omega} + \|q - q_{h}\|_{L^{2}(0,t;L^{2})} \leq Ch^{k+1}, \tag{5.15}$$

where C may depend on $|u|_{H^{1}(0,L;H^{k+1})}$, $\|q\|_{L^{2}(0,L;H^{k+1})}$, $|u|_{H^{k+1}(\Omega)}$ and $|g|_{H^{k+1}(\Omega)}$. $\qquad\square$

On Cartesian mesh $\mathcal{K}_h$ with the tensor polynomial space S_h^k being the solution and test function spaces in scheme (5.3), we are able to extend the above optimal error bound to a wider class of parameters for $(\alpha, c_1, c_2) \in \Theta_{GR}$. The main tool is the Gauss-Raudu type projection we construct in Section 3.2, and its superconvergent property in Lemma 3.5.

Theorem 5.3 (Error Estimate on Cartesian Mesh). *Let $d \geq 2$, $d < 2(k+1)$, $(\alpha, c_1, c_2) \in \Theta_{GR}$, assume the exact solution $u \in H^1(0, L; H^{k+1}) \cap L^2(0, L; H^{k+5})$ and initial condition $g \in H^{k+1}(\mathcal{K}_h)$, then we have the following error estimate for scheme (5.3) on Cartesian mesh $\mathcal{K}_h$ with the tensor polynomial space S_h^k being the solution and test function spaces: for any fixed $t \in [0, L]$,*

$$\|u - u_{h}\|_{\Omega} + \|q - q_{h}\|_{L^{2}(0,t;L^{2})} \leq Ch^{k+1}, \tag{5.16}$$

where the constant C depends on $|u|_{H^{1}(0,L;H^{k+1})}$, $\|u\|_{L^{2}(0,L,H^{k+3})}$, $\|q\|_{L^{2}(0,L,H^{k+3})}$, $|g|_{H^{k+1}}$ and $|u|_{H^{k+1}}$.

Proof. We again denote $\eta_{u,h}^{\star} = \Pi_h^{\mathsf{GR}} u - u$, $\xi_{u,h}^{\star} = \Pi_h^{\mathsf{GR}} u - u_h$, $\eta_{q,h}^{\star} = \Pi_h^{\mathsf{GR}} q - q$ and $\xi_{q,h}^{\star} = \Pi_h^{\mathsf{GR}} q - q_h$. Here the projections are the tensor Gauss-Raudu type projection defined in (3.37). The error term can be decomposed into $e_u = \xi_{u,h}^{\star} - \eta_{u,h}^{\star}$ and $e_q = \xi_{q,h}^{\star} - \eta_{q,h}^{\star}$. We take $v_h = \xi_{u,h}^{\star}$, $w_h = \xi_{q,h}^{\star}$ in error equations associated with scheme (5.3) to get:

$$\begin{aligned}
&((\xi_{u,h}^{\star})_{t}, \xi_{u,h}^{\star})_{\Omega} - a_{h}(\xi_{q,h}^{\star}, \xi_{u,h}^{\star}) + a_{h}(\eta_{q,h}^{\star}, \xi_{u,h}^{\star}) = ((\eta_{u,h}^{\star})_{t}, \xi_{u,h}^{\star})_{\Omega}, \\
&(\xi_{q,h}^{\star}, \xi_{q,h}^{\star})_{\Omega} + a_{h}(\xi_{u,h}^{\star}, \xi_{q,h}^{\star}) - a_{h}(\eta_{u,h}^{\star}, \xi_{q,h}^{\star}) = (\eta_{q,h}^{\star}, \xi_{q,h}^{\star})_{\Omega}.
\end{aligned} \tag{5.17}$$

We add the two equations and use symmetricity to have:

$$\frac{d}{dt}\left\|\xi_{u,h}^{\star}\right\|_{\Omega}^{2} + \left\|\xi_{q,h}^{\star}\right\|_{\Omega}^{2} = ((\eta_{u,h}^{\star})_{t}, \xi_{u,h}^{\star})_{\Omega} + (\eta_{q,h}^{\star}, \xi_{q,h}^{\star})_{\Omega} + a_{h}(\eta_{u,h}^{\star}, \xi_{q,h}^{\star}) - a_{h}(\eta_{q,h}^{\star}, \xi_{u,h}^{\star}). \tag{5.18}$$

By Cauchy-Schwarz inequality and Young's inequality,

$$\frac{d}{dt}\left\|\xi_{u,h}^{\star}\right\|_{\Omega}^{2} + \left\|\xi_{q,h}^{\star}\right\|_{\Omega}^{2} \leq \frac{1}{2}\left(\left\|(\eta_{u,h}^{\star})_{t}\right\|_{\Omega}^{2} + \left\|\xi_{u,h}^{\star}\right\|_{\Omega}^{2} + \left\|\eta_{q,h}^{\star}\right\|_{\Omega}^{2} + \left\|\xi_{q,h}^{\star}\right\|_{\Omega}^{2} \right) + |a_{h}(\eta_{u,h}^{\star}, \xi_{q,h}^{\star}) - a_{h}(\eta_{q,h}^{\star}, \xi_{u,h}^{\star})|. \tag{5.19}$$

We use the superconvergent property of Π_h^{GR} in Lemma 3.5 to bound the last term on the right:

$$|a_{h}(\eta_{u,h}^{\star}, \xi_{q,h}^{\star}) - a_{h}(\eta_{q,h}^{\star}, \xi_{u,h}^{\star})| \leq Ch^{k+1}(|u|_{H^{k+3}(\mathcal{K}_h)} \left\|\xi_{q,h}^{\star}\right\|_{\Omega} + |q|_{H^{k+3}(\mathcal{K}_h)} \left\|\xi_{u,h}^{\star}\right\|_{\Omega}). \tag{5.20}$$

Then we apply Young's inequality again and use the approximation capability of projection to obtain

$$\frac{d}{dt}\left\|\xi_{u,h}^{\star}\right\|_{\Omega}^{2} + \left\|\xi_{q,h}^{\star}\right\|_{\Omega}^{2} \leq C\left\|\xi_{u,h}^{\star}\right\|_{\Omega}^{2} + Ch^{2k+2}\left(|u_{t}|_{H^{k+1}(\mathcal{K}_h)}^{2} + |u|_{H^{k+3}(\mathcal{K}_h)}^{2} + |q|_{H^{k+3}(\mathcal{K}_h)}^{2} \right). \tag{5.21}$$

27

We take integration over $[0,t]$ and use Gronwall inequality to obtain:

$$\left\|\xi_{u,h}^\star(t)\right\|_\Omega^2 + \int_0^t \left\|\xi_{q,h}^\star(s)\right\|_\Omega^2 ds$$
$$\leq Ch^{2k+2}\left(|u|_{H^1(0,L;H^{k+1})}^2 + \|u\|_{L^2(0,L,H^{k+3})}^2 + \|q\|_{L^2(0,L,H^{k+3})}^2 + |g|_{H^{k+1}(\Omega)}^2\right). \tag{5.22}$$

Then by triangular inequality and approximation capability of ultra-weak projection, we have the following estimates:
$$\|u - u_h\|_\Omega + \|q - q_h\|_{L^2(0,t;L^2)} \leq Ch^{k+1}, \tag{5.23}$$
where C may depend on $|u|_{H^1(0,L;H^{k+1})}$, $\|u\|_{L^2(0,L,H^{k+3})}$, $\|q\|_{L^2(0,L,H^{k+3})}$, $|g|_{H^{k+1}}$ and $|u|_{H^{k+1}}$. $\qquad\square$

Remark 5.2. *Our result can be viewed as a generalization of the study in [49] to a wider range of numerical fluxes on both simplex and Cartesian mesh. Compared with [49], a lower regularity requirement is needed because of the ultra-weak projection and Lemma 3.5.*

Remark 5.3. *We also remark that the technique and tool we built in the paper can be directly extended to other equations in a general setting of dimension and numerical fluxes, e.g., the Schrödinger equation [15], wave equation [50], fifth and general higher order problems [49].*

6 Numerical Experiments

In this section, numerical examples are presented to validate theoretical results in previous sections. Various sets of the parameters α, c_1 and c_2 will be tested. Periodic boundary conditions are adopted for all numerical examples.

For the temporal discretization of the convection-diffusion equation, we use an L-stable third-order implicit-explicit (IMEX) Runge-Kutta (RK) (3,4,3) scheme [3]. The coefficients of the scheme are listed in Table 6.1, which contains two butcher tableaus of Runge-Kutta schemes. The left one is the implicit RK scheme for the linear diffusion term, while the right one is the explicit RK scheme to discretize the nonlinear convection term. The constants in these schemes are taken as: $\gamma \approx 0.435866521508459$ which is the middle root of $6x^3 - 18x^2 + 9x - 1 = 0$; $\beta_1 = -\frac{3}{2}\gamma^2 + 4\gamma - \frac{1}{4}$; $\beta_2 = \frac{3}{2}\gamma^2 - 5\gamma + \frac{5}{4}$. The parameter α_1 is chosen as -0.35 and $\alpha_2 = (\frac{1}{3} - 2\gamma^2 - 2\beta_2\alpha_1\gamma)/[\gamma(1-\gamma)]$. The time marching step size τ is chosen to adapt the convergence order of spatial discretization. In the numerical tests, we take $\tau = \mathcal{O}(h^{\max\{1,\frac{k+1}{3}\}})$ to observe clean convergence rate for each k, as we expect to observe $k+1$ order of spatial convergence for $\mathcal{P}_k$. For the temporal discretization of the biharmonic equation, we apply the L-stable third order Diagonal RK method, which is a degenerating case of the IMEX RK method used for convection-diffusion equations.

	0	0	0	0	0	0	0	0
0	0	0	0	0	0	0	0	0
γ	0	γ	0	0	γ	0	0	0
$\frac{\gamma+1}{2}$	0	$\frac{1-\gamma}{2}$	γ	0	$\frac{\gamma+1}{2} - \alpha_1$	α_1	0	0
1	0	β_1	β_2	γ	0	$1-\alpha_2$	α_2	0
	0	β_1	β_2	γ	0	β_1	β_2	γ

Table 6.1: Coefficients of IMEX (4,4,3) method used in numerical experiments

28

Example 6.1. We first consider the one-dimensional nonlinear convection-diffusion equation

$$u_t + \left(\frac{u^2}{2}\right)_x - u_{xx} = R, \qquad (6.1)$$

with the exact solution set to be

$$u(x,t) = \sin(\pi x)e^t. \qquad (6.2)$$

The right-hand side R can be computed from the exact solution (6.2). The computational domain is set to be $\Omega = [-1, 1]$ which is discretized into N equidistant cells. This leads to a uniform partition mesh with size $h = 2/N$. We apply the ultra-weak DG scheme (4.4) to solve the above equation, with the global Lax-Friedrich flux taking the form:

$$\widehat{\mathbf{f}}(u_h^+, u_h^-) \cdot \mathbf{n} = \{\!\{ \mathbf{f}(u_h) \cdot \mathbf{n} \}\!\} + \frac{\sigma}{2} [\![u_h]\!], \qquad (6.3)$$

where $\sigma = \max_{1 \leq i \leq d, X \in \Omega} |f_i'(u(X))|$.

We choose different sets of the parameters α, c_1 and c_2, and test this example with the final time $L = 1$. We summarize the convergence rates into one table which can be seen in Table 6.2. In the table, we take some representative parameters from Θ_{UW}, for which we could prove the optimal performance for both accuracy and stability analytically. The numerical examples exhibit optimal convergence, confirming the validity of our theoretical results. The detailed results and numerical orders can be seen through the hyperlink in the column 'Table'. Apart from these parameters, we also test some well-known numerical fluxes which actually do not belong to the set of Θ_{UW} (but in the set of Θ_{GR}). Our numerical examples show that most of them work well in 1D cases. However, the stability of these semi-discrete schemes (using parameters in Θ_{GR}) cannot be proved rigorously, therefore further investigation of these results will be needed. It is also notable that the central flux with $k = 1$ does not belong to either Θ_{UW} or Θ_{GR}, for which we observe an unstable numerical behavior.

Flux	Table	Parameters			$\mathcal{P}_1$	$\mathcal{P}_2$	$\mathcal{P}_3$
		α	c_1	c_2			
Θ_{UW}							
General Flux	6.3	1/2	-17	1	k+1	k+1	k+1
IPDG	6.3	0	-17	0	k+1	k+1	k+1
$\alpha\beta$ Flux [18]	6.4	1/2	-26	0	k+1	k+1	k+1
Θ_{GR}							
General Flux	6.4	1/2	0	1	k+1	k+1	k+1
Alternating Flux	6.5	1/2	0	0	k+1	k+1	k+1
$\alpha\beta$ Flux	6.5	0.3	0.4	0.4	k+1	k+1	k+1
Central Flux ($k \geq 2$)	-	0	0	0	-	k+1	k+1
Other fluxes							
Central Flux ($k = 1$)	-	0	0	0	U	-	-

Table 6.2: Summary of numerical experiments of 1D ultra-weak DG scheme with parameters (work for three equations) where 'U' means unstable numerical results are observed, 'k+1' means optimal convergence.

In addition, we have considered the heat equation and the linear convection-diffusion equation

taking the form

$$u_t - u_{xx} = R, \tag{6.4a}$$

$$u_t + u_x - u_{xx} = R, \tag{6.4b}$$

with different source terms R leading to the same exact solution (6.2). The same convergence rates as in Table 6.2 have been observed, and we skip these results to save space.

Parameters		$(1/2,-17,1)$				$(0,-17,0)$			
k	N	L^2 error	order	H^1 error	order	L^2 error	order	H^1 error	order
1	320	6.0454×10^{-2}	-	4.4358×10^{-1}	-	5.4919×10^{-3}	-	3.8987×10^{-1}	-
	640	3.8440×10^{-3}	2.00	9.8611×10^{-2}	1.04	1.3774×10^{-3}	2.00	1.9445×10^{-1}	1.00
	1280	3.8440×10^{-3}	2.00	9.8611×10^{-2}	1.04	3.4920×10^{-4}	1.98	9.7094×10^{-2}	1.00
	2560	9.6142×10^{-4}	2.00	4.8887×10^{-2}	1.01	8.8090×10^{-5}	1.99	4.8496×10^{-2}	1.00
2	20	4.1958×10^{-4}	-	3.2051×10^{-2}	-	4.1078×10^{-4}	-	3.1693×10^{-2}	-
	40	5.2066×10^{-5}	3.01	7.9526×10^{-3}	2.01	5.1899×10^{-5}	2.98	7.9273×10^{-3}	2.00
	80	6.5303×10^{-6}	3.00	1.9844×10^{-3}	2.00	6.5386×10^{-6}	2.99	1.9821×10^{-3}	2.00
	160	8.1926×10^{-7}	2.99	4.9586×10^{-4}	2.00	8.2120×10^{-7}	2.99	4.9555×10^{-4}	2.00
3	10	3.1112×10^{-4}	-	1.1114×10^{-2}	-	1.1252×10^{-4}	-	6.7292×10^{-3}	-
	20	2.1506×10^{-5}	3.85	1.4284×10^{-3}	2.96	7.2730×10^{-6}	3.95	8.3611×10^{-4}	3.01
	40	1.3814×10^{-6}	3.96	1.7969×10^{-4}	2.99	4.5910×10^{-7}	3.99	1.0432×10^{-4}	3.00
	80	8.6992×10^{-8}	3.99	2.2496×10^{-5}	3.00	2.8913×10^{-8}	3.99	1.3033×10^{-5}	3.00

Table 6.3: Numerical error and convergence rate for the 1D quadratic convection-diffusion equation, with parameter $(1/2,-17,1)$ (Left) and $(0,-17,0)$ (Right)

Parameters		$(1/2,-26,0)$				$(1/2,0,1)$			
k	N	L^2 error	order	H^1 error	order	L^2 error	order	H^1 error	order
1	320	5.0640×10^{-3}	-	3.9042×10^{-1}	-	1.2135×10^{-3}	-	9.2393×10^{-2}	-
	640	1.2719×10^{-3}	1.99	1.9479×10^{-1}	1.00	3.0301×10^{-4}	2.00	4.6537×10^{-2}	0.99
	1280	3.2378×10^{-4}	1.97	9.7282×10^{-2}	1.00	7.5709×10^{-5}	2.00	2.3436×10^{-2}	0.99
	2560	8.1868×10^{-5}	1.98	4.8596×10^{-2}	1.00	1.8923×10^{-5}	2.00	1.1792×10^{-2}	0.99
2	20	4.3872×10^{-4}	-	3.2020×10^{-2}	-	2.2745×10^{-3}	-	7.1868×10^{-2}	-
	40	5.5524×10^{-5}	2.98	8.0109×10^{-3}	2.00	2.7159×10^{-4}	3.07	1.7143×10^{-2}	2.07
	80	6.9953×10^{-6}	2.99	2.0031×10^{-3}	2.00	3.3202×10^{-5}	3.03	4.1898×10^{-3}	2.03
	160	8.7834×10^{-7}	2.99	5.0081×10^{-4}	2.00	4.1054×10^{-6}	3.02	1.0359×10^{-3}	2.02
3	10	8.2688×10^{-5}	-	7.3153×10^{-3}	-	3.5836×10^{-4}	-	1.1584×10^{-2}	-
	20	5.2400×10^{-6}	3.98	9.1816×10^{-4}	2.99	2.2370×10^{-5}	4.00	1.4457×10^{-3}	3.00
	40	3.2937×10^{-7}	3.99	1.1494×10^{-4}	3.00	1.3988×10^{-6}	4.00	1.8075×10^{-4}	3.00
	80	2.0820×10^{-8}	3.98	1.4374×10^{-5}	3.00	8.7492×10^{-8}	4.00	2.2596×10^{-5}	3.00

Table 6.4: Numerical error and convergence rate for the 1D quadratic convection-diffusion equation, with parameter $(1/2,-26,0)$ (Left) and $(1/2,0,1)$ (Right)

Example 6.2. In this example, we present numerical results for the two-dimensional convection-diffusion equation

$$u_t + u(u_x + u_y) - \Delta u = R, \tag{6.5}$$

with a suitable choice of R leading to the exact solution

$$u(x,y,t) = \sin(\pi x)\sin(\pi y)e^t. \tag{6.6}$$

Parameters		$(1/2,0,0)$				$(0.3,0.4,0.4)$			
k	N	L^2 error	order	H^1 error	order	L^2 error	order	H^1 error	order
1	320	3.3188×10^{-4}	-	9.2363×10^{-2}	-	4.9457×10^{-4}	-	5.9011×10^{-2}	-
	640	8.2852×10^{-5}	2.00	4.6532×10^{-2}	0.99	1.2353×10^{-4}	2.00	2.9605×10^{-2}	1.00
	1280	2.0718×10^{-5}	2.00	2.3435×10^{-2}	0.99	3.0868×10^{-5}	2.00	1.4850×10^{-2}	1.00
	2560	5.1839×10^{-6}	2.00	1.1791×10^{-2}	0.99	7.7156×10^{-6}	2.00	7.4460×10^{-3}	1.00
2	20	1.0528×10^{-3}	-	4.8030×10^{-2}	-	1.8232×10^{-3}	-	5.8216×10^{-2}	-
	40	1.3092×10^{-4}	3.01	1.1893×10^{-2}	2.01	2.2104×10^{-4}	3.04	1.4122×10^{-2}	2.04
	80	1.6327×10^{-5}	3.00	2.9589×10^{-3}	2.01	2.7217×10^{-5}	3.02	3.4788×10^{-3}	2.02
	160	2.0388×10^{-6}	3.00	7.3796×10^{-4}	2.00	3.3771×10^{-6}	3.01	8.6343×10^{-4}	2.01
3	10	2.1821×10^{-4}	-	8.9797×10^{-3}	-	3.3354×10^{-4}	-	1.0817×10^{-2}	-
	20	1.3608×10^{-5}	4.00	1.1186×10^{-3}	3.00	2.0842×10^{-5}	4.00	1.3513×10^{-3}	3.00
	40	8.4867×10^{-7}	4.00	1.3945×10^{-4}	3.00	1.3035×10^{-6}	4.00	1.6896×10^{-4}	3.00
	80	5.3037×10^{-8}	4.00	1.7406×10^{-5}	3.00	8.1538×10^{-8}	4.00	2.1122×10^{-5}	3.00

Table 6.5: Numerical error and convergence rate for the 1D quadratic convection-diffusion equation, with parameter $(1/2,0,0)$ (Left) and $(0.3,0.4,0.4)$ (Right)

We set the domain to be $\Omega = [-1,1] \times [-1,1]$ which is partitioned into a $N \times N$ Cartesian mesh. A line with slope -1 is used to split each rectangular into two right-angle triangles. The spatial discretization used on the triangular mesh is piecewise $\mathcal{P}$ space. Meanwhile, we also test the performance of tensor $\mathcal{Q}$ space on the Cartesian mesh.

We apply the ultra-weak DG scheme (4.4) with the global Lax-Friedrich flux to solve the above equation. We choose different sets of the parameters α, c_1 and c_2, and test this example with the final time $L = 1$. The summary of 2D numerical examples can be found in Table 6.6. It can be seen that we obtain optimal convergence for Θ_{UW} which verifies our theoretical results. However, when using parameters in Θ_{GR}, unlike the 1D case, the 2D numerical results are less clean and even unstable, due to stability issues arising from spatial discretization.

In addition, we have tested the performance of ultra-weak DG methods on the 2D heat and linear convection-diffusion equations, which (if they converge) seem to have cleaner order of convergence compared with nonlinear models. This may partially result from the nonlinearity of the convection term and the use of global Lax-Friedrich flux. The same convergence rate as in Table 6.6 has been observed, with only one difference marked by $\mathtt{U}^\star$. For this test, the ultra-weak DG method is unstable for the heat equation, while optimal for the convection-diffusion equation with linear or quadratic convection, probably due to the existence of numerical viscosity in approximating the convection term.

Example 6.3. In this example, we consider the one-dimensional biharmonic equation with source term R, written as:
$$u_t + u_{xxxx} = R, \tag{6.7}$$

with the exact solution
$$u(x,t) = e^t \sin(x), \quad \text{on } [0, 2\pi] \times [0, 1]. \tag{6.8}$$

The local ultra-weak DG scheme (5.3) is applied to solve the above equation. We choose different sets of the parameters α, c_1 and c_2, and test this example with the final time $L = 1$. We summarize the numerical results for polynomial order $1 \le k \le 3$ in Table 6.10. For all the numerical fluxes tested, $\mathtt{k+1}$ order optimal convergence is observed. It is remarkable that central flux with $k = 1$ does not belong to either Θ_{UW} or Θ_{GR}. However, the numerical test shows the ultra-weak DG scheme still works well under this setting.

Flux	Table	Parameters			$\mathcal{P}_1$	$\mathcal{P}_2$	$\mathcal{P}_3$	$\mathcal{Q}_1$	$\mathcal{Q}_2$	$\mathcal{Q}_3$
		α	c_1	c_2						
Θ_{UW}										
General Flux	6.7	1/2	-41	1	k+1	k+1	k+1	k+1	k+1	k+1
IPDG	6.8	0	-40	0	k+1	k+1	k+1	k+1	k+1	k+1
$\alpha\beta$ Flux [18]	6.9	1/2	-121	0	k+1	k+1	k+1	k+1	k+1	k+1
Θ_{GR}										
General Flux	-	1/2	-10	1	k+1	k+1	U	k+1	k+1	k+1
Alternating Flux	-	1/2	0	0	U	U	k+1	U	U	U
$\alpha\beta$ Flux	-	0.3	0.4	0.4	k+1	U	U*	U	U	k+1
Central Flux ($k \geq 2$)	-	0	0	0	-	U	U	-	U	U
Other fluxes										
Central Flux ($k = 1$)	-	0	0	0	U	-	-	U	-	-

Table 6.6: Summary of numerical experiments for 2D ultra-weak DG scheme with parameters, where 'U' means unstable numerical results are observed, 'k+1' means optimal convergence, U* means unstable for the heat equation, but optimal for the convection-diffusion equation with linear or quadratic convection.

Parameters		$\mathcal{P}_k$ Spaces				$\mathcal{Q}_k$ Spaces			
k	N	L^2 error	order	H^1 error	order	L^2 error	order	H^1 error	order
1	20	5.2441×10^{-1}	-	2.8334×10^{0}	-	2.4117×10^{-1}	-	1.5622×10^{0}	-
	40	1.5928×10^{-1}	1.72	1.0862×10^{0}	1.38	6.4138×10^{-2}	1.91	6.3800×10^{-1}	1.29
	80	4.2071×10^{-2}	1.92	4.4173×10^{-1}	1.30	1.6264×10^{-2}	1.98	2.9090×10^{-1}	1.13
	160	1.0668×10^{-2}	1.98	1.9615×10^{-1}	1.17	4.0867×10^{-3}	1.99	1.4029×10^{-1}	1.05
2	10	3.7067×10^{-2}	-	3.8097×10^{-1}	-	9.7826×10^{-3}	-	2.0086×10^{-1}	-
	20	2.7829×10^{-3}	3.74	8.7515×10^{-2}	2.12	1.5256×10^{-3}	2.68	4.6569×10^{-2}	2.11
	40	2.7454×10^{-4}	3.34	2.1666×10^{-2}	2.01	2.2942×10^{-4}	2.73	1.1302×10^{-2}	2.04
	80	3.4569×10^{-5}	2.99	5.4034×10^{-3}	2.00	3.2648×10^{-5}	2.81	2.7950×10^{-3}	2.02
3	10	1.1902×10^{-3}	-	4.3722×10^{-2}	-	7.8639×10^{-4}	-	1.6524×10^{-2}	-
	20	7.3350×10^{-5}	4.02	5.1458×10^{-3}	3.09	5.7909×10^{-5}	3.76	2.0549×10^{-3}	3.01
	40	4.7716×10^{-6}	3.94	6.3026×10^{-4}	3.03	3.9769×10^{-6}	3.86	2.5560×10^{-4}	3.01
	50	1.9782×10^{-6}	3.95	3.2186×10^{-4}	3.01	1.6628×10^{-6}	3.91	1.3074×10^{-4}	3.00

Table 6.7: Numerical error and convergence rate for the 2D quadratic convection-diffusion equation, with parameter $(1/2, -41, 1)$

Example 6.4. We consider the two-dimensional time-dependent biharmonic equation with the source term R:

$$u_t + \Delta^2 u = R, \tag{6.9}$$

with the exact solution written in the form

$$u(x, y, t) = e^{-t} \sin(\pi(x + y)), \quad \text{on } [-2, 2]^2 \times [0, 1]. \tag{6.10}$$

We test this example with the final time $L = 1$, using represented numerical fluxes with polynomial order $1 \leq k \leq 3$. The summarized results are listed in Table 6.15. When $(\alpha, c_1, c_2) \in \Theta_{UW}$, it can be observed that the numerical results verify our theoretical findings. For $(\alpha, c_1, c_2) \in \Theta_{GR}$, the ultra-weak scheme works well on $\mathcal{Q}_k$ spaces which can be proved rigorously. There are no analytical results on $\mathcal{P}_k$ spaces with the triangular mesh. Numerically, most of these methods work well, as

Parameters		$\mathcal{P}_k$ Spaces				$\mathcal{Q}_k$ Spaces			
k	N	L^2 error	order	H^1 error	order	L^2 error	order	H^1 error	order
1	20	7.4724×10^{-2}	-	1.8625×10^0	-	3.4415×10^{-2}	-	1.1401×10^0	-
	40	1.9602×10^{-2}	1.93	9.2906×10^{-1}	1.00	1.0251×10^{-2}	1.75	5.6201×10^{-1}	1.02
	80	5.3142×10^{-3}	1.88	4.6301×10^{-1}	1.00	3.3298×10^{-3}	1.62	2.7924×10^{-1}	1.01
	160	1.3826×10^{-3}	1.94	2.2979×10^{-1}	1.01	9.2290×10^{-4}	1.85	1.3857×10^{-1}	1.01
2	10	1.1708×10^{-2}	-	4.2302×10^{-1}	-	9.5696×10^{-3}	-	1.9432×10^{-1}	-
	20	1.7251×10^{-3}	2.76	1.0648×10^{-1}	1.99	1.5201×10^{-3}	2.65	4.6144×10^{-2}	2.07
	40	2.5072×10^{-4}	2.78	2.6622×10^{-2}	2.00	2.2923×10^{-4}	2.73	1.1274×10^{-2}	2.03
	80	3.5036×10^{-5}	2.84	6.6517×10^{-3}	2.00	3.2639×10^{-5}	2.81	2.7933×10^{-3}	2.01
3	10	8.0828×10^{-4}	-	3.4523×10^{-2}	-	6.6334×10^{-4}	-	1.0888×10^{-2}	-
	20	5.7426×10^{-5}	3.82	4.2895×10^{-3}	3.01	5.0207×10^{-5}	3.72	1.2469×10^{-3}	3.13
	40	3.9211×10^{-6}	3.87	5.3461×10^{-4}	3.00	3.5217×10^{-6}	3.83	1.5014×10^{-4}	3.05
	50	1.6391×10^{-6}	3.91	2.7359×10^{-4}	3.00	1.4795×10^{-6}	3.89	7.6422×10^{-5}	3.03

Table 6.8: Numerical error and convergence rate for the 2D quadratic convection-diffusion equation, with parameter $(0, -40, 0)$

Parameters		$\mathcal{P}_k$ Spaces				$\mathcal{Q}_k$ Spaces			
k	N	L^2 error	order	H^1 error	order	L^2 error	order	H^1 error	order
1	20	7.6357×10^{-2}	-	1.8862×10^0	-	3.4214×10^{-2}	-	1.1403×10^0	-
	40	1.9964×10^{-2}	1.94	9.4490×10^{-1}	1.00	1.0217×10^{-2}	1.74	5.6207×10^{-1}	1.02
	80	5.3951×10^{-3}	1.89	4.7213×10^{-1}	1.00	3.3251×10^{-3}	1.62	2.7928×10^{-1}	1.01
	160	1.4019×10^{-3}	1.94	2.3524×10^{-1}	1.01	9.2198×10^{-4}	1.85	1.3858×10^{-1}	1.01
2	10	1.2530×10^{-2}	-	4.4638×10^{-1}	-	9.7027×10^{-3}	-	1.9387×10^{-1}	-
	20	1.8284×10^{-3}	2.78	1.1284×10^{-1}	1.98	1.5351×10^{-3}	2.66	4.6091×10^{-2}	2.07
	40	2.6252×10^{-4}	2.80	2.8243×10^{-2}	2.00	2.3089×10^{-4}	2.73	1.1263×10^{-2}	2.03
	80	3.6389×10^{-5}	2.85	7.0589×10^{-3}	2.00	3.2826×10^{-5}	2.81	2.7906×10^{-3}	2.01
3	10	8.2583×10^{-4}	-	3.5959×10^{-2}	-	6.6158×10^{-4}	-	1.0882×10^{-2}	-
	20	5.8060×10^{-5}	3.83	4.4801×10^{-3}	3.00	5.0097×10^{-5}	3.72	1.2489×10^{-3}	3.12
	40	3.9525×10^{-6}	3.88	5.5894×10^{-4}	3.00	3.5153×10^{-6}	3.83	1.5048×10^{-4}	3.05
	50	1.6514×10^{-6}	3.91	2.8609×10^{-4}	3.00	1.4770×10^{-6}	3.89	7.6601×10^{-5}	3.03

Table 6.9: Numerical error and convergence rate for the 2D quadratic convection-diffusion equation, with parameter $(1/2, -121, 0)$

seen in Table 6.15. It is worth mentioning that if central flux is taken, similar optimal results in the 1D case are observed, although the case with $k = 1$ is not included in either set Θ_{GR} or Θ_{UW}. However, when the alternating flux and generalized alternating flux are taken on triangular mesh and $\mathcal{P}_1$ space, the local ultra-weak DG scheme converges to a wrong solution, and we observe that the numerical error converges to constants larger than 0 (see Table 6.20 and 6.22). This observation has been cross validated with multiple software codes. For spaces $\mathcal{P}_2$ and $\mathcal{P}_3$, the method behaves optimally. These observations suggest the preference to use high order spatial spaces ($k \geq 1$) of the ultra-weak scheme, which is also reflected in Figure 3.2, where we found the range of Θ_{GR} varies significantly when $k = 1$ switches to $k \geq 1$.

Flux	Table	α	c_1	c_2	$\mathcal{P}_1$	$\mathcal{P}_2$	$\mathcal{P}_3$
		Parameters				
Θ_{UW}							
General Flux	6.11	1/2	-17	1	k+1	k+1	k+1
IPDG	6.11	0	-17	0	k+1	k+1	k+1
$\alpha\beta$ Flux [18]	6.12	1/2	-26	0	k+1	k+1	k+1
Θ_{GR}							
General Flux	6.12	1/2	0	1	k+1	k+1	k+1
Alternating Flux	6.13	1/2	0	0	k+1	k+1	k+1
$\alpha\beta$ Flux	6.13	0.3	0.4	0.4	k+1	k+1	k+1
generalized Alternating Flux	6.14	0.8	0	0	k+1	k+1	k+1
Central Flux ($k \geq 2$)	6.14	0	0	0	-	k+1	k+1
Other flux							
Central Flux ($k = 1$)	6.14	0	0	0	k+1	-	-

Table 6.10: Summary of numerical experiments of 1D Local ultra-weak DG scheme with parameters for the biharmonic equation.

Parameters		$(1/2, -17, 1)$				$(0, -17, 0)$			
k	N	L^2 error	order	H^1 error	order	L^2 error	order	H^1 error	order
1	320	1.2291×10^{-3}	-	1.9311×10^{-2}	-	1.1989×10^{-4}	-	1.9610×10^{-2}	-
	640	3.0730×10^{-4}	2.00	9.6411×10^{-3}	1.00	2.9972×10^{-5}	2.00	9.8049×10^{-3}	1.00
	1280	7.6826×10^{-5}	2.00	4.8188×10^{-3}	1.00	7.4930×10^{-6}	2.00	4.9025×10^{-3}	1.00
	2560	1.9207×10^{-5}	2.00	2.4092×10^{-3}	1.00	1.8735×10^{-6}	2.00	2.4512×10^{-3}	1.00
2	20	5.0644×10^{-4}	-	1.3652×10^{-2}	-	4.9537×10^{-4}	-	1.3620×10^{-2}	-
	40	6.1881×10^{-5}	3.03	3.3901×10^{-3}	2.01	6.1803×10^{-5}	3.00	3.4080×10^{-3}	2.00
	80	7.6909×10^{-6}	3.01	8.4608×10^{-4}	2.00	7.7218×10^{-6}	3.00	8.5218×10^{-4}	2.00
	160	9.5999×10^{-7}	3.00	2.1143×10^{-4}	2.00	9.6513×10^{-7}	3.00	2.1306×10^{-4}	2.00
3	10	4.0354×10^{-4}	-	4.5411×10^{-3}	-	1.7014×10^{-4}	-	3.1849×10^{-3}	-
	20	2.7745×10^{-5}	3.86	5.7434×10^{-4}	2.98	1.0786×10^{-5}	3.98	3.9658×10^{-4}	3.01
	40	1.7796×10^{-6}	3.96	7.1891×10^{-5}	3.00	6.7658×10^{-7}	3.99	4.9513×10^{-5}	3.00
	80	1.1316×10^{-7}	3.98	8.9882×10^{-6}	3.00	4.4973×10^{-8}	3.91	6.1882×10^{-6}	3.00

Table 6.11: Numerical error and convergence rate for the 1D biharmonic equation, with parameter $(1/2, -17, 1)$ (Left) and $(0, -17, 0)$ (Right)

Parameters		$\mathcal{P}_k$ Spaces				$\mathcal{Q}_k$ Spaces			
k	N	L^2 error	order	H^1 error	order	L^2 error	order	H^1 error	order
1	20	5.8711×10^{-1}	-	2.7270×10^{0}	-	5.2541×10^{-1}	-	2.3969×10^{0}	-
	40	2.3134×10^{-1}	1.34	1.1079×10^{0}	1.30	1.9029×10^{-1}	1.47	9.2241×10^{-1}	1.38
	80	6.7007×10^{-2}	1.79	3.5095×10^{-1}	1.66	5.3271×10^{-2}	1.84	3.1169×10^{-1}	1.57
	160	1.7431×10^{-2}	1.94	1.1708×10^{-1}	1.58	1.3722×10^{-2}	1.96	1.2056×10^{-1}	1.37
2	10	1.3733×10^{-2}	-	3.0145×10^{-1}	-	2.1371×10^{-2}	-	3.2248×10^{-1}	-
	20	1.0946×10^{-3}	3.65	6.7930×10^{-2}	2.15	1.8186×10^{-3}	3.55	7.1052×10^{-2}	2.18
	40	1.1754×10^{-4}	3.22	1.6516×10^{-2}	2.04	2.0104×10^{-4}	3.18	1.7211×10^{-2}	2.05
	80	1.4089×10^{-5}	3.06	4.0998×10^{-3}	2.01	2.4305×10^{-5}	3.05	4.2689×10^{-3}	2.01
3	10	1.3157×10^{-3}	-	3.9173×10^{-2}	-	2.0996×10^{-3}	-	4.2032×10^{-2}	-
	20	1.0608×10^{-4}	3.63	5.3911×10^{-3}	2.86	1.7184×10^{-4}	3.61	5.9497×10^{-3}	2.82
	40	7.2544×10^{-6}	3.87	6.8897×10^{-4}	2.97	1.1676×10^{-5}	3.88	7.7066×10^{-4}	2.95
	50	2.9907×10^{-6}	3.97	3.5361×10^{-4}	2.99	4.8347×10^{-6}	3.95	3.9632×10^{-4}	2.98

Table 6.16: Numerical error and convergence rate for the 2D quadratic convection-diffusion equation, with parameter $(1/2, -41, 1)$

Parameters		(1/2, −26, 0)				(1/2, 0, 1)			
k	N	L^2 error	order	H^1 error	order	L^2 error	order	H^1 error	order
1	320	1.0989×10^{-4}	-	1.9369×10^{-2}	-	1.5026×10^{-3}	-	4.2225×10^{-2}	-
	640	2.7473×10^{-5}	2.00	9.6844×10^{-3}	1.00	3.7555×10^{-4}	2.00	2.1112×10^{-2}	1.00
	1280	6.8683×10^{-6}	2.00	4.8422×10^{-3}	1.00	9.3880×10^{-5}	2.00	1.0556×10^{-2}	1.00
	2560	1.7177×10^{-6}	2.00	2.4211×10^{-3}	1.00	2.3469×10^{-5}	2.00	5.2781×10^{-3}	1.00
2	20	5.2064×10^{-4}	-	1.2675×10^{-2}	-	2.5193×10^{-3}	-	2.6150×10^{-2}	-
	40	6.5141×10^{-5}	3.00	3.1721×10^{-3}	2.00	3.1721×10^{-4}	2.99	6.5810×10^{-3}	1.99
	80	8.1448×10^{-6}	3.00	7.9323×10^{-4}	2.00	3.9724×10^{-5}	3.00	1.6480×10^{-3}	2.00
	160	1.0182×10^{-6}	3.00	1.9832×10^{-4}	2.00	4.9678×10^{-6}	3.00	4.1219×10^{-4}	2.00
3	10	1.4050×10^{-4}	-	2.6762×10^{-3}	-	4.5029×10^{-4}	-	4.6036×10^{-3}	-
	20	8.7958×10^{-6}	4.00	3.3584×10^{-4}	2.99	2.8275×10^{-5}	3.99	5.7808×10^{-4}	2.99
	40	5.4995×10^{-7}	4.00	4.2021×10^{-5}	3.00	1.7692×10^{-6}	4.00	7.2340×10^{-5}	3.00
	80	3.8043×10^{-8}	3.85	5.2548×10^{-6}	3.00	1.1164×10^{-7}	3.99	9.0451×10^{-6}	3.00

Table 6.12: Numerical error and convergence rate for the 1D biharmonic equation, with parameter $(1/2, -26, 0)$ (Left) and $(1/2, 0, 1)$ (Right)

Parameters		(1/2, 0, 0)				(0.3, 0.4, 0.4)			
k	N	L^2 error	order	H^1 error	order	L^2 error	order	H^1 error	order
1	320	4.1225×10^{-4}	-	4.2223×10^{-2}	-	6.2801×10^{-4}	-	2.6643×10^{-2}	-
	640	1.0306×10^{-4}	2.00	2.1112×10^{-2}	1.00	1.5699×10^{-4}	2.00	1.3322×10^{-2}	1.00
	1280	2.5764×10^{-5}	2.00	1.0556×10^{-2}	1.00	3.9245×10^{-5}	2.00	6.6609×10^{-3}	1.00
	2560	6.4409×10^{-6}	2.00	5.2781×10^{-3}	1.00	9.8112×10^{-6}	2.00	3.3304×10^{-3}	1.00
2	20	1.1591×10^{-3}	-	2.1975×10^{-2}	-	2.0656×10^{-3}	-	2.2263×10^{-2}	-
	40	1.4539×10^{-4}	2.99	5.5090×10^{-3}	2.00	2.5977×10^{-4}	2.99	5.5941×10^{-3}	1.99
	80	1.8191×10^{-5}	3.00	1.3782×10^{-3}	2.00	3.2521×10^{-5}	3.00	1.4003×10^{-3}	2.00
	160	2.2744×10^{-6}	3.00	3.4461×10^{-4}	2.00	4.0667×10^{-6}	3.00	3.5020×10^{-4}	2.00
3	10	2.5672×10^{-4}	-	4.4929×10^{-3}	-	4.1812×10^{-4}	-	4.3513×10^{-3}	-
	20	1.6086×10^{-5}	4.00	5.6472×10^{-4}	2.99	2.6241×10^{-5}	3.99	5.4618×10^{-4}	2.99
	40	1.0061×10^{-6}	4.00	7.0688×10^{-5}	3.00	1.6417×10^{-6}	4.00	6.8342×10^{-5}	3.00
	80	6.4098×10^{-8}	3.97	8.8404×10^{-6}	3.00	1.0373×10^{-7}	3.98	8.5452×10^{-6}	3.00

Table 6.13: Numerical error and convergence rate for the 1D biharmonic equation, with parameter $(1/2, 0, 0)$ (Left) and $(0.3, 0.4, 0.4)$ (Right)

Parameters		$\mathcal{P}_k$ Spaces				$\mathcal{Q}_k$ Spaces			
k	N	L^2 error	order	H^1 error	order	L^2 error	order	H^1 error	order
1	20	6.0177×10^{-2}	-	8.1167×10^{-1}	-	6.6194×10^{-2}	-	8.4803×10^{-1}	-
	40	1.5483×10^{-2}	1.96	4.0213×10^{-1}	1.01	1.7006×10^{-2}	1.96	4.2056×10^{-1}	1.01
	80	3.8989×10^{-3}	1.99	2.0053×10^{-1}	1.00	4.2807×10^{-3}	1.99	2.0979×10^{-1}	1.00
	160	9.7648×10^{-4}	2.00	1.0020×10^{-1}	1.00	1.0720×10^{-3}	2.00	1.0483×10^{-1}	1.00
2	10	7.7278×10^{-3}	-	2.4104×10^{-1}	-	1.3269×10^{-2}	-	2.6963×10^{-1}	-
	20	8.2848×10^{-4}	3.22	6.1475×10^{-2}	1.97	1.5652×10^{-3}	3.08	6.7929×10^{-2}	1.99
	40	9.8957×10^{-5}	3.07	1.5449×10^{-2}	1.99	1.9266×10^{-4}	3.02	1.7019×10^{-2}	2.00
	80	1.2227×10^{-5}	3.02	3.8674×10^{-3}	2.00	2.3991×10^{-5}	3.01	4.2570×10^{-3}	2.00
3	10	5.1967×10^{-4}	-	2.4046×10^{-2}	-	9.3230×10^{-4}	-	2.8650×10^{-2}	-
	20	3.3442×10^{-5}	3.96	2.9855×10^{-3}	3.01	6.0347×10^{-5}	3.95	3.6057×10^{-3}	2.99
	40	2.1044×10^{-6}	3.99	3.7200×10^{-4}	3.00	3.8057×10^{-6}	3.99	4.5130×10^{-4}	3.00
	50	8.6313×10^{-7}	3.99	1.9038×10^{-4}	3.00	1.5607×10^{-6}	3.99	2.3110×10^{-4}	3.00

Table 6.17: Numerical error for 2D, biharmonic equation, with parameter $(0, -40, 0)$

Parameters		(0.8, 0, 0)				(0, 0, 0)			
k	N	L^2 error	order	H^1 error	order	L^2 error	order	H^1 error	order
1	320	8.3592×10^{-4}	-	6.0787×10^{-2}	-	1.1991×10^{-4}	-	1.9611×10^{-2}	-
	640	2.0898×10^{-4}	2.00	3.0396×10^{-2}	1.00	2.9973×10^{-5}	2.00	9.8051×10^{-3}	1.00
	1280	5.2243×10^{-5}	2.00	1.5198×10^{-2}	1.00	7.4930×10^{-6}	2.00	4.9025×10^{-3}	1.00
	2560	1.3061×10^{-5}	2.00	7.5992×10^{-3}	1.00	1.8732×10^{-6}	2.00	2.4512×10^{-3}	1.00
2	20	8.8953×10^{-4}	-	1.9209×10^{-2}	-	2.8862×10^{-3}	-	2.9622×10^{-2}	-
	40	1.1056×10^{-4}	3.01	4.7950×10^{-3}	2.00	3.7750×10^{-4}	2.93	7.6032×10^{-3}	1.96
	80	1.3800×10^{-5}	3.00	1.1983×10^{-3}	2.00	4.7743×10^{-5}	2.98	1.9138×10^{-3}	1.99
	160	1.7244×10^{-6}	3.00	2.9955×10^{-4}	2.00	5.9855×10^{-6}	3.00	4.7927×10^{-4}	2.00
3	10	3.0395×10^{-4}	-	4.6108×10^{-3}	-	1.8758×10^{-4}	-	3.2446×10^{-3}	-
	20	1.9517×10^{-5}	3.96	5.8291×10^{-4}	2.98	1.1060×10^{-5}	4.08	3.9836×10^{-4}	3.03
	40	1.2284×10^{-6}	3.99	7.3071×10^{-5}	3.00	6.8085×10^{-7}	4.02	4.9568×10^{-5}	3.01
	80	7.7935×10^{-8}	3.98	9.1415×10^{-6}	3.00	4.4897×10^{-8}	3.92	6.1900×10^{-6}	3.00

Table 6.14: Numerical error and convergence rate for the 1D biharmonic equation, with parameter $(0.8, 0, 0)$ (Left) and $(0, 0, 0)$ (Right)

Flux	Table	Parameters			$\mathcal{P}_1$	$\mathcal{P}_2$	$\mathcal{P}_3$	$\mathcal{Q}_1$	$\mathcal{Q}_2$	$\mathcal{Q}_3$
		α	c_1	c_2						
Θ_{UW}										
General Flux	6.16	1/2	-41	1	k+1	k+1	k+1	k+1	k+1	k+1
IPDG	6.17	0	-40	0	k+1	k+1	k+1	k+1	k+1	k+1
$\alpha\beta$ Flux [18]	6.18	1/2	-121	0	k+1	k+1	k+1	k+1	k+1	k+1
Θ_{GR}										
General Flux	6.19	1/2	-10	1	k+1	k+1	S	k+1	k+1	k+1
Alternating Flux	6.20	1/2	0	0	D	k+1	k+1	k+1	k+1	k+1
$\alpha\beta$ Flux	6.21	0.3	0.4	0.4	k+1	S	k+1	k+1	k+1	k+1
Generalized Alternating Flux	6.22	0.8	0	0	D	k+1	k+1	k+1	k+1	k+1
Central Flux ($k \geq 2$)	6.23	0	0	0	-	k+1	k+1	-	k+1	k+1
Other flux										
Central Flux ($k = 1$)	6.23	0	0	0	k+1	-	-	k+1	-	-

Table 6.15: Summary of numerical experiments of 2D ultra-weak DG scheme with parameters for the time-dependent biharmonic equation. In the table, D represents stable, but the numerical algorithm converges to a solution which is not an exact solution. S means a convergent result is observed, but the convergence order is not clean.

Parameters		$\mathcal{P}_k$ Spaces				$\mathcal{Q}_k$ Spaces			
k	N	L^2 error	order	H^1 error	order	L^2 error	order	H^1 error	order
1	20	6.1496×10^{-2}	-	8.3224×10^{-1}	-	6.4815×10^{-2}	-	8.4615×10^{-1}	-
	40	1.5751×10^{-2}	1.97	4.1382×10^{-1}	1.01	1.6600×10^{-2}	1.97	4.2032×10^{-1}	1.01
	80	3.9615×10^{-3}	1.99	2.0658×10^{-1}	1.00	4.1750×10^{-3}	1.99	2.0978×10^{-1}	1.00
	160	9.9184×10^{-4}	2.00	1.0325×10^{-1}	1.00	1.0455×10^{-3}	2.00	1.0484×10^{-1}	1.00
2	10	1.0002×10^{-2}	-	2.5340×10^{-1}	-	1.4046×10^{-2}	-	2.6992×10^{-1}	-
	20	1.1376×10^{-3}	3.14	6.4707×10^{-2}	1.97	1.7023×10^{-3}	3.04	6.7916×10^{-2}	1.99
	40	1.3813×10^{-4}	3.04	1.6267×10^{-2}	1.99	2.1111×10^{-4}	3.01	1.7007×10^{-2}	2.00
	80	1.7137×10^{-5}	3.01	4.0725×10^{-3}	2.00	2.6339×10^{-5}	3.00	4.2535×10^{-3}	2.00
3	10	6.0022×10^{-4}	-	2.5546×10^{-2}	-	9.2133×10^{-4}	-	2.8611×10^{-2}	-
	20	3.6689×10^{-5}	4.03	3.2194×10^{-3}	2.99	5.7451×10^{-5}	4.00	3.6095×10^{-3}	2.99
	40	2.2787×10^{-6}	4.01	4.0319×10^{-4}	3.00	3.5866×10^{-6}	4.00	4.5225×10^{-4}	3.00
	50	9.3394×10^{-7}	4.00	2.0648×10^{-4}	3.00	1.4700×10^{-6}	4.00	2.3162×10^{-4}	3.00

Table 6.18: Numerical error for 2D, biharmonic equation, with parameter $(1/2, -121, 0)$

Parameters		$\mathcal{P}_k$ Spaces				$\mathcal{Q}_k$ Spaces			
k	N	L^2 error	order	H^1 error	order	L^2 error	order	H^1 error	order
1	20	4.3028×10^{-1}	-	2.3548×10^{0}	-	5.0671×10^{-1}	-	2.4043×10^{0}	-
	40	1.5915×10^{-1}	1.43	9.2726×10^{-1}	1.34	1.8533×10^{-1}	1.45	9.3813×10^{-1}	1.36
	80	4.5056×10^{-2}	1.82	3.0572×10^{-1}	1.60	5.2116×10^{-2}	1.83	3.1813×10^{-1}	1.56
	160	1.1646×10^{-2}	1.95	1.1235×10^{-1}	1.44	1.3443×10^{-2}	1.95	1.2289×10^{-1}	1.37
2	10	7.9854×10^{-3}	-	3.9107×10^{-1}	-	1.5439×10^{-2}	-	3.2937×10^{-1}	-
	20	6.6730×10^{-4}	3.58	8.4283×10^{-2}	2.21	1.0817×10^{-3}	3.84	7.3154×10^{-2}	2.17
	40	7.1666×10^{-5}	3.22	2.0257×10^{-2}	2.06	1.0573×10^{-4}	3.35	1.7737×10^{-2}	2.04
	80	8.5792×10^{-6}	3.06	5.0142×10^{-3}	2.01	1.2219×10^{-5}	3.11	4.4002×10^{-3}	2.01
3	10	8.4568×10^{-3}	-	2.7429×10^{-1}	-	1.7430×10^{-3}	-	4.8199×10^{-2}	-
	20	1.7262×10^{-4}	5.61	1.0341×10^{-2}	4.73	1.5955×10^{-4}	3.45	6.5142×10^{-3}	2.89
	40	7.9633×10^{-6}	4.44	8.5127×10^{-4}	3.60	1.1407×10^{-5}	3.81	7.9708×10^{-4}	3.03
	50	3.8125×10^{-6}	3.30	4.0748×10^{-4}	3.30	4.7574×10^{-6}	3.92	4.0545×10^{-4}	3.03

Table 6.19: Numerical error for 2D, biharmonic equation, with parameter $(1/2, -10, 1)$

Parameters		$\mathcal{P}_k$ Spaces				$\mathcal{Q}_k$ Spaces			
k	N	L^2 error	order	H^1 error	order	L^2 error	order	H^1 error	order
1	20	4.6236×10^{2}	-	3.2641×10^{0}	-	2.6103×10^{-1}	-	1.6419×10^{0}	-
	40	4.7880×10^{2}	-	3.3518×10^{0}	-	7.0139×10^{-2}	1.90	8.3404×10^{-1}	0.98
	80	4.8606×10^{2}	-	3.4100×10^{0}	-	1.7841×10^{-2}	1.98	4.1869×10^{-1}	0.99
	160	4.8942×10^{2}	-	3.4400×10^{0}	-	4.4793×10^{-3}	1.99	2.0956×10^{-1}	1.00
2	10	3.6567×10^{-2}	-	4.6001×10^{-1}	-	3.3958×10^{-2}	-	4.0885×10^{-1}	-
	20	3.8861×10^{-3}	3.23	1.0083×10^{-1}	2.19	4.2845×10^{-3}	2.99	1.0220×10^{-1}	2.00
	40	4.8886×10^{-4}	2.99	2.5171×10^{-2}	2.00	5.3733×10^{-4}	3.00	2.5522×10^{-2}	2.00
	80	6.1471×10^{-5}	2.99	6.3003×10^{-3}	2.00	6.7226×10^{-5}	3.00	6.3782×10^{-3}	2.00
3	10	1.6826×10^{-3}	-	3.7294×10^{-2}	-	1.8272×10^{-3}	-	3.8179×10^{-2}	-
	20	9.4890×10^{-5}	4.15	4.3465×10^{-3}	3.10	1.1541×10^{-4}	3.98	4.8054×10^{-3}	2.99
	40	5.5928×10^{-6}	4.08	5.1669×10^{-4}	3.07	7.2283×10^{-6}	4.00	6.0165×10^{-4}	3.00
	50	2.2617×10^{-6}	4.06	2.6155×10^{-4}	3.05	2.9615×10^{-6}	4.00	3.0810×10^{-4}	3.00

Table 6.20: Numerical error for 2D, biharmonic equation, with parameter $(1/2, 0, 0)$

Parameters		$\mathcal{P}_k$ Spaces				$\mathcal{Q}_k$ Spaces			
k	N	L^2 error	order	H^1 error	order	L^2 error	order	H^1 error	order
1	20	2.7281×10^{-1}	-	1.0641×10^{0}	-	3.9476×10^{-1}	-	1.4447×10^{0}	-
	40	7.7330×10^{-2}	1.82	4.5818×10^{-1}	1.22	1.0944×10^{-1}	1.85	5.8052×10^{-1}	1.32
	80	2.0011×10^{-2}	1.95	2.1757×10^{-1}	1.07	2.8049×10^{-2}	1.96	2.6874×10^{-1}	1.11
	160	5.0553×10^{-3}	1.98	1.0713×10^{-1}	1.02	7.0557×10^{-3}	1.99	1.3151×10^{-1}	1.03
2	10	2.0988×10^{0}	-	2.2654×10^{1}	-	5.5724×10^{-2}	-	4.9949×10^{-1}	-
	20	2.9742×10^{-2}	6.14	6.3146×10^{-1}	5.16	7.2119×10^{-3}	2.95	1.2100×10^{-1}	2.05
	40	4.9696×10^{-3}	2.58	1.9670×10^{-1}	1.68	9.1042×10^{-4}	2.99	2.9859×10^{-2}	2.02
	80	1.5805×10^{-4}	4.97	1.3428×10^{-2}	3.87	1.1408×10^{-4}	3.00	7.4368×10^{-3}	2.01
3	10	1.7105×10^{-3}	-	3.4995×10^{-2}	-	2.8104×10^{-3}	-	4.6772×10^{-2}	-
	20	1.0043×10^{-4}	4.09	4.3282×10^{-3}	3.02	1.7880×10^{-4}	3.97	5.8547×10^{-3}	3.00
	40	6.1956×10^{-6}	4.02	5.4046×10^{-4}	3.00	1.1219×10^{-5}	3.99	7.3183×10^{-4}	3.00
	50	2.5367×10^{-6}	4.00	2.7671×10^{-4}	3.00	4.5977×10^{-6}	4.00	3.7469×10^{-4}	3.00

Table 6.21: Numerical error for 2D, biharmonic equation, with parameter $(0.3, 0.4, 0.4)$

Parameters		$\mathcal{P}_k$ Spaces				$\mathcal{Q}_k$ Spaces			
k	N	L^2 error	order	H^1 error	order	L^2 error	order	H^1 error	order
1	20	3.8323×10^1	-	4.5664×10^1	-	4.5023×10^{-1}	-	2.3601×10^0	-
	40	3.7348×10^1	-	4.5257×10^1	-	1.4078×10^{-1}	1.68	1.2251×10^0	0.95
	80	3.7269×10^1	-	4.5392×10^1	-	3.7390×10^{-2}	1.91	6.1650×10^{-1}	0.99
	160	3.7329×10^1	-	4.5541×10^1	-	9.4931×10^{-3}	1.98	3.0867×10^{-1}	1.00
2	10	5.2535×10^{-2}	-	6.1377×10^{-1}	-	2.9523×10^{-2}	-	3.7521×10^{-1}	-
	20	3.5989×10^{-3}	3.87	9.5501×10^{-2}	2.68	3.2049×10^{-3}	3.20	8.7506×10^{-2}	2.10
	40	4.2267×10^{-4}	3.09	2.2787×10^{-2}	2.07	3.8521×10^{-4}	3.06	2.1481×10^{-2}	2.03
	80	5.2348×10^{-5}	3.01	5.6516×10^{-3}	2.01	4.7669×10^{-5}	3.01	5.3454×10^{-3}	2.01
3	10	4.8013×10^{-3}	-	9.7740×10^{-2}	-	2.0124×10^{-3}	-	4.0358×10^{-2}	-
	20	2.1666×10^{-4}	4.47	9.3581×10^{-3}	3.38	1.4097×10^{-4}	3.84	5.3643×10^{-3}	2.91
	40	1.0510×10^{-5}	4.37	9.2560×10^{-4}	3.34	9.0996×10^{-6}	3.95	6.8214×10^{-4}	2.98
	50	4.0172×10^{-6}	4.31	4.4337×10^{-4}	3.30	3.7421×10^{-6}	3.98	3.5000×10^{-4}	2.99

Table 6.22: Numerical error for 2D, biharmonic equation, with parameter $(0.8, 0, 0)$

Parameters		$\mathcal{P}_k$ Spaces				$\mathcal{Q}_k$ Spaces			
k	N	L^2 error	order	H^1 error	order	L^2 error	order	H^1 error	order
1	20	3.3726×10^{-2}	-	8.4539×10^{-1}	-	7.8927×10^{-2}	-	8.4553×10^{-1}	-
	40	8.3518×10^{-3}	2.01	4.2012×10^{-1}	1.01	1.7818×10^{-2}	2.15	4.2032×10^{-1}	1.01
	80	2.0830×10^{-3}	2.00	2.0973×10^{-1}	1.00	4.3316×10^{-3}	2.04	2.0977×10^{-1}	1.00
	160	5.2046×10^{-4}	2.00	1.0483×10^{-1}	1.00	1.0752×10^{-3}	2.01	1.0483×10^{-1}	1.00
2	10	1.6036×10^{-2}	-	2.9862×10^{-1}	-	4.5358×10^{-2}	-	4.9135×10^{-1}	-
	20	1.9435×10^{-3}	3.04	7.6181×10^{-2}	1.97	8.5739×10^{-3}	2.40	1.5206×10^{-1}	1.69
	40	2.4054×10^{-4}	3.01	1.9119×10^{-2}	1.99	1.2450×10^{-3}	2.78	4.0680×10^{-2}	1.90
	80	2.9991×10^{-5}	3.00	4.7841×10^{-3}	2.00	1.6231×10^{-4}	2.94	1.0353×10^{-2}	1.97
3	10	1.1052×10^{-3}	-	2.8789×10^{-2}	-	1.4260×10^{-3}	-	3.3482×10^{-2}	-
	20	6.0359×10^{-5}	4.19	3.2449×10^{-3}	3.15	6.8372×10^{-5}	4.38	3.7552×10^{-3}	3.16
	40	3.6805×10^{-6}	4.04	3.9871×10^{-4}	3.02	3.9326×10^{-6}	4.12	4.5596×10^{-4}	3.04
	50	1.5033×10^{-6}	4.01	2.0374×10^{-4}	3.01	1.5939×10^{-6}	4.05	2.3263×10^{-4}	3.02

Table 6.23: Numerical error for 2D, biharmonic equation, with parameter $(0, 0, 0)$

Example 6.5. In this example, we examine how the parameter ε affects the performance of ultra-weak DG scheme on the convection-diffusion equation. We consider the following equation on general dimension d:

$$u_t + \nabla \cdot (\mathbf{c}u) - \varepsilon \Delta u = R, \tag{6.11}$$

where $\mathbf{c}$ taken as $\mathbf{1}$, the vector full of 1. We conduct tests using the following exact solution for $d \geq 1$ [16, 24]:

$$u(x_1, ...x_d, t) = \sin\left(\sum_{i=1}^{d} x_i - t\right) e^{-\varepsilon t}. \tag{6.12}$$

For one-dimension $(d = 1)$, we test the numerical accuracy with same setting as examples above for mild values $\varepsilon = 0.1, 0.01$ and vanishing values $\varepsilon = 10^{-4}, 10^{-6}$. The convergence results are shown in Tables 6.24 and 6.25. For two-dimension $(d = 2)$, we only present vanishing values cases $\varepsilon = 10^{-5}, 10^{-6}$ in Table 6.26 and 6.27. Similar optimal results are observed for other ε values. All of these numerical examples validate our theoretical results.

Parameters		$\varepsilon = 0.1$				$\varepsilon = 0.01$			
k	N	L^2 error	order	H^1 error	order	L^2 error	order	H^1 error	order
1	320	8.4921×10^{-5}	-	6.4187×10^{-3}	-	4.8458×10^{-5}	-	7.0556×10^{-3}	-
	640	2.1234×10^{-5}	2.00	3.2085×10^{-3}	1.00	1.2130×10^{-5}	2.00	3.5184×10^{-3}	1.00
	1280	5.3088×10^{-6}	2.00	1.6040×10^{-3}	1.00	3.0350×10^{-6}	2.00	1.7570×10^{-3}	1.00
	2560	1.3271×10^{-6}	2.00	8.0196×10^{-4}	1.00	7.5907×10^{-7}	2.00	8.7796×10^{-4}	1.00
2	20	1.7356×10^{-4}	-	4.5901×10^{-3}	-	2.0062×10^{-4}		5.5358×10^{-3}	
	40	2.0915×10^{-5}	3.05	1.1333×10^{-3}	2.02	2.4305×10^{-5}	3.05	1.3004×10^{-3}	2.09
	80	2.5808×10^{-6}	3.02	2.8218×10^{-4}	2.01	2.9537×10^{-6}	3.04	3.1547×10^{-4}	2.04
	160	3.2097×10^{-7}	3.01	7.0443×10^{-5}	2.00	3.6100×10^{-7}	3.03	7.7833×10^{-5}	2.02
3	10	1.5686×10^{-4}		1.9252×10^{-3}		1.7818×10^{-4}	-	2.6674×10^{-3}	-
	20	1.0074×10^{-5}	3.96	2.1788×10^{-4}	3.14	1.7543×10^{-5}	3.34	4.6635×10^{-4}	2.52
	40	6.1312×10^{-7}	4.04	2.4945×10^{-5}	3.13	1.2166×10^{-6}	3.85	5.9734×10^{-5}	2.96
	80	3.8335×10^{-8}	4.00	3.0272×10^{-6}	3.04	5.8908×10^{-8}	4.37	5.4124×10^{-6}	3.46

Table 6.24: Numerical error and convergence rate for the 1D linear convection-diffusion equation, with $\varepsilon = 0.1$ (Left) and $\varepsilon = 0.01$ (Right)

Parameters		$\varepsilon = 10^{-4}$				$\varepsilon = 10^{-6}$			
k	N	L^2 error	order	H^1 error	order	L^2 error	order	H^1 error	order
1	320	4.7792×10^{-5}	-	8.4630×10^{-3}	-	4.9115×10^{-5}	-	8.7944×10^{-3}	-
	640	1.1709×10^{-5}	2.03	4.1118×10^{-3}	1.04	1.2264×10^{-5}	2.00	4.3953×10^{-3}	1.00
	1280	2.8572×10^{-6}	2.03	1.9776×10^{-3}	1.06	3.0627×10^{-6}	2.00	2.1957×10^{-3}	1.00
	2560	6.9952×10^{-7}	2.03	9.4917×10^{-4}	1.06	7.6449×10^{-7}	2.00	1.0959×10^{-3}	1.00
2	20	2.7554×10^{-4}	-	8.0228×10^{-3}	-	2.8046×10^{-4}	-	8.1095×10^{-3}	-
	40	3.3964×10^{-5}	3.02	1.9914×10^{-3}	2.01	3.5160×10^{-5}	3.00	2.0343×10^{-3}	2.00
	80	4.1148×10^{-6}	3.05	4.8819×10^{-4}	2.03	4.3974×10^{-6}	3.00	5.0894×10^{-4}	2.00
	160	4.8643×10^{-7}	3.08	1.1758×10^{-4}	2.05	5.4941×10^{-7}	3.00	1.2721×10^{-4}	2.00
3	10	9.9388×10^{-5}	-	2.2827×10^{-3}	-	9.9319×10^{-5}	-	2.2567×10^{-3}	-
	20	5.7282×10^{-6}	4.12	2.8076×10^{-4}	3.02	5.7324×10^{-6}	4.11	2.8011×10^{-4}	3.01
	40	3.6199×10^{-7}	3.98	3.5309×10^{-5}	2.99	3.5332×10^{-7}	4.02	3.3983×10^{-5}	3.04
	80	2.3962×10^{-8}	3.92	4.5753×10^{-6}	2.95	2.2056×10^{-8}	4.00	4.2007×10^{-6}	3.02

Table 6.25: Numerical error and convergence rate for the 1D linear convection-diffusion equation, with $\varepsilon = 10^{-4}$ (Left) and $\varepsilon = 10^{-6}$ (Right)

Parameters		$\mathcal{P}_k$ Spaces				$\mathcal{Q}_k$ Spaces			
k	N	L^2 error	order	H^1 error	order	L^2 error	order	H^1 error	order
1	20	3.9743×10^{-2}	-	5.4830×10^{-1}	-	7.6490×10^{-2}	-	6.3544×10^{-1}	-
	40	9.7720×10^{-3}	2.02	2.6949×10^{-1}	1.02	1.8988×10^{-2}	2.01	3.0855×10^{-1}	1.04
	80	2.4195×10^{-3}	2.01	1.3356×10^{-1}	1.01	4.7233×10^{-3}	2.01	1.5220×10^{-1}	1.02
	160	6.0156×10^{-4}	2.01	6.6432×10^{-2}	1.01	1.1772×10^{-3}	2.00	7.5576×10^{-2}	1.01
2	10	3.2490×10^{-3}	-	9.3911×10^{-2}	-	9.1038×10^{-3}	-	1.4855×10^{-1}	-
	20	3.9410×10^{-4}	3.04	2.3403×10^{-2}	2.00	1.1990×10^{-3}	2.92	3.8735×10^{-2}	1.94
	40	4.8898×10^{-5}	3.01	5.8518×10^{-3}	2.00	1.5218×10^{-4}	2.98	9.8000×10^{-3}	1.98
	80	6.0566×10^{-6}	3.01	1.4594×10^{-3}	2.00	1.9002×10^{-5}	3.00	2.4490×10^{-3}	2.00
3	10	1.6417×10^{-4}	-	5.2240×10^{-3}	-	2.6459×10^{-4}	-	6.8108×10^{-3}	-
	20	9.7445×10^{-6}	4.07	6.5899×10^{-4}	2.99	1.7136×10^{-5}	3.95	8.3040×10^{-4}	3.04
	40	5.8612×10^{-7}	4.06	7.9534×10^{-5}	3.05	9.9821×10^{-7}	4.10	1.0326×10^{-4}	3.01
	50	2.4256×10^{-7}	3.95	4.0865×10^{-5}	2.98	4.0474×10^{-7}	4.05	5.1776×10^{-5}	3.09

Table 6.26: Numerical error and convergence rate for the 2D linear convection-diffusion equation, with $\varepsilon = 10^{-5}$

Parameters		$\mathcal{P}_k$ Spaces				$\mathcal{Q}_k$ Spaces			
k	N	L^2 error	order	H^1 error	order	L^2 error	order	H^1 error	order
1	20	3.9740×10^{-2}	-	5.4845×10^{-1}	-	7.6493×10^{-2}	-	6.3557×10^{-1}	-
	40	9.7723×10^{-3}	2.02	2.6963×10^{-1}	1.02	1.8990×10^{-2}	2.01	3.0866×10^{-1}	1.04
	80	2.4202×10^{-3}	2.01	1.3370×10^{-1}	1.01	4.7246×10^{-3}	2.01	1.5230×10^{-1}	1.02
	160	6.0201×10^{-4}	2.01	6.6568×10^{-2}	1.01	1.1779×10^{-3}	2.00	7.5675×10^{-2}	1.01
2	10	3.2554×10^{-3}	-	9.3990×10^{-2}	-	9.1137×10^{-3}	-	1.4866×10^{-1}	-
	20	3.9565×10^{-4}	3.04	2.3435×10^{-2}	2.00	1.2019×10^{-3}	2.92	3.8800×10^{-2}	1.94
	40	4.9283×10^{-5}	3.01	5.8672×10^{-3}	2.00	1.5295×10^{-4}	2.97	9.8348×10^{-3}	1.98
	80	6.1509×10^{-6}	3.00	1.4670×10^{-3}	2.00	1.9199×10^{-5}	2.99	2.4666×10^{-3}	2.00
3	10	1.6421×10^{-4}	-	5.2417×10^{-3}	-	2.6438×10^{-4}	-	6.8032×10^{-3}	-
	20	9.7091×10^{-6}	4.08	6.6144×10^{-4}	2.99	1.7153×10^{-5}	3.95	8.3137×10^{-4}	3.03
	40	5.8036×10^{-7}	4.06	7.9948×10^{-5}	3.05	9.9388×10^{-7}	4.11	1.0316×10^{-4}	3.01
	50	2.3955×10^{-7}	3.97	4.1186×10^{-5}	2.97	4.0319×10^{-7}	4.04	5.1637×10^{-5}	3.10

Table 6.27: Numerical error and convergence rate for the 2D linear convection-diffusion equation, with $\varepsilon = 10^{-6}$

Example 6.6. In the last example, we demonstrate the usability of the ultra-weak DG method on a contaminant transport problem. Consider the following convection-diffusion equation on a two-dimensional domain $\Omega = [0, 10] \times [-1.25, 1.25]$ inspired by [40]: For $j = 1, ..., 5$,

$$
\begin{aligned}
u_t + \nabla \cdot (\mathbf{c}(x,y)u) - \varepsilon \Delta u &= 0, \text{ on } \Omega \times ((j-1)T, jT], \\
u(X, (j-1)T) &= u_0, \text{ on } \Omega,
\end{aligned}
\tag{6.13}
$$

where $\mathbf{c}(x, y)$ is a velocity field taken as $\mathbf{c}(x,y) = \left(1 - e^{\gamma x} \cos(2\pi y), \frac{\gamma}{2\pi} e^{\gamma x} \sin(2\pi y)\right)$ with $\gamma = Re/2 - \sqrt{Re^2/4 + 4\pi^2}$ and Reynolds number taken to be $Re = 100$. The above system satisfies the following homogenous boundary condition:

$$
u = 0, \text{ on } \Gamma_D, \qquad \partial_{\mathbf{n}} u = 0, \text{ on } \Gamma_N,
\tag{6.14}
$$

where the inflow boundary is specified as $\Gamma_D = \{x = 0\} \times [-1.25, 1.25]$, and the outflow boundary is $\Gamma_N = \partial\Omega \backslash \Gamma_D$. This system models transport of the contaminant under velocity field $\mathbf{c}(x, y)$. Moreover, the same amount of contaminant is injected every T seconds, while the contaminant is transported to the downstream. So the initial condition can be modeled by the following:

$$
u_0 = \begin{cases} w_0, & \text{if } j = 1, \\ w_0 + u((j-1)T), & \text{if } j > 1, \end{cases}
\tag{6.15}
$$

with the initial concentration $w_0 = e^{-\frac{(x-1)^2 + y^2}{0.5^2}} + e^{-\frac{(x-1)^2 + (y-0.5)^2}{0.5^2}} + e^{-\frac{(x-1)^2 + (y+0.5)^2}{0.5^2}}$.

We use the proposed ultra-weak DG method to solve this problem with the diffusive coefficient $\varepsilon = 0.01$. We take the unstructured triangular mesh as in Example 6.2 and $\mathcal{P}_2$ space for space discretization. The IMEX RK (3,4,3) method as time discretization. In our test, we take $N = 40$, $\tau = 0.0025$, the time period is taken as $T = 2$. The flux parameters are taken as $(\alpha, c_1, c_2) = (0.5, -80, 1.0)$. The heatplot of u at time points 0, T, $2T$, $3T$, $4T$, $5T$ is shown in Figure 6.1. It agrees with the results of an implicit Hybrid DG method studied in [40] very well.

7 Conclusions

In this paper, we studied multi-dimensional ultra-weak discontinuous Galerkin methods on unstructured and rectangular meshes with generalized numerical fluxes. The key contribution of our work
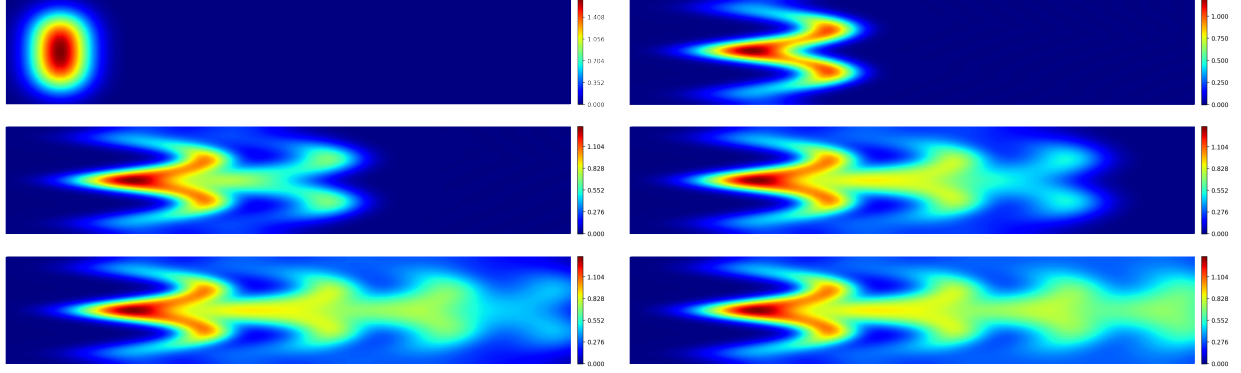
Figure 6.1: The Heatplot (from left to right, from upper to lower) of $T = 0, T, 2T, 3T, 4T, 5T$ of contaminant concentration for Example 6.6.

is on the study of the global projections designed and analyzed for ultra-weak schemes. For simplex meshes, global projections are defined directly from the ultra-weak schemes. For Cartesian meshes, we have taken advantage of the tensor product structure of meshes and spaces to define tensor product projections from one-dimensional Gauss-Radau type projections. These tensor product projections could extend the range of parameters. These projections are applied to derive the stability analysis and provide optimal error estimates for convection-diffusion and biharmonic equations. Extensive numerical examples are provided to validate our theoretic results in both one and two dimensions.

Acknowledgement

A   Proofs

A.1   Proof of Lemma 2.1

Proof. The case of $d = 1$ coincides with trace inequality for $\mathcal{P}_k$, so we only consider the case of $d > 1$. Without loss of generality, e can be written as $I_{\alpha_1}^1 \times I_{\alpha_2}^2 \times ... \times \{x_{\alpha_d - 1/2}^d\}$. We can apply the one-dimensional case of (2.10) (with $\sigma = 1$) to have:

$$\|v\|_{L^2(e)}^2 = \int_e v^2(x^1, x^2, ..., x^{d-1}, x_{\alpha_d - 1/2}^d) ds \leq (k+1)^2 \left| x_{\alpha_d - 1/2}^d - x_{\alpha_d + 1/2}^d \right|^{-1} \int_e \int_{x_{\alpha_d - 1/2}^d}^{x_{\alpha_d + 1/2}^d} v^2 dx^d \widehat{dx^d}, \tag{A.1}$$

where $\widehat{dx^i} = \prod_{j=1, j \neq i}^d dx^j$. Here we applied trace inequality on interval $\widehat{x_e^d} \times [x_{\alpha_d - 1/2}^d, x_{\alpha_d + 1/2}^d]$ for every $\widehat{x_e^d} \in I_{\alpha_1}^1 \times I_{\alpha_2}^2 \times ... \times I_{\alpha_{d-1}}^{d-1}$, and use the fact that $v(\widehat{x_e^d}, \cdot) \in \mathcal{P}_k([x_{\alpha_d - 1/2}^d, x_{\alpha_d + 1/2}^d])$ since $v \in \mathcal{Q}_k(T)$. Then we can use the assumption (2.2) of mesh $\mathcal{K}_h$ to obtain:

$$\|v\|_{L^2(e)}^2 \leq (k+1)^2 \frac{|e|}{|T|} \|v\|_{L^2(T)}^2 \leq \frac{\sigma(k+1)^2}{h_e} \|v\|_{L^2(T)}^2, \tag{A.2}$$

which finishes the proof. $\qquad \square$

A.2 Proof of Lemma 3.3

Proof. This proof is based on the analysis of [15, Lemmas 3.2, 3.4], and readers could refer to two lemmas therein for more details. The well-posedness follows from Lemma 3.2 and 3.3 there. We only prove the approximation capability in this proof.

Case 1. $\alpha^2 + c_1 c_2 = \frac{1}{4}, \Gamma \neq 0$.

By Lemma 3.1 of [15], this projection is locally defined. Then we can apply Bramble-Hilbert Lemma on each interval I_j and use a standard scaling argument to obtain the L^2 estimate. The estimate on $\mathcal{E}_h$ is obtained using trace inequality (2.7).

Case 2. $\alpha^2 + c_1 c_2 \neq \frac{1}{4}, |\Gamma| > |\Lambda|$.

In this case, we note that Π_h^{GR} is a global projection. Let $\Pi_h^1 u$ to be the projection Π_h^{GR} with $(\alpha, c_1, c_2) = (1/2, 0, 0)$, also known as the alternating flux. By Case 1, the optimal approximation capability holds for this projection. We will use this optimal projection as a reference. In this proof, we inherit the computations and notations of [15], and the corresponding equation number of the original definitions therein will be commented. We denote $P_l(\xi)$ to be the lth Legendre polynomial on $[-1, 1]$, with $\xi = 2(x - x_j)/h$ on I_j. For any Π_h^{GR}, using the first condition of (3.31), we could decompose $(\Pi_h^{\mathrm{GR}} u - \Pi_h^1 u)|_{I_j}(x) = \sum_{l=0}^{k} \alpha_{j,l} P_l(\xi) = \sum_{l=k-1}^{k} \alpha_{j,l} P_l(\xi)$, $l = 0, 1, ..., k-2$, $j = 1, ..., N$. Using the other two conditions of (3.31), these coefficients can thus be written as the solution of a linear system $\mathbb{M}\tilde{\alpha} = \mathbb{b}$, where $\tilde{\alpha} = [\alpha_{1,k-1}, \alpha_{1,k}, ..., \alpha_{N,k-1}, \alpha_{N,k}]$, $\mathbb{b} = [\tau_1, \iota_1, ..., \tau_N, \iota_N]$ with τ_j, ι_j defined as:

$$\begin{bmatrix} \tau_j \\ \iota_j \end{bmatrix} = \begin{bmatrix} \frac{1}{2} + \alpha & c_2 h \\ -c_1/h & \frac{1}{2} + \alpha \end{bmatrix} \begin{bmatrix} \eta_j \\ \theta_j \end{bmatrix}, \quad \begin{bmatrix} \eta_j \\ \theta_j \end{bmatrix} = \begin{bmatrix} u - (\Pi_h^1 u)^+ \\ u_x - (\Pi_h^1 u)_x^- \end{bmatrix}_{j+\frac{1}{2}}. \tag{A.3}$$

$\mathbb{M}$ is a block circulant matrix, and the inverse of $\mathbb{M}$ can be computed explicitly, which reads (we refer to [15] for details):

$$\mathbb{M}^{-1} = \tilde{\mathbb{M}} \otimes A^{-1}, \tag{A.4}$$

where $\otimes$ denotes Kronecker product for block matrices, $\tilde{\mathbb{M}} = \mathrm{circ}(r_0, r_1, ..., r_{N-1})$ with circ denoting the circulant matrix, and

$$A = \begin{bmatrix} \frac{1}{2} - \alpha & c_2 h \\ \frac{c_1}{h} & \frac{1}{2} + \alpha \end{bmatrix} \begin{bmatrix} P_{k-1}(1) & P_k(1) \\ \frac{2}{h} P_{k-1}'(1) & \frac{2}{h} P_k'(1) \end{bmatrix}, \quad r_j = d_1^j Q_1 + d_2^j (I_2 - Q_1), \tag{A.5}$$

with $d_1^j = \lambda_1^j/(1 - \lambda_1^N)$ and $d_2^j = \lambda_2^j/(1 - \lambda_2^N)$. Here $\lambda_1, \lambda_2 \in \mathbb{R}$ are two eigenvalues of a parameter matrix satisfying $\lambda_1, \lambda_2 \neq 1$. Under our scale invariant numerical fluxes setting, we have λ_1, λ_2 and Q_1 [15, in Eq. (60)] independent of h. We therefore have:

$$\tilde{\alpha} = \mathbb{M}^{-1} \mathbb{b} = \tilde{\mathbb{M}} \tilde{\mathbb{b}} \tag{A.6}$$

where $\tilde{\mathbb{b}} = [A^{-1}[\tau_j, \iota_j]]_{j=1}^N = [\eta_j V_1 + \theta_j V_2]_{j=1}^N$. Note that $V_1, V_2 \in \mathbb{R}^2$ [15, in Eq. (65)], and $V_1 \sim \mathcal{O}(1)$, $V_2 \sim \mathcal{O}(h)$ in our context. We can analyze $\tilde{\mathbb{M}}$ as the following:

$$\|\tilde{\mathbb{M}}\|_1 = \|\tilde{\mathbb{M}}\|_\infty \leq C \sum_{j=1}^N (|d_1^j| + |d_2^j|) \leq C \left(\frac{1}{1 - |\lambda_1|} \frac{1 - |\lambda_1|^N}{|1 - \lambda_1^N|} + \frac{1}{1 - |\lambda_2|} \frac{1 - |\lambda_2|^N}{|1 - \lambda_2^N|} \right) \leq C, \tag{A.7}$$

where the last inequality results from the independence of λ_1, λ_2 and h. Therefore we have:

$$\|\tilde{\alpha}\|_2^2 \le \|\tilde{\mathbb{M}}\|_2^2 \|\tilde{\mathbb{b}}\|_2^2 \le \|\tilde{\mathbb{M}}\|_1 \|\tilde{\mathbb{M}}\|_\infty \left(\sum_{j=1}^N |\eta_j|^2 + h^2 |\theta_j|^2 \right) \le C \left(\left\| u - \Pi_h^1 u \right\|_{L^2(\mathcal{E}_h)}^2 + h^2 |u - \Pi_h^1 u|_{H^1(\mathcal{E}_h)}^2 \right).$$
(A.8)

Note that:

$$\begin{aligned} \left\| u - \Pi_h^{\mathtt{GR}} u \right\|_{L^2(\mathcal{T}_h)}^2 &\le \left\| u - \Pi_h^1 u \right\|_{L^2(\mathcal{T}_h)}^2 + \left\| \Pi_h^{\mathtt{GR}} u - \Pi_h^1 u \right\|_{L^2(\mathcal{T}_h)}^2 \\ &\le \left\| u - \Pi_h^1 u \right\|_{L^2(\mathcal{T}_h)}^2 + \sum_{j=1}^N \sum_{l=k-1}^k \alpha_{j,l}^2 \left\| P_l(\xi) \right\|_{L^2(\mathcal{T}_h)}^2 \\ &\le \left\| u - \Pi_h^1 u \right\|_{L^2(\mathcal{T}_h)}^2 + h \left\| \tilde{\alpha} \right\|_2^2 . \end{aligned}$$
(A.9)

The estimate in L^2 norm follows the approximation capability in Case 1, and the estimate on $\mathcal{E}_h$ follows directly from $\|\tilde{\alpha}\|_2$. This completes the proof. $\qquad\square$

References

[1] Douglas N. Arnold. An interior penalty finite element method with discontinuous elements. *SIAM J. Numer. Anal.*, 19(4):742–760, 1982.

[2] Douglas N. Arnold, Franco Brezzi, Bernardo Cockburn, and L. Donatella Marini. Unified analysis of discontinuous Galerkin methods for elliptic problems. *SIAM J. Numer. Anal.*, 39(5):1749–1779, 2001/02.

[3] Uri M. Ascher, Steven J. Ruuth, and Raymond J. Spiteri. Implicit-explicit Runge-Kutta methods for time-dependent partial differential equations. volume 25, pages 151–167. 1997. Special issue on time integration (Amsterdam, 1996).

[4] I. Babuška, J. Osborn, and J. Pitkäranta. Analysis of mixed methods using mesh dependent norms. *Math. Comp.*, 35(152):1039–1062, 1980.

[5] Garth A. Baker. Finite element methods for elliptic equations using nonconforming elements. *Math. Comp.*, 31(137):45–59, 1977.

[6] F. Bassi and S. Rebay. A high-order accurate discontinuous finite element method for the numerical solution of the compressible Navier-Stokes equations. *J. Comput. Phys.*, 131(2):267–279, 1997.

[7] Carlos Erik Baumann and J. Tinsley Oden. A discontinuous hp finite element method for convection-diffusion problems. *Comput. Methods Appl. Mech. Engrg.*, 175(3-4):311–341, 1999.

[8] J. L. Bona, H. Chen, O. Karakashian, and Y. Xing. Conservative, discontinuous Galerkin-methods for the generalized Korteweg-de Vries equation. *Math. Comp.*, 82(283):1401–1432, 2013.

[9] Susanne C. Brenner and L. Ridgway Scott. *The mathematical theory of finite element methods*, volume 15 of *Texts in Applied Mathematics*. Springer, New York, third edition, 2008.

[10] Susanne C. Brenner and Li-Yeng Sung. C^0 interior penalty methods for fourth order elliptic boundary value problems on polygonal domains. *J. Sci. Comput.*, 22/23:83–118, 2005.

[11] F. Brezzi, G. Manzini, D. Marini, P. Pietra, and A. Russo. Discontinuous Galerkin approximations for elliptic problems. *Numer. Methods Partial Differential Equations*, 16(4):365–378, 2000.

[12] Paul Castillo. An optimal estimate for the local discontinuous Galerkin method. In *Discontinuous Galerkin methods (Newport, RI, 1999)*, volume 11 of *Lect. Notes Comput. Sci. Eng.*, pages 285–290. Springer, Berlin, 2000.

[13] Paul Castillo, Bernardo Cockburn, Dominik Schötzau, and Christoph Schwab. Optimal a priori error estimates for the hp-version of the local discontinuous Galerkin method for convection-diffusion problems. *Math. Comp.*, 71(238):455–478, 2002.

[14] Anqi Chen, Yingda Cheng, Yong Liu, and Mengping Zhang. Superconvergence of ultra-weak discontinuous Galerkin methods for the linear Schrödinger equation in one dimension. *J. Sci. Comput.*, 82(1):Paper No. 22, 44, 2020.

[15] Anqi Chen, Fengyan Li, and Yingda Cheng. An ultra-weak discontinuous Galerkin method for Schrödinger equation in one dimension. *J. Sci. Comput.*, 78(2):772–815, 2019.

[16] Yao Cheng, Xiong Meng, and Qiang Zhang. Application of generalized Gauss-Radau projections for the local discontinuous Galerkin method for linear convection-diffusion equations. *Math. Comp.*, 86(305):1233–1267, 2017.

[17] Yingda Cheng, Ching-Shan Chou, Fengyan Li, and Yulong Xing. L^2 stable discontinuous Galerkin methods for one-dimensional two-way wave equations. *Math. Comp.*, 86(303):121–155, 2017.

[18] Yingda Cheng and Chi-Wang Shu. A discontinuous Galerkin finite element method for time dependent partial differential equations with higher order derivatives. *Math. Comp.*, 77(262):699–730, 2008.

[19] P. G. Ciarlet and P.-A. Raviart. General Lagrange and Hermite interpolation in $\mathbf{R}^n$ with applications to finite element methods. *Arch. Rational Mech. Anal.*, 46:177–199, 1972.

[20] P. G. Ciarlet and P.-A. Raviart. A mixed finite element method for the biharmonic equation. In *Mathematical aspects of finite elements in partial differential equations (Proc. Sympos., Math. Res. Center, Univ. Wisconsin, Madison, Wis., 1974)*, pages 125–145. Academic Press, New York-London, 1974.

[21] Philippe G. Ciarlet. *The finite element method for elliptic problems*, volume 40 of *Classics in Applied Mathematics*. Society for Industrial and Applied Mathematics (SIAM), Philadelphia, PA, 2002. Reprint of the 1978 original [North-Holland, Amsterdam; MR0520174 (58 #25001)].

[22] Bernardo Cockburn, Jayadeep Gopalakrishnan, and Francisco-Javier Sayas. A projection-based error analysis of HDG methods. *Math. Comp.*, 79(271):1351–1367, 2010.

[23] Bernardo Cockburn, Guido Kanschat, Ilaria Perugia, and Dominik Schötzau. Superconvergence of the local discontinuous Galerkin method for elliptic problems on Cartesian grids. *SIAM J. Numer. Anal.*, 39(1):264–285, 2001.

[24] Bernardo Cockburn and Chi-Wang Shu. The local discontinuous Galerkin method for time-dependent convection-diffusion systems. *SIAM J. Numer. Anal.*, 35(6):2440–2463, 1998.

[25] V. Dolejší, M. Feistauer, and V. Sobotíková. Analysis of the discontinuous Galerkin method for nonlinear convection-diffusion problems. *Comput. Methods Appl. Mech. Engrg.*, 194(25-26):2709–2733, 2005.

[26] Vít Dolejší and Miloslav Feistauer. Error estimates of the discontinuous Galerkin method for nonlinear nonstationary convection-diffusion problems. *Numer. Funct. Anal. Optim.*, 26(3):349–383, 2005.

[27] Jim Douglas, Jr. and Todd Dupont. Interior penalty procedures for elliptic and parabolic Galerkin methods. In *Computing methods in applied sciences (Second Internat. Sympos., Versailles, 1975)*, Lecture Notes in Phys., Vol. 58, pages 207–216. Springer, Berlin, 1976.

[28] G. Engel, K. Garikipati, T. J. R. Hughes, M. G. Larson, L. Mazzei, and R. L. Taylor. Continuous/discontinuous finite element approximations of fourth-order elliptic problems in structural and continuum mechanics with applications to thin beams and plates, and strain gradient elasticity. *Comput. Methods Appl. Mech. Engrg.*, 191(34):3669–3750, 2002.

[29] Guosheng Fu and Chi-Wang Shu. An energy-conserving ultra-weak discontinuous Galerkin method for the generalized Korteweg–de Vries equation. *J. Comput. Appl. Math.*, 349:41–51, 2019.

[30] Pei Fu, Yingda Cheng, Fengyan Li, and Yan Xu. Discontinuous Galerkin methods with optimal L^2 accuracy for one dimensional linear PDEs with high order spatial derivatives. *J. Sci. Comput.*, 78(2):816–863, 2019.

[31] Juntao Huang, Yong Liu, Yuan Liu, Zhanjing Tao, and Yingda Cheng. A class of adaptive multiresolution ultra-weak discontinuous Galerkin methods for some nonlinear dispersive wave equations. *SIAM J. Sci. Comput.*, 44(2):A745–A769, 2022.

[32] Guang Shan Jiang and Chi-Wang Shu. On a cell entropy inequality for discontinuous Galerkin methods. *Math. Comp.*, 62(206):531–538, 1994.

[33] Hailiang Liu. Optimal error estimates of the direct discontinuous Galerkin method for convection-diffusion equations. *Math. Comp.*, 84(295):2263–2295, 2015.

[34] Hailiang Liu. Analysis of direct discontinuous Galerkin methods for multi-dimensional convection-diffusion equations. *Numer. Math.*, 147(4):839–867, 2021.

[35] Hailiang Liu and Jue Yan. The direct discontinuous Galerkin (DDG) methods for diffusion problems. *SIAM J. Numer. Anal.*, 47(1):675–698, 2008/09.

[36] Wenying Lu, Yunqing Huang, and Hailiang Liu. Mass preserving discontinuous Galerkin methods for Schrödinger equations. *J. Comput. Phys.*, 282:210–226, 2015.

[37] Xiong Meng, Chi-Wang Shu, and Boying Wu. Optimal error estimates for discontinuous Galerkin methods based on upwind-biased fluxes for linear hyperbolic equations. *Math. Comp.*, 85(299):1225–1261, 2016.

[38] Igor Mozolevski and Endre Süli. A priori error analysis for the *hp*-version of the discontinuous Galerkin finite element method for the biharmonic equation. *Comput. Methods Appl. Math.*, 3(4):596–607, 2003.

[39] Igor Mozolevski, Endre Süli, and Paulo R. Bösing. *hp*-version a priori error analysis of interior penalty discontinuous Galerkin finite element approximations to the biharmonic equation. *J. Sci. Comput.*, 30(3):465–491, 2007.

[40] N. C. Nguyen, J. Peraire, and B. Cockburn. An implicit high-order hybridizable discontinuous Galerkin method for linear convection-diffusion equations. *J. Comput. Phys.*, 228(9):3232–3254, 2009.

[41] J. Tinsley Oden, Ivo Babuška, and Carlos Erik Baumann. A discontinuous *hp* finite element method for diffusion problems. *J. Comput. Phys.*, 146(2):491–519, 1998.

[42] William H Reed and Thomas R Hill. Triangular mesh methods for the neutron transport equation. Technical report, Los Alamos Scientific Lab., N. Mex.(USA), 1973.

[43] Béatrice Rivière, Mary F. Wheeler, and Vivette Girault. Improved energy estimates for interior penalty, constrained and discontinuous Galerkin methods for elliptic problems. I. *Comput. Geosci.*, 3(3-4):337–360 (2000), 1999.

[44] Gilbert Strang. The finite element method and approximation theory. In *Numerical Solution of Partial Differential Equations, II (SYNSPADE 1970) (Proc. Sympos., Univ. of Maryland, College Park, Md., 1970)*, pages 547–583. Academic Press, New York, 1971.

[45] Jiawei Sun, Chi-Wang Shu, and Yulong Xing. Multi-symplectic discontinuous Galerkin methods for the stochastic Maxwell equations with additive noise. *J. Comput. Phys.*, 461:Paper No. 111199, 30, 2022.

[46] Jiawei Sun, Chi-Wang Shu, and Yulong Xing. Discontinuous Galerkin methods for stochastic Maxwell equations with multiplicative noise. *ESAIM Math. Model. Numer. Anal.*, 57(2):841–864, 2023.

[47] Zheng Sun and Yulong Xing. Optimal error estimates of discontinuous Galerkin methods with generalized fluxes for wave equations on unstructured meshes. *Math. Comp.*, 90(330):1741–1772, 2021.

[48] Zheng Sun and Yulong Xing. On generalized Gauss-Radau projections and optimal error estimates of upwind-biased DG methods for the linear advection equation on special simplex meshes. *J. Sci. Comput.*, 95(2):Paper No. 40, 36, 2023.

[49] Qi Tao, Yan Xu, and Chi-Wang Shu. An ultraweak-local discontinuous Galerkin method for PDEs with high order spatial derivatives. *Math. Comp.*, 89(326):2753–2783, 2020.

[50] Qi Tao, Yan Xu, and Chi-Wang Shu. A discontinuous Galerkin method and its error estimate for nonlinear fourth-order wave equations. *J. Comput. Appl. Math.*, 386:Paper No. 113230, 16, 2021.

[51] R. Verfürth. A posteriori error estimation and adaptive mesh-refinement techniques. In *Proceedings of the Fifth International Congress on Computational and Applied Mathematics (Leuven, 1992)*, volume 50, pages 67–83, 1994.

[52] T. Warburton and J. S. Hesthaven. On the constants in *hp*-finite element trace inverse inequalities. *Comput. Methods Appl. Mech. Engrg.*, 192(25):2765–2773, 2003.

[53] Yan Xu and Chi-Wang Shu. Error estimates of the semi-discrete local discontinuous Galerkin method for nonlinear convection-diffusion and KdV equations. *Comput. Methods Appl. Mech. Engrg.*, 196(37-40):3805–3822, 2007.

[54] Qiang Zhang and Chi-Wang Shu. Error estimates to smooth solutions of Runge-Kutta discontinuous Galerkin methods for scalar conservation laws. *SIAM J. Numer. Anal.*, 42(2):641–666, 2004.

[55] Qiang Zhang and Chi-Wang Shu. Stability analysis and a priori error estimates of the third order explicit Runge-Kutta discontinuous Galerkin method for scalar conservation laws. *SIAM J. Numer. Anal.*, 48(3):1038–1063, 2010.